

LA-11152-T

Thesis

C.3

Los Alamos National Laboratory is operated by the University of California for the United States Department of Energy under contract W-7405-ENG-36.

CIC-14 REPORT COLLECTION
REPRODUCTION
COPY

*Effects of Electric Fields on the
Photodetachment Cross Section of the H⁻ Ion
Near Threshold*



Los Alamos Los Alamos National Laboratory
Los Alamos, New Mexico 87545

rw

This thesis was accepted by the Department of Physics, University of New Mexico, Albuquerque, New Mexico, in partial fulfillment of the requirements for the degree of Doctor of Philosophy. It is the independent work of the author and has not been edited by the Writing and Editing staff.

DISCLAIMER

This report was prepared as an account of work sponsored by an agency of the United States Government. Neither the United States Government nor any agency thereof, nor any of their employees, makes any warranty, express or implied, or assumes any legal liability or responsibility for the accuracy, completeness, or usefulness of any information, apparatus, product, or process disclosed, or represents that its use would not infringe privately owned rights. Reference herein to any specific commercial product, process, or service by trade name, trademark, manufacturer, or otherwise, does not necessarily constitute or imply its endorsement, recommendation, or favoring by the United States Government or any agency thereof. The views and opinions of authors expressed herein do not necessarily state or reflect those of the United States Government or any agency thereof.

LA-11152-T
Thesis

UC-34
Issued: December 1987

Effects of Electric Fields on the Photodetachment Cross Section of the H⁻ Ion Near Threshold

James Edward Stewart





EFFECTS OF ELECTRIC FIELDS ON THE
PHOTODETACHMENT CROSS SECTION OF THE H^- ION
NEAR THRESHOLD

BY

JAMES EDWARD STEWART

B.A., University of North Dakota, 1968

B.S., University of North Dakota, 1971

M.S., University of New Mexico, 1985

DISSERTATION

Submitted in Partial Fulfillment of the
Requirements for the Degree of
Doctor of Philosophy in Physics

The University of New Mexico
Albuquerque, New Mexico

December, 1987

ACKNOWLEDGMENTS

The support of my advisor, Dr. Howard Bryant, has made a difficult task relatively painless. The nature of the experiment is such that the help of many people is necessary. Dr. Stan Cohen, a fellow traveller, has given invaluable advice on the arcane world of computing. Dr. Dave Clark has given technical advice and material support. Dr. Bernd Bassalleck has always been willing to listen and to give useful advice. Dr. Randy Reeder, Amir Mohagheghi, Phil Harris, Dr. Vincent Yuan, Dr. Bob Quick, Dr. Win Smith and Dr. Chuck Hummer all helped set up and run the experiment. Alan Lucero's help with analysis of the data was invaluable. Peggy Stewart's support and assistance have been indispensable.

TABLE OF CONTENTS

	Page
CHAPTER 1: INTRODUCTION	1
CHAPTER 2: THEORY	6
Zero Field.	6
Pi Polarization	8
Time Dependent Auto-Correlation Approach.	9
Frame Transformation Approach	12
Simple Theory to Find Minima.	14
Sigma Polarization.	22
CHAPTER 3: APPARATUS AND EXPERIMENTAL TECHNIQUE	24
Overview of Experiment.	24
H Minus Particle Beam	28
Nd:YAG Laser.	31
Vacuum.	33
Scattering Chamber.	34
Methods to Generate Electric Fields	37
Laser Polarization.	45
Detection of Particles.	47
Electron Spectrometer	48
Tune Up	64
A Typical Run	65
Timing and Electronics.	66
CHAPTER 4: DATA AND ANALYSIS.	72
Data Reduction and Curve Fitting.	74

TABLE OF CONTENTS (Cont.)

	Page
Determination of Encoder Zero and Steps	
per Degree.	79
Analysis of 1985 Data	83
1985 "Zero Field" Data.	84
1985 σ Polarization Field Data.	89
Analysis of 1986 Data	91
1986 "Zero Field" Data.	96
1986 σ Polarization Field Data.102
1986 π Polarization Field Data.102
CHAPTER 5: CONCLUSIONS.123
APPENDICES127
1. 1985 "Zero Field" Data.127
2. 1985 Sigma Polarization Field Data.131
3. 1986 "Zero Field" Data.138
4. 1986 Sigma Polarization Field Data.142
5. 1986 Pi Polarization Field Data145
REFERENCES159

LIST OF FIGURES

Figure	Page
2.1 Prediction of W.P. Reinhardt.	11
2.2 Prediction of Rau and Wong.	15
2.3 Illustration of simple theory	18
2.4 H.C. Bryant's comparison of a Michelson interferometer with his "atomic interferometer"	20
3.1 Layout of experiment, 1986.	25
3.2 Schematic of LAMPF photodetachment apparatus (1986 electromagnet in place)	26
3.3 Schematic of LAMPF photodetachment apparatus (1986 potential well in place)	27
3.4 Error due to misalignment of laser.	36
3.5 Schematic of interaction region with electromagnet	39
3.6 Magnetic field of magnets used in 1986.	40
3.7 Schematic of interaction region with potential well.	42
3.8 Energy tagging in potential well.	43
3.9 Schematic of polarizer.	46
3.10 Electron trajectories	51
3.11 Coordinate system for calculating trajectories.	53

LIST OF FIGURES (Cont.)

	Page
3.12 Design parameters for detector location	57
3.13 Electron spectrometer assembly.	58
3.14 Effect of energy tagging on position of electron peak in spectrometer.	61
3.15 Hydrogen series	63
3.16 Block diagram of electronics.	67
3.17 Timing scheme	69
3.18 Examples of H^- ion pulse with laser and background gates.	71
4.1 Ideogram 1985 zero field data	86
4.2 1985 threshold power law.	90
4.3 1985 σ polarization field data.	93
4.4 Effect of electric field on power and threshold	94
4.5 1986 threshold power law.	98
4.6 Ideogram 1986 zero field data101
4.7 Overview of 1986 data comparing σ and π polarization at different fields.104
4.8 Relative cross sections for π polarization compared with the theory of W. P. Reinhardt106
4.9 Example of the subtraction method107

LIST OF FIGURES (Cont.)

	Page
4.10 Relative cross section for π polarization compared with the theory of Rau and Wong.109
4.11 Summaries of ripple minima vs. electric field.115
4.12 Summary of ripple minima vs. energy116
4.13 Summary of amplitudes118

LIST OF TABLES

Table	Page
1. Overview of experiments	73
2. 1985 data, summary of zero field fits	87
3. 1985 data, summary of all runs.	92
4. 1986 data, summary of zero field fits	99
5. 1986 data, summary of σ polarization runs103
6. Ripple summary.110
7. Average values for a' and n117
8. Ripple minima from data taken with potential well.120

EFFECTS OF ELECTRIC FIELDS ON THE
PHOTODETACHMENT CROSS SECTION OF THE H^- ION
NEAR THRESHOLD

James Edward Stewart

B.A. Social Sciences, University of North Dakota, 1968

B.S. Education, University of North Dakota, 1971

M.S. Physics, University of New Mexico, 1985

Ph.D. Physics, University of New Mexico, 1987

The photodetachment cross section of the H^- ion near the one electron threshold in electric fields ranging from approximately 5×10^{-7} atomic units up to 2.4×10^{-4} atomic units has been studied using an 800 MeV beam at the Los Alamos National Laboratory. The lowest field data, analyzed as though at zero field, are consistent with the Wigner prediction for p wave processes. At greater field values, photodetachment using σ polarized laser light displays the expected lowering of apparent threshold and evidence of tunneling. Using π polarized laser light the same features are seen with the addition of oscillations superimposed on the cross section. Three complementary explanations are presented for the oscillations.

CHAPTER 1: INTRODUCTION

The experiments described here are the most recent in a series exploring the H^- ion using the relativistic H^- beam at the Clinton P. Anderson Meson Physics Facility (commonly known as LAMPF for Los Alamos Meson Physics Facility) at the Los Alamos National Laboratory. The recent experiments have explored the behavior of the photodetachment cross section of the H minus ion in moderate electric fields.

The H^- ion is of interest for several reasons. It is arguably the simplest three body system available for study, consisting of a single proton binding two electrons. Neutral hydrogen binds its single electron with approximately 13.6 electron volts. The H^- ion is formed when a free electron approaches close enough to polarize the neutral atom to allow capture of the electron. The second electron is bound by a mere 0.75 eV.

The H^- ion is a major constituent of solar atmospheres contributing to solar spectra by absorbing radiation from the solar surface. As one considers the phenomenon described in this paper one wonders whether the H^- minus spectrum of stars could yield information about the electric and magnetic fields which surround a star.

In recent years the H^- ion has been of great interest to scientists and engineers designing neutral particle

beams. The negatively charged ion can be accelerated and then stripped of the loosely bound electron to produce a neutral particle beam.

H^- provides a simple test of theoretical models of negative ions. This paper describes experiments which tested two such models.

In the first experiments in the series exploring the H^- ion, Sharifian (1977) and Tootoonchi (1977) used the technique described below to explore the H^- cross section from 1.5 eV to 12 eV where the shape and Feshbach resonances (auto-ionizing states wherein the residual neutral atom is left in an excited state) near $n = 2$ were observed. Frost (1981) looked at the threshold for both one and two electron photodetachment of the H^- ion. The present work is a direct extension of the work of Frost. Butterfield (1984) explored the behavior of the shape and Feshbach resonances in electric fields. Most recently, Cohen (1986) has examined the $^1P^0$ resonance near $n = 3$ in external electric fields.

All of these experiments are based on a technique, devised by H.C. Bryant (Bryant et al., 1980), which makes elegant use of the relativistic (0.84c) particle beam. We make use of two facets of Special Relativity. It is commonly known that light from a source moving at an appreciable fraction of the speed of light will appear to an observer at rest to be shifted in wavelength - the

familiar red shift of astronomical use is an example. We use this relativistic Doppler shift,

$$E_{\text{cm}} = \gamma E_{\text{lab}} (1 + \beta \cos \alpha), \quad (1)$$

to achieve a photon energy which is continuously tunable over a wide range in the rest frame of the target

particles. $\beta = v/c$; $\gamma = 1/\sqrt{1-\beta^2}$; α is the angle between laser beam and particle beam defined such that head-on is zero degrees; E_{lab} is the laboratory photon energy.

Evaluating the factor $(1 + \beta \cos \alpha)$ for $\beta = 0.84$ we find that the barycentric energy of the laser photon can be varied by a factor ranging from 0.3 to 3.4 depending on α .

We also make use of the Lorentz transformation for electric and magnetic fields (in S.I. units),

$$\vec{F}'_{\perp} = \gamma(\vec{F}_{\perp} + \vec{v} \times \vec{B}). \quad (2)$$

$$\vec{F}'_{\parallel} = \vec{F}_{\parallel}$$

In particular, we are able to impose upon the interaction region a barycentric electric field about two orders of magnitude larger than can reasonably be accomplished in the laboratory frame. This is done by using a modest magnetic field in the laboratory which then transforms to crossed electric and magnetic fields in the H minus frame.

The experiments described herein were mounted to explore the behavior of the H^- ion near the one electron threshold in electric fields. In particular we were motivated by a prediction of W.P. Reinhardt (1984) that we would observe oscillations in the cross section in the particular case where the photons were polarized parallel to the imposed electric field.

Two series of experiments were conducted. One, in the summer of 1985, looked at the effect of photodetaching the loosely bound (0.75 eV) second electron of the H^- ion in electric fields of as much as 1.3×10^6 volts/cm using σ polarized light. Sigma (σ) polarization is perpendicular to the electric field and π is parallel to the electric field. In the summer of 1986, a modified apparatus allowed us to look at the effect of π polarization although with smaller fields, of the order of 2×10^5 volts/cm.

The field-induced oscillations are a phenomenon similar to that observed by a number of other workers looking at neutral atoms of Rb, Ba, and Na (Feneuille et al., 1979; Littman et al., 1981; Freeman et al., 1978; Luk et al., 1981; Sandner et al., 1981). Theoretical explanations have been put forward by Harmin (1982); Luc-Koenig and Bachelier (1979, 1980); Rau (1979); Rau and Lu (1980). Blumberg et al., (1978) have reported observation of oscillations in the S^- photodetachment

cross section in the presence of a magnetic field where they presume the oscillations are due to the excitation of the detached electron to discrete levels.

Recently, Rau and Wong (1987) have also formulated a theory which predicts field induced oscillations in photodetachment.

For the π polarization experiments we constructed several new pieces of apparatus. An "electrostatic potential well" was built to be able to look at the effects of a pure electric field on the cross section and an electron spectrometer was made to use in conjunction with the potential well to detect electrons which, once photodetached, were tagged with an energy different from background electrons. Most of the data was taken using an older setup with one of two electro-magnets supplying a motional electric field.

The potential well, spectrometer combination was useful to prove that the ripple effect is due to the electric field and not a combination of crossed electric and magnetic fields. In addition, the spectrometer was used in an unrelated experiment which is discussed briefly as it is relevant to the function and testing of the spectrometer.

CHAPTER 2: THEORY

We are concerned with three different situations for which we must invoke different theories. These cases are photodetachment in zero field, in a d.c. electric field with a photon polarized perpendicular to the field, (σ), and in a d.c. electric field with a photon polarized parallel to the field, (π).

ZERO FIELD

Wigner (1948) was able to determine the form of the cross section near threshold for any two-body process. He showed that the form did not depend on the details of the interaction process. Wigner found that the cross section was proportional to

$$(E-E_0)^{(2\ell+1)/2}, \quad (3)$$

where E is the energy of the photon and E_0 is the binding energy so that $(E-E_0)$ gives the kinetic energy of the detached electron. The angular momentum quantum number of the final two body state is ℓ . In the case of photodetachment of the H^- ion, $\ell = 1$. We expect that the cross section will depend on $(E-E_0)^{3/2}$. Wigner does not tell us how far in energy above threshold this law should apply.

Armstrong (1963) obtained a simple characterization of the H^- threshold over a wider energy range than Wigner's prediction applies. This prediction gives the overall shape of the curve beyond the broad maximum which occurs at 1.5 eV. Armstrong's prediction for the cross section, σ , as a function of energy is

$$\sigma(E) \propto \frac{E_0^{1/2} [E - E_0]^{3/2}}{E^3} \left[1 + \frac{g_0}{2} E_0 [2E_0 - E] \right]^2. \quad (4)$$

The term in the square brackets is an empirical correction factor introduced to produce better agreement with the data of Smith and Burch (1959). Frost found that the correction factor was unnecessary; so, it has not been used in my analysis.

Fano and Rau (1986) obtain a comparable formula, atomic units:

$$\sigma = \frac{16\pi}{3(137)} \frac{E_0^{1/2} [E - E_0]^{3/2}}{E^3}. \quad (5)$$

Also of interest is the prediction of Greene and Rau (1985) that there are oscillations even in the zero field cross section above threshold. Using Quantum Defect Theory they expect oscillations of very small amplitude to appear - a prediction which remains unconfirmed.

dominated by the nucleus moving to that dominated by the electrostatic field.

Several authors have explained similar oscillations which appear in the photoionization cross section of neutral atoms. Harmin (1982) modeled the data of Freeman et al., (1978) by considering two distinct regions: one where the Coulomb potential was dominant and the imposed electric field could be ignored and one where the electric field was dominant. This work provided a partial basis for Rau and Wong's predictions for negative ions.

Luc-Koenig and Bachelier (1979) proposed that the oscillations arise from cancellations of oscillator strengths of different Stark states due to symmetries between the wave functions and the light.

Rau (1979) and Rau and Lu (1980), by considering neutral hydrogen in an electric field in parabolic

coordinates, find that oscillations with equal spacing dependent on $F^{3/2}$ are present. They state further that this is a general phenomenon to be expected whenever there is a mixing of fields.

Time Dependent Auto-Correlation Approach

Reinhardt gives a specific theory for negative ions. The photodetachment cross section is given as

$$\sigma(\omega) = 2\pi \alpha a_0^2 \omega \int \exp(i\omega t) \langle \phi(t) | \phi(0) \rangle dt^1. \quad (6)$$

Reinhardt assumed a Gaussian, p wave initial state of the form

$$\phi(0) = 2\sqrt{\alpha} \left[\frac{2a}{\pi} \right]^{3/4} z \exp\left\{ -a \left[x^2 + y^2 + z^2 \right] \right\}, \quad (7)$$

where $a = 1/(8\rho^2)$ with ρ equal to the ionic radius (Overman, 1986). A further assumption is that there is no final state interaction between the detached electron and the neutral atom - a reasonable assumption in light of the fact that the multipole elements which describe the polarized atom decay rapidly with distance.

¹The matrix element has, in fact, been squared as expected, but is not explicitly displayed due to a mathematical trick which is exposed in Heller (1978).

The final state, $\phi(t)$, is given by

$$\phi(t) = \int dx' U(x, x', t) \phi(0), \quad (8)$$

where $U(x, x', t)$ is the propagator for an electron in a d.c. electric field.

A substantial amount of algebra leads to the result

$$\sigma(\omega) = 2\pi\alpha a_0^2 \int_{-\infty}^{\infty} e^{i\omega t} \left[\frac{4a - F^2 t^2 (1 + iat)}{4a(1 + iat)^{5/2}} \right] \times \exp\left\{ \frac{-F^2 t^2}{24a} (3 + iat) \right\} dt, \quad (9)$$

(Reeder, 1986), which must now be numerically integrated. Figure 2.1 shows Reinhardt's initial prediction of ripples in a constant field, with $a = 1$.

The integration program as written by Reinhardt calculates the cross section in a constant electric field. However, our experimental setup is such that, as the angle of intersection between the laser and the H^- beam is changed the electric field is also changed. So, to correctly model our experiment, I modified the program to recalculate the wave functions at each angle. This seemingly simple change increases the run time of the program on our Micro-vax II from about 7 minutes to 13.5

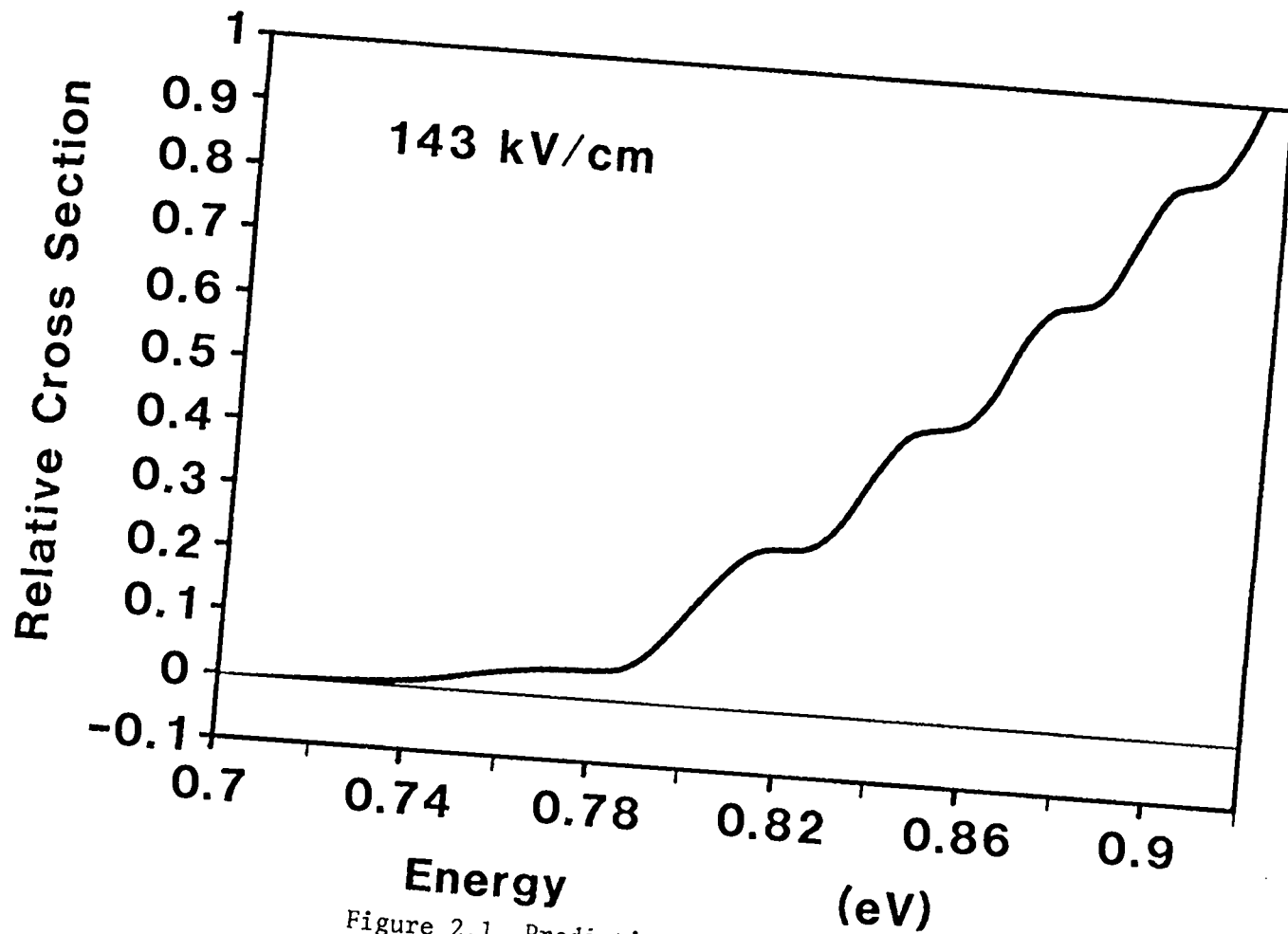


Figure 2.1 Prediction of W. P. Reinhardt.

hours! Rather than calculating the 200,000 element complex arrays in the program one time, the modification requires calculating them 200 times. The end result is a smooth curve that can be compared with our data.

Frame Transformation Approach

Rau and Wong's (1987) 'frame transformation' is based on the work of Harmin (1982) and Fano (1981). The problem is considered in spherical symmetry while the electron is close to the atom and essentially uninfluenced by the external field. At some appropriate distance a transformation is made to the cylindrically symmetric wave function which describes the electron in an electrostatic field.

For the outgoing p wave electron Rau and Wong use the spherically symmetric wave function

$$f_{1m}(\vec{r}) = (2k/\pi)^{1/2} j_1(kr) Y_{1m}(\hat{r}) , \quad (10)$$

where j_1 is the spherical Bessel function and Y_{1m} are spherical harmonics. The wave function in cylindrical coordinates is

$$\psi_{qm}(\vec{r}) = (2\pi)^{-1/2} e^{im\phi} J_m \left[(k^2 - q^2)^{1/2} \rho \right]$$

$$(\pi q)^{-1/2} \begin{cases} \cos qz & \pi_z = + \\ \sin qz & \pi_z = - \end{cases} . \quad (11)$$

For any energy $1/2 k^2$, there are two degenerate solutions of even and odd parity. The initial energy, $1/2 k^2$, is divided into energy in the z direction, along the field, $1/2 q^2$, and transverse energy, $1/2(k^2 - q^2)$. J_m is the regular Bessel function.

We now look for a transformation of the form,

$$\psi_{qm}(\vec{r}) = \sum_l U_{ql}^{F=0} f_{lm}(\vec{r}). \quad (12)$$

The summation runs over even (odd) $l-m$ for $\pi_z = +(-)$.

The $l = 1$ coefficient of $U_{ql}^{F=0}$ can be found by considering small values of the coordinates for ψ and f .

Once we know $\psi^{F=0}$ in terms of f_{lm} we can find a transformation U^F for ψ^F knowing ψ^F is given by

$$\psi_{qm}^F(\vec{r}) = (2\pi)^{-1/2} e^{im\phi} J_m \left[(k^2 - q^2)^{1/2} \rho \right] Ai \left[(2F)^{1/3} \left(z - \frac{q^2}{2F} \right) \right], \quad (13)$$

where Ai is the Airy function. U^F is found to be

$$U_{ql}^F = \begin{cases} \left[\frac{3\pi}{k^3} \right]^{1/2} \left[16F \right]^{1/6} Ai \left[\frac{-q^2}{(2F)^{2/3}} \right] & m = 0 \\ \left[\frac{3\pi}{2k} \right]^{1/2} \left[\frac{4}{F} \right]^{1/6} \left[1 - \frac{q^2}{k^2} \right] Ai \left[\frac{-q^2}{(2F)^{2/3}} \right] & m = \pm 1 \end{cases} \quad (14)$$

The photodetachment cross section can now be written

$$\begin{aligned}\sigma^F(k) &= \sigma^{F=0}(k) \int_{-\infty}^{1/2k^2} d(1/2q^2) \left| U_q^F \right|^2 \\ &= \sigma^{F=0}(k) H^F(k)\end{aligned}\quad (15)$$

where $H^F(k)$ is the "modulating factor."

A numerical integration of eq. 15, for $m = 0$, gives the result shown in Figure 2.2. Note that this is an absolute cross section.

Rau and Wong point out three characteristics of the cross section. 1) Above threshold σ^F oscillates about σ^0 with an amplitude proportional to $F^{1/3}$. 2) σ^F is finite and positive at the zero field threshold with a value proportional to F . 3) σ^F decreases rapidly and monotonically below threshold.

Additionally, Rau and Wong point out that the location of maxima in the cross section is given by

$$\frac{(3\pi F n)^{2/3}}{2} \quad \text{where } n = 1, 2, 3, \dots \quad (16)$$

Simple Theory to Find Minima

A simpler approach enables us to predict the location of minima in the cross section (Bryant et al., 1987). We consider the final state of the electron simply to be that

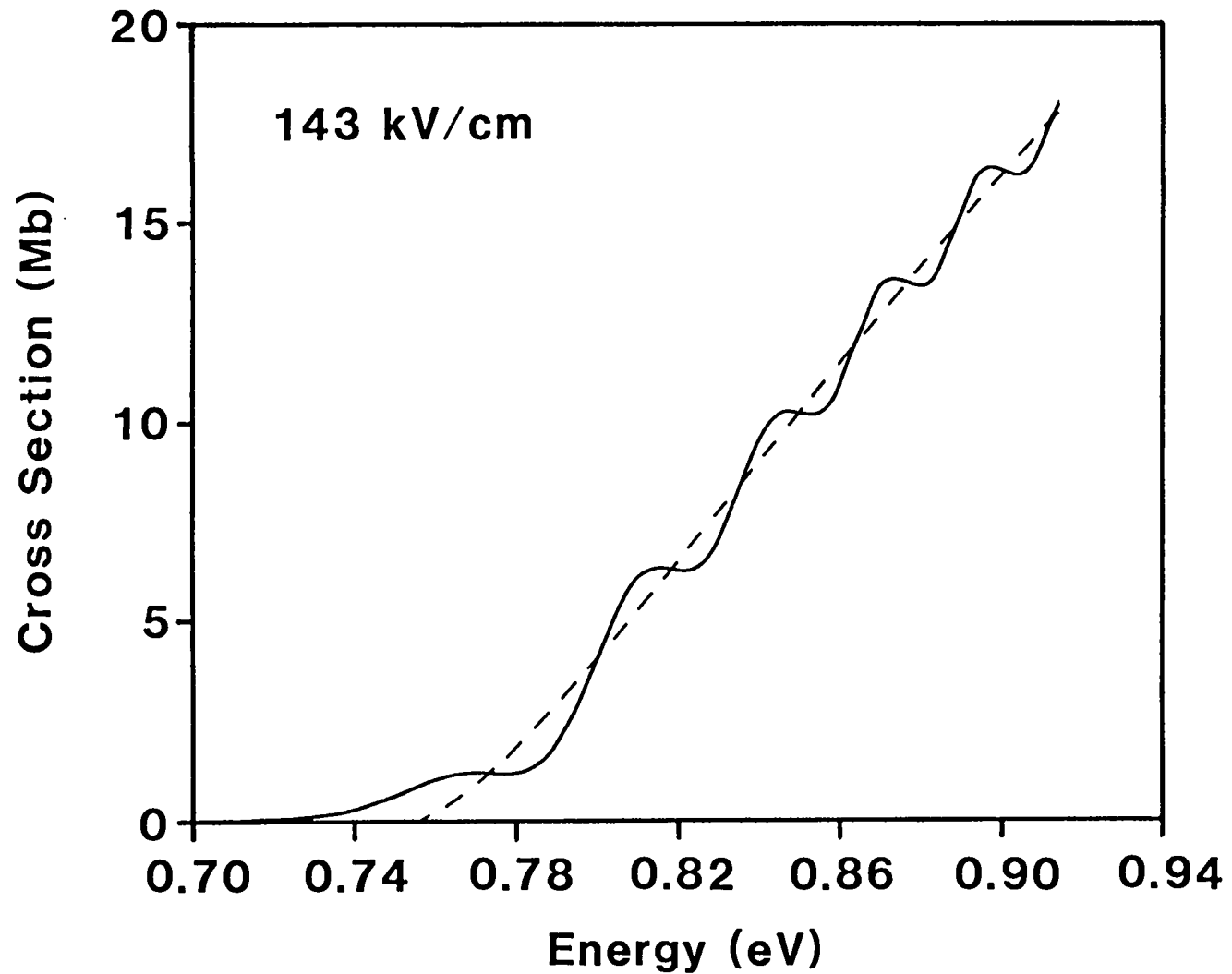


Figure 2.2 Prediction of Rau and Wong

of an electron in a d.c. field, i.e. no final state interaction. The final state wave function, $\psi(t)$, is the solution of the one dimensional Schroedinger equation:

$$\frac{\hbar^2}{2m} \frac{d^2}{dx^2} \psi + \left[E - xeF \right] \psi = 0 , \quad (17)$$

where E is the kinetic energy of the detached electron and F is the electric field. By writing

$$x = bz + E/eF , \quad (18)$$

where

$$b^3 = \hbar^2/2meF . \quad (19)$$

The equation becomes

$$\frac{d^2\psi}{dz^2} - z\psi = 0 . \quad (20)$$

Requiring ψ to vanish as $z \rightarrow \infty$, the solution is the Airy function, $Ai(z)$ (Abramowitz and Stegun 1964). The dipole matrix element between the initial state and final state is proportional to

$$\int_{-\infty}^{\infty} dx \psi^*(x) x \phi(x) , \quad (21)$$

where the initial state, $\phi(x)$, is assumed to be a symmetric function localized around $x = 0$. The integrand can be considered to be approximately an odd function when a maximum or minimum of the Airy function occurs at $x = 0$ (Figure 2.3). Then the matrix element will be a minimum. The values of z for which $Ai(z)$ is maximum or minimum are denoted a'_s where $s = 1, 2, 3, \dots$ (Abramowitz and Stegun 1964). From eq. 19 we can solve for the energy corresponding to a minimum in the cross section,

$$E = -(eF)^{2/3} \left[\frac{\hbar^2}{2m} \right]^{1/3} a'_s . \quad (22)$$

Then the photon energy required to make a transition to a minimum is E plus the electron affinity of H^- (0.7542 eV, Pekeris, 1958).

By considering how the spreading wave function of the photodetached electron reflects off of the barrier formed by the d.c. potential we can learn something about the coherence time of the process. If the time to travel to the barrier and back exceeds the coherence time of the photodetachment process, the reflected wave cannot interfere with that still emerging from the ion and we will see no ripples.

The time to travel to the classical turning point and back is given by

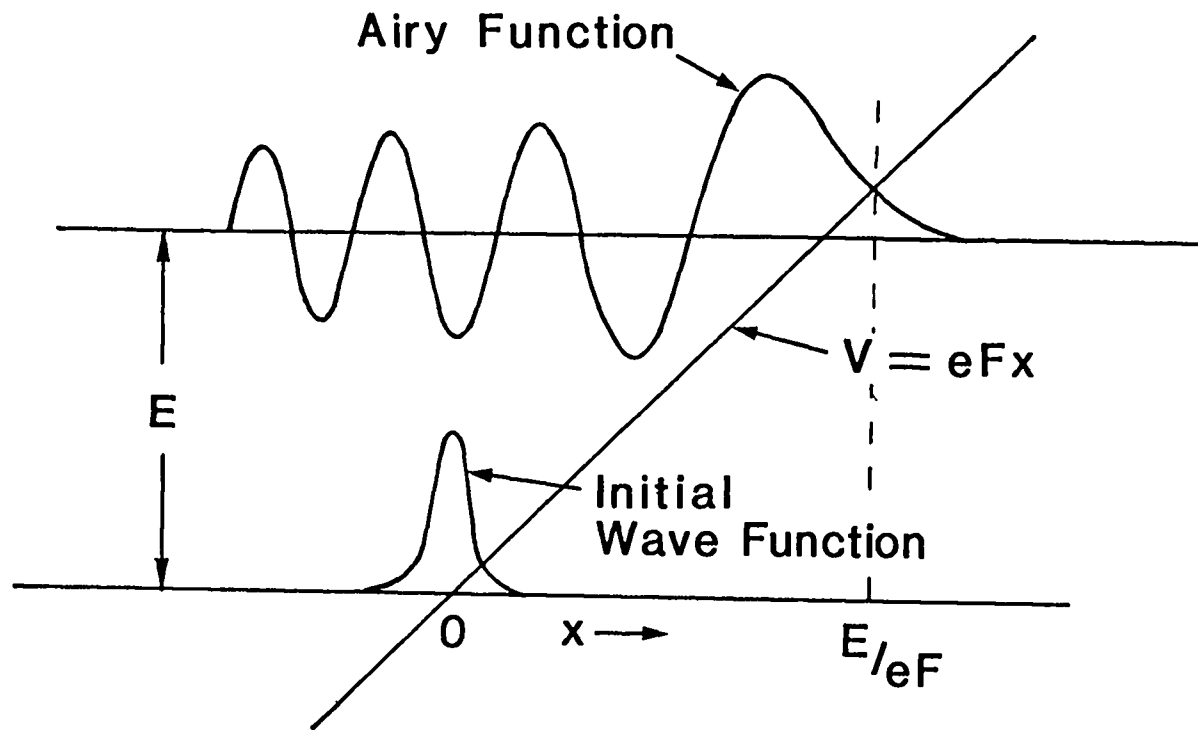


Figure 2.3 Illustration of Simple Theory. The absorbed photon causes transitions from the initial bound wave function to that of an electron in a constant electric field. E is the energy above the zero-field threshold. The classical turning point for the ejected electron in the constant field, F , is a distance E/eF from the center of the atom.

$$\tau = 2 \int_0^{E/eF} \frac{dx}{v} = \frac{\sqrt{8mE}}{eF} . \quad (23)$$

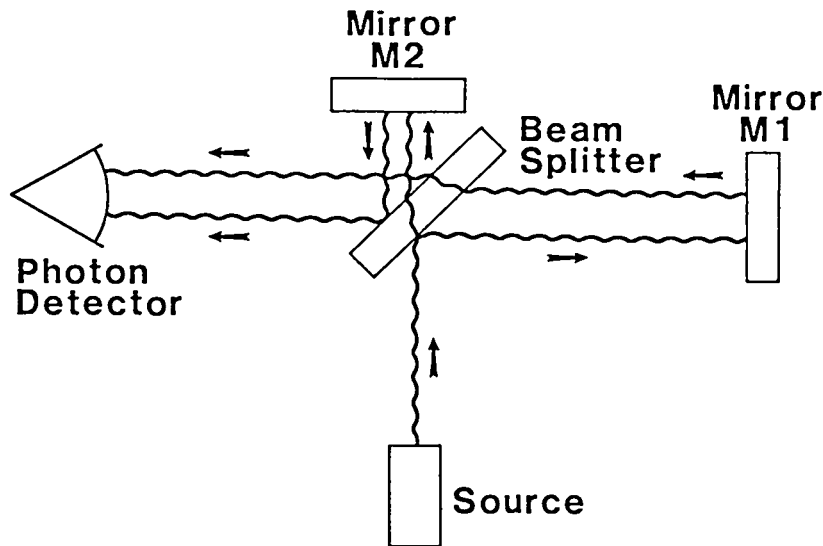
By observing the approximate energy where ripples fade away we have a measure of the coherence time and, through Heisenberg's Uncertainty Principle, a measure of experimental resolution.

Bryant (1987) has called the system an "atomic interferometer" based on this analysis. By considering an unequal arm interferometer as sketched in Figure 2.4, Bryant recovers the $F^{2/3}$ scaling for ripples that we have seen is characteristic.

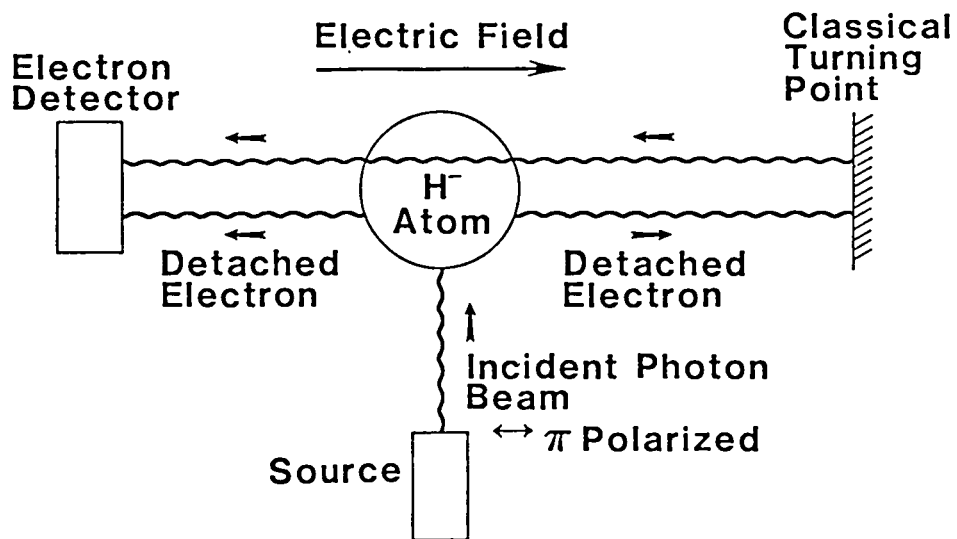
Consider an electron wave packet prepared at the beam splitter which then divides. One path is very short reflecting the wave packet promptly towards the detector and the other path is considerably longer so that that part of the packet arrives at the detector after a delay of time τ . We can write the wave packet as

$$f_1(t) = \int_{-\infty}^{\infty} e^{-\frac{(\omega-\omega_0)^2}{2s^2}} e^{i(kx-\omega t)} d\omega , \quad (24)$$

where x is along the path to the detector and s is the Gaussian energy spread. Taking the detector to be at $x = 0$ simplifies the form somewhat.



A MICHELSON INTERFEROMETER



AN ATOMIC INTERFEROMETER

Figure 2.4 H. C. Bryant's comparison of a Michelson interferometer with his "atomic interferometer."

The amplitude from the longer branch is more complicated because τ is a function of ω . Equation 23 gives the appropriate τ . Including a phase shift term to account for the transit time and the delay due to reflection at the barrier, the amplitude can be written as

$$f_2(t) = a \int_{-\infty}^{\infty} \exp\left\{-\frac{(\omega - \omega_0)^2}{2s^2} - i\left(\omega t - \frac{2}{3}\omega\tau + \Delta\right)\right\} d\omega, \quad (25)$$

where $\frac{2}{3}\omega\tau$ and Δ give the phase shifts due to transit time and delay at the barrier, respectively.

The probability amplitude for an electron to arrive at the detector at time t is

$$f(t) = f_1(t) + f_2(t). \quad (26)$$

The total probability is

$$P = \int_{-\infty}^{\infty} f^*(t) f(t) dt. \quad (27)$$

From this the cross section can be written

$$\sigma = 4\pi^{3/2} a^2 s \left[1 + e^{-\tau^2 s^2 / 9} \cos\left[\frac{2}{3}\omega_0\tau - \Delta\right] \right]. \quad (28)$$

Making the ad hoc replacement of $\sigma_0 E^{3/2}/(E+E_0)^3$ for $4\pi^{3/2} a^2 s$ to model the zero field situation, the cross section becomes

$$\sigma = \sigma_0 E^{3/2} \left[1 + e^{-\tau^2 s^2 / 9} \cos \left[\frac{2}{3} \omega_0 \tau - \Delta \right] \right] / (E+E_0)^3 . \quad (29)$$

Maxima occur when

$$\frac{2}{3} \omega_0 \tau - \Delta = (2n-1)\pi = \frac{4E}{3\hbar} \sqrt{\frac{2mE}{eF}}, \quad n = 1, 2, 3, \dots \quad (30)$$

Therefore,

$$E_{\min} = (eF)^{2/3} \left[\frac{\hbar}{2m} \right]^{1/3} \left\{ \frac{3}{4} \left[(2n-1)\pi + \Delta \right] \right\}^{2/3} . \quad (31)$$

We have recovered the $F^{2/3}$ dependence and we see that, qualitatively, we have an "atomic interferometer."

SIGMA POLARIZATION

Although we use no specific theory to describe this case we can make some assumptions about the form of the cross section. As an electrostatic potential is imposed on the binding potential of the ion, one side of that binding well will be depressed and tunneling becomes possible. In fact, even without a photon to increase the energy of the bound electron, it can still tunnel out if an electric field has depressed the barrier. We expect

then to see, in an electric field, an exponential decrease in the cross section below the zero field threshold.

We can define a classical threshold in an electric field. It is simply the energy needed to raise the electron up to the now depressed top of the well. But, as seen above we must add to this the effect of tunneling. As the kinetic energy of the ejected electron is increased the details of the potential at threshold must become less and less important so that we expect the cross section to approach that of zero field.

A simple characterization of the potential is

$$V(z) = - ezF - 1/2 \frac{\alpha e^2}{(r + r_p)^4} \quad (32)$$

(Delone et al., 1985), where α is the polarizability of the atom and $r_p = 0.583a_0$ (Schiff, 1968). We can use this to make a rough calculation of the classical threshold for comparison to the experimental result.

Rau and Wong's (1987) work accomodates σ polarization as well as π . Equation 14 includes an $m \pm 1$ result which is the σ polarization case. We became aware of this work too late to include a comprehensive analysis in this paper.

CHAPTER 3: APPARATUS AND EXPERIMENTAL TECHNIQUE

OVERVIEW OF EXPERIMENT

The experimental setup was simple in concept and can be understood by reference to Figures 3.1, 3.2 and 3.3. Figure 3.1 shows a large scale view of the experiment as set up for the 318 MeV run in 1986. Several pieces of equipment are shown which played no role in these experiments. These are: polarimeter, foil box, fluorescent well, and the Rydberg well.

Figure 3.2 shows the vertical benders detection scheme and Figure 3.3 shows the electron spectrometer scheme. The vertical bender scheme was used in 1985 and for the bulk of the 1986 data. The electron spectrometer was used for a small portion of the 1986 experiment. The changes to different detection schemes were small variations on the large scale setup, so Figure 3.1 serves as a reasonable descriptor of all cases. The H^- beam entered the scattering chamber where it was intersected by light at 1.06 microns from our Nd:YAG laser. The photon energy as seen by the H^- particles was dependent on the angle of intersection and is given by the Doppler formula, equation 1.

The products of the interaction were then detected downstream using one of two methods. In the first and most commonly used method, the different charge states

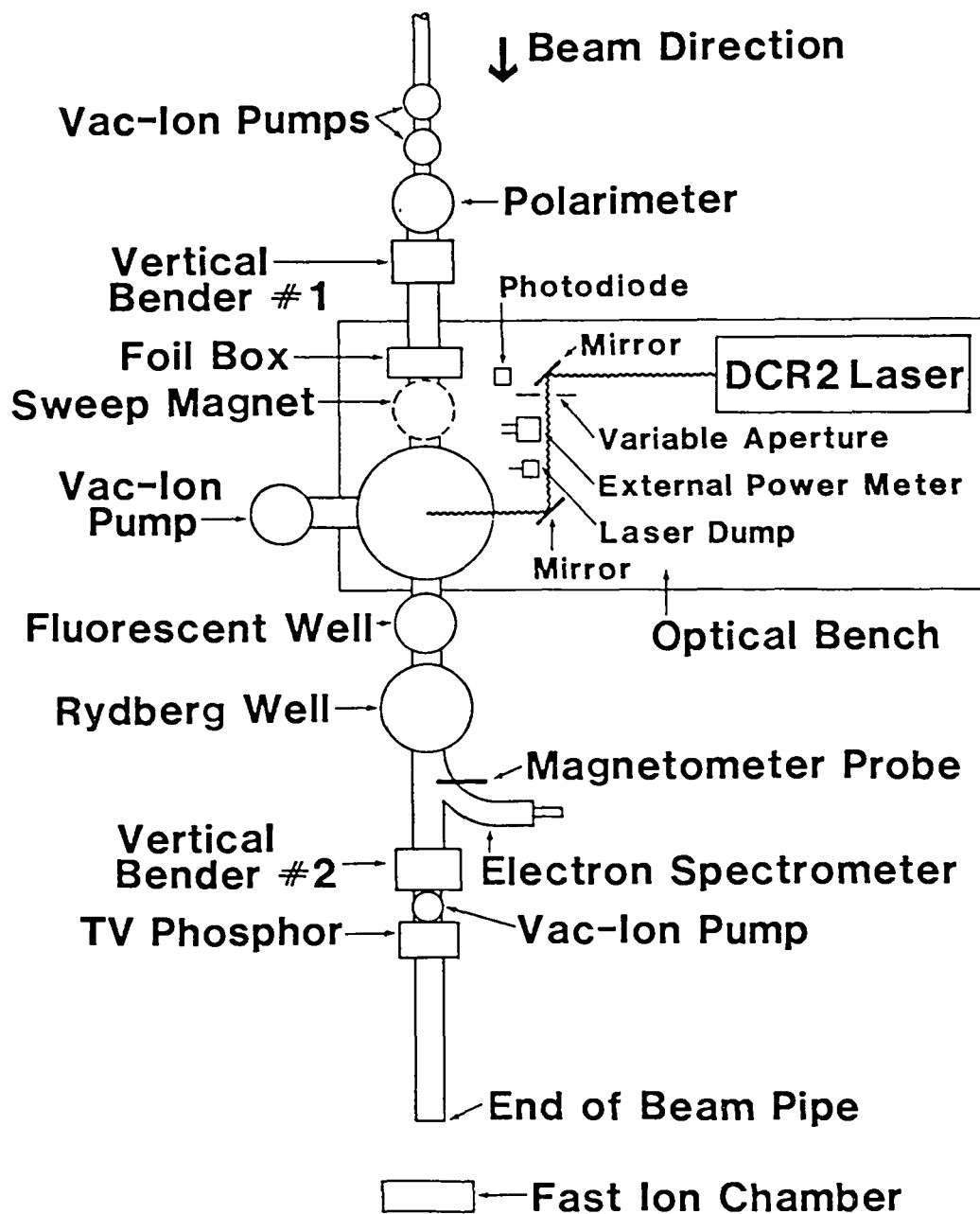
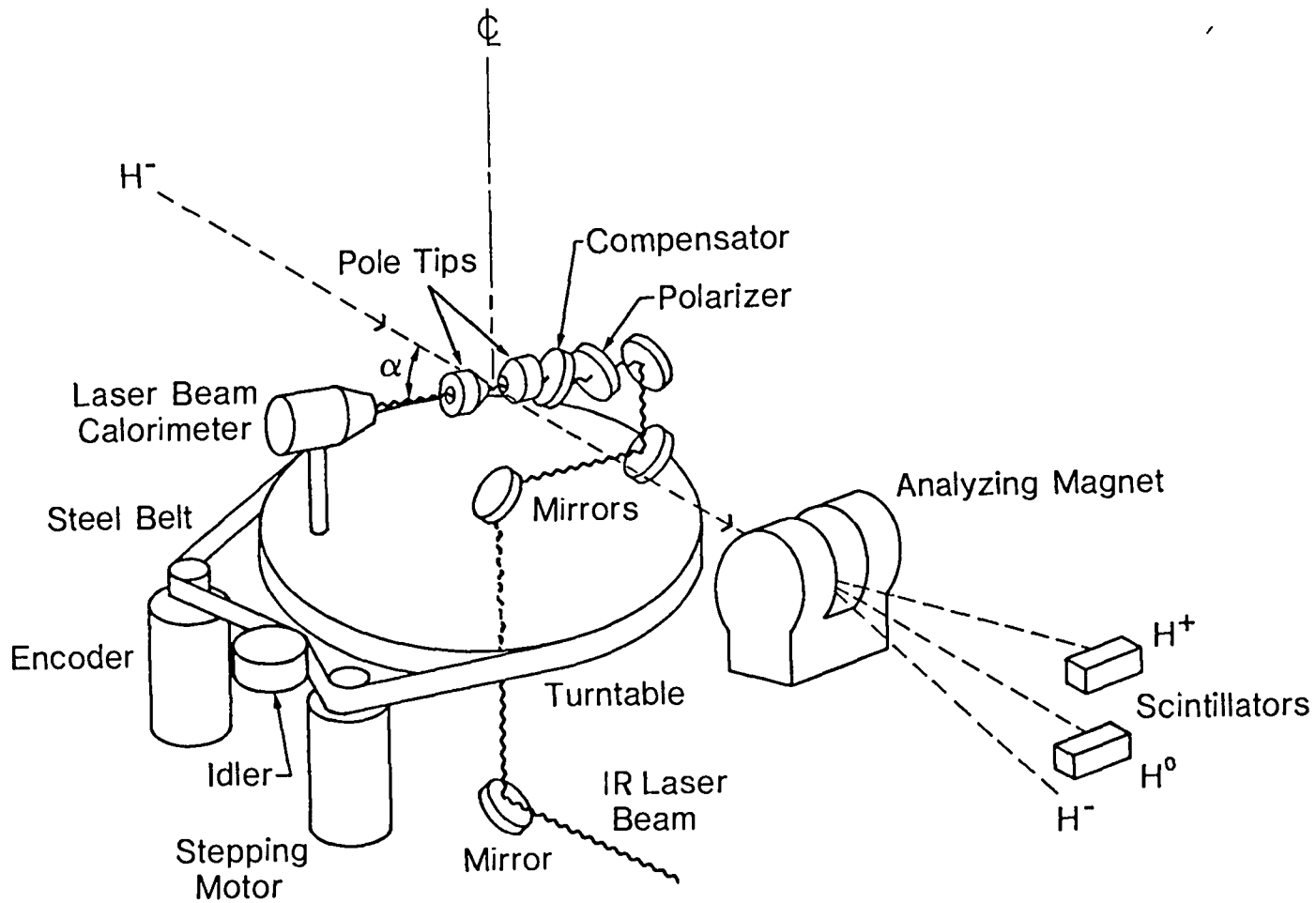
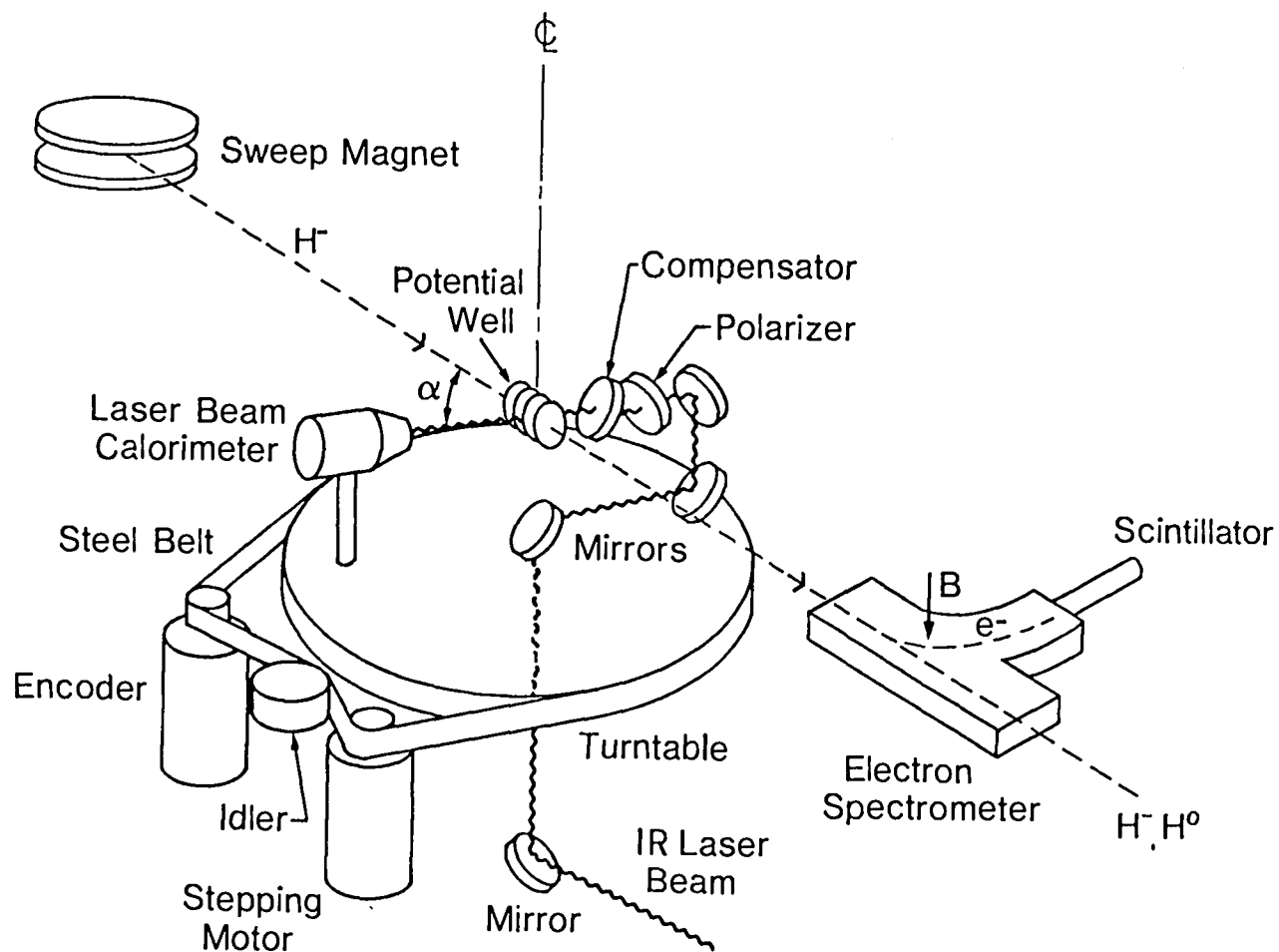


Figure 3.1 Layout of the experiment, 1986.



SCHEMATIC OF LAMPF PHOTODETACHMENT APPARATUS

Figure 3.2 Schematic of LAMPF photodetachment apparatus, 1986 electromagnet in place.



SCHEMATIC OF LAMPF PHOTODETACHMENT APPARATUS

Figure 3.3 Schematic of LAMPF photodetachment apparatus, 1986 potential well in place.

were magnetically separated and then the neutral products of the process were detected in a scintillator. In the second method the electron resulting from the photodetachment process was separated in an electron spectrometer and detected by a scintillator. In this case we could distinguish electrons tagged with an energy difference of as little as 5 keV and so were able to discriminate against background electrons.

We also monitored the ion current and the laser intensity.

H MINUS PARTICLE BEAM

LAMPF can deliver H^- ions with an energy of up to 800 MeV corresponding to a velocity of $0.84c$. The accelerator runs at a nominal 120 Hz although we took only 40 pulses per second and could use only 10 of those due to the laser repetition rate. Each macropulse of about 700 microseconds contained micropulses which were about 0.25 nanoseconds wide and separated by 5 nanoseconds. We normally ran with a current of about one nanoamp; hence, each micropulse contained some 10^3 particles.

The accelerator exists primarily to do meson physics and accelerates protons for this purpose. The H^- ion is accelerated on the second half of the RF cycle used for protons. The accelerator is tuned to provide maximum stability and current for protons; hence, the

characteristics of the H^- beam are often less than optimum. Additionally, most of our run time in 1987 was officially 'development.' Our status was such that we had to make do with the beam tuning required by another experiment on an adjacent beam line.

Local tuning of the beam was accomplished with two quadrupole magnets and an adjustable stripper aperture. These devices were under control of technicians in the Central Control Room (CCR) with whom we communicated by telephone. For a consistent, steady beam it was necessary for the beam to be centered very well on the stripper, which required constant monitoring by the CCR personnel. Our experiment was perhaps the most sensitive to beam tune at the accelerator.

We used a cylindrical lens to focus the laser beam in the vertical direction to attempt to improve the overlap between beam and laser. With the laser focused to overlap precisely the approximately 1 millimeter diameter particle beam, we soon discovered ripples in our data similar to those predicted by Reinhardt. On careful examination we found that we were sensitive to a slight change in the tune of the beam when the polarization of the proton in the ion was changed at the ion source on a two minute cycle. This was a requirement for other experiments. A small vertical movement in the beam changed the overlap of laser and particle beam so that we saw "beam bumps" in our

data. Very careful tuning of the beam in our experimental area could eliminate the beam bumps temporarily, but the ultimate solution was to replace the lens with one of longer focal length so that the laser beam was about two millimeters high to the particle beam's one millimeter. Then we were not sensitive to small vertical movements of the beam. We did run for a time taking data for only one half the cycle.

Monitoring of beam current was not done with a calibrated Faraday cup as in the past. The Faraday cup in the beam stop was inoperative, apparently due to damage during the major construction that was in progress in the area.

We used instead a fast (~ 10 microseconds) ion chamber to give relative beam currents. The ion chamber was pressurized with hydrogen gas. When a charged particle passed through the gas, the hydrogen was ionized and the electrons were attracted to a charged plate and the current was measured. A current-to-voltage preamplifier fed an amplifier in the counting house. This signal was then fed into a CAMAC ADC (Analog-to-Digital Converter) where it was digitized and subsequently recorded on magnetic tape. The signal was also sent to a preset NIM scaler which determined how long we ran at each angle. This scaler was preset to a certain value and when that

number of beam counts was reached the apparatus stepped to a new angle and started the cycle again.

We also recorded a signal provided by CCR from a slow (~1 sec.) ion chamber.

Nd:YAG LASER

As in past years we used a Quanta-Ray DCR-2, Nd:YAG laser which we had overhauled by a Spectra Physics technician immediately prior to the summer runs. We used the fundamental wavelength of 1.064 μm . The tuned up laser running at 10 hertz put out an average power of 11 watts implying greater than one joule per pulse. A photon energy of 1.16 eV gives 5×10^{18} photons per pulse.

In past experiments we have used the laser in the Q-switched mode with a pulse width of ~8 nsecs and, due to jitter in the laser firing circuits comparable to the spacing of the H^- micropulses, the laser has been fired randomly into a macropulse giving a random overlap with any given micropulse. This technique gives high power densities and extremely low background counts. However, it requires relatively precise timing of detector circuits and may even saturate the micropulse. In 1986 we decided to try using the same laser in non-Q-switched mode. We simplified timing at the expense of additional background. The laser pulse was now ~100 micro secs, so, with roughly the same number of photons, our detector gates had to be

open about 10^4 times as long as with the Q-switched mode. This change also eliminated our concern about saturating the H^- beam or the detector.

We monitored the laser intensity in two places, one, a fast photodiode on the laser table and the other a Scientech calorimeter inside the scattering chamber immediately after the interaction region. The photodiode easily resolved structure within the 100 microsecond laser pulse. The calorimeter integrates the signal over a period of about ten seconds. The photodiode signal was recorded on the data tape. The calorimeter signal was recorded in the log book several times during each run.

Because the length of time we took data at each angle was determined by the total amount of H^- that passed through the chamber, a low beam current resulted in a large number of photons being counted at a given angle. There were occasional circumstances where the beam current could drop to essentially zero but we would still be counting photons.

A more appropriate measure was the rate at which photons crossed the interaction region. In 1986, after run 307, we set up the Q software so that an approximate rate was available by recording the time spent at each angle.

In the final analysis, we found that there were wide fluctuations in the photon current as measured by the

photodiode which were not consistent with the observations of the calorimeter readings which remained very constant over time. So, in 1986, the data was not normalized to photon current. We made the assumption based on an analysis of both the calorimeter and the photodiode data that we introduced less error by not explicitly including the laser normalization.

The mirrors used to transport the laser light to the interaction region were dielectric mirrors, manufactured by Airtron, and coated for greater than 99% reflectivity.

VACUUM

A common vacuum must be maintained over the entire 800 meter length of the accelerator and the various branches and experimental areas. Our experiment was served locally by four vacuum-ion pumps: two approximately two meters upstream of the interaction region; one on the scattering chamber itself; and one about two meters downstream. The principal source of background was collisions with the residual gas particles in the beam line. We were normally able to maintain a vacuum of 10^{-7} Torr. Any improvement in vacuum leads to a reduction of background.

Historically, we have been able to achieve vacuum at least an order of magnitude better. Our poor showing on this account is probably due to two factors. The heating of the coils of the electromagnet must have caused some

outgassing and, secondly, we were probably not as careful as we might have been to keep things clean when assembling the apparatus.

We burned out our vacuum gauge early on and had to rely on an indirect measurement - the current drawn by the ion pumps attached to the scattering chamber.

SCATTERING CHAMBER

The heart of the scattering chamber was the stepper-spider-encoder assembly. The stepping motor was controlled from the counting house and rotated the mirror assembly (known as the spider) inside the chamber changing the angle of intersection of the laser with the H^- beam. The 14-bit optical encoder returned to the counting house an absolute angle.

Laser light passed through a window at the bottom of the chamber and then was reflected around three dielectric mirrors to intersect with the H^- beam. This was tricky business. The point of intersection had to remain constant so that we could be certain the interaction was taking place in the carefully controlled environment that we prepared. Additionally, if the laser entered the chamber at any angle other than exactly normal to the entry window and if there was any misalignment of the mirrors mounted in the spider, there could be substantial error in the true angle of intersection of laser with

particle beam which in turn determined the true energy of the photon in the barycentric frame. The result of a calculation assuming misalignment at the entry window of 1 mrad and misalignment of the three mirrors on the spider of 1 mrad is shown in Figure 3.4 (Harris, 1987). Unfortunately, we have no way of measuring the magnitude of this error which certainly must have existed.

The spider was belt driven with a stepping motor which was controlled from the equipment trailer. The belt was often a weak link in the system. Since we desired to measure precisely small angles, the belt drive should have small thermal expansion and should not stretch appreciably. We have used belts made from high carbon shim stock which have been soldered with a lap joint to form a belt. If the joint was weak or if it was subjected to much flexing as it drove the spider it might break, shutting down the experiment for about 12 hours while we broke vacuum and installed a new one.

For the runs in 1986 we found a stainless steel material which could be fabricated with a butt joint using a laser welding process. This proved to be very satisfactory. We experienced no breaks in the hundreds of hours we ran.

The 14 bit optical encoder was used to determine the angle of intersection. The 14 bits yield 2^{14} or 16,384 steps per revolution of the encoder. The system is

ERROR DUE TO MISALIGNMENT OF LASER

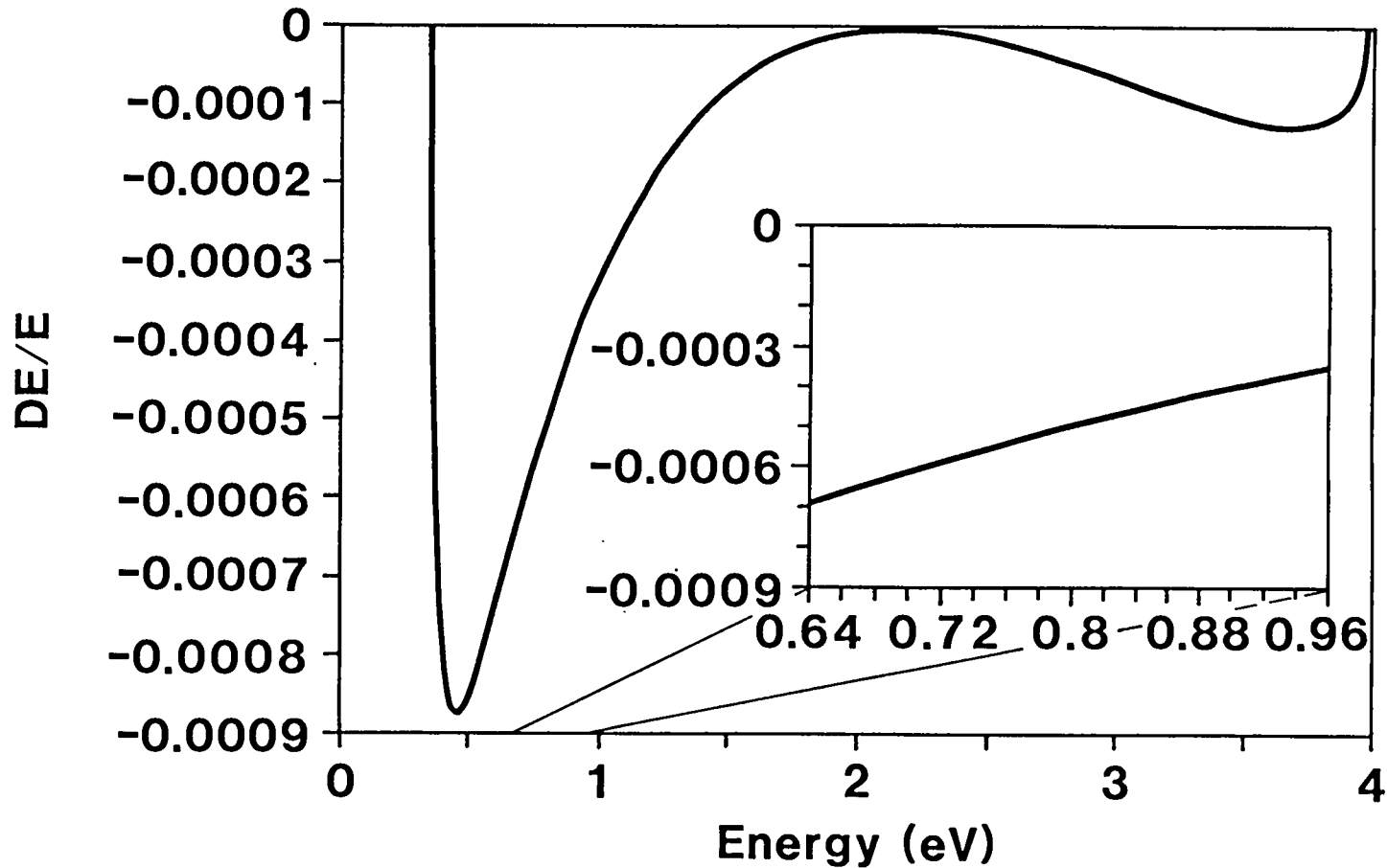


Figure 3.4 Error due to misalignment of laser. Shows possible error due to misalignment as spider is rotated 180 degrees. The angle scale has been converted to energy. The energy range for these experiments has been expanded.

designed so that the encoder makes approximately 12.5 revolutions for one revolution of the spider. A potentiometer keeps track of which of twelve sectors we are operating in. In this experiment we looked at a fairly narrow range of angles so the sector measurement was not particularly important.

The encoder was also belt driven from the spider table. Prior to the 1986 runs the bearings in the system were replaced with the exception of that on the encoder drive - a mistake.

During the runs we noticed that when we used very small steps the encoder reading might stay constant through a step or two or even appear to reverse direction. After the fact, when we dismantled the apparatus, we found that bearings both in the external shaft which drove the encoder and in the encoder itself were bad, causing jerky movements which must have been the source of the problems noted during the run.

METHODS TO GENERATE ELECTRIC FIELD

We used three methods to impose an electrostatic field onto the interaction region in this experiment. Most of our field measurements were taken using one of two electromagnets. In 1985 we used an electromagnet which imposed a constant field normal to the plane of the H^- beam and laser beam.

In 1986 most of our field measurements were taken using an electromagnet with holes through the pole tips to allow the laser beam to pass through, Figure 3.5. This put the constant field in the same plane as the ion and laser beams. The magnet was mounted on the laser table and thus rotated with the laser beam. Because the electric field seen by the ion is dependent on the angle between the velocity vector and the magnetic field vector the electric field changed as the angle of the laser changed.

It was necessary to put the laser through the pole tips in order to accomplish polarization of the laser light parallel to the barycentric electric field. When using the electromagnets we detected the neutral hydrogen product of the photodetachment in a scintillator downstream.

The pole tips of the 1986 magnet were so small that they saturated with a current of about 1 amp in the coil, as can be seen from Figure 3.6 which shows the magnetic field against current. We began the runs with the small pole tips but immediately asked the machine shop to make a set of larger ones. The magnet still saturated at about one amp, but we were able to increase the maximum field by a factor of about two.

Another problem with the magnet was how to keep it cool. We had 300 turns of 1/16" square copper wire which

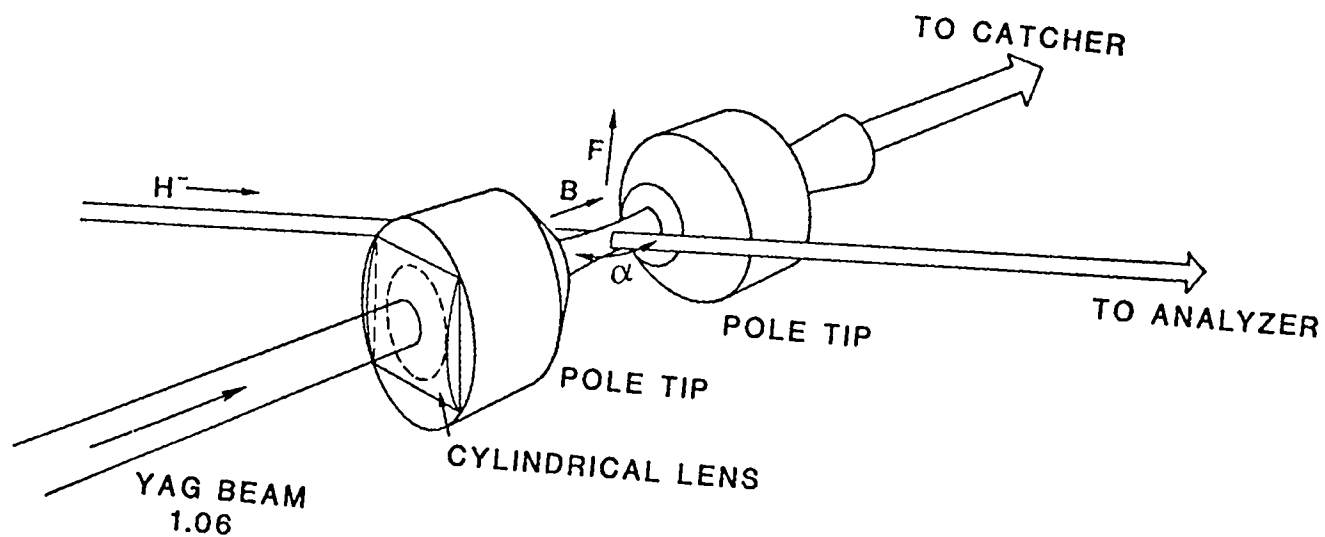


Figure 3.5 Schematic of interaction region with electromagnet. The magnetic field, B , is kept parallel to the laser direction so that states for which the laser light is pure pi or sigma in the center-of-mass system can be prepared.

Magnetic Field vs. Current

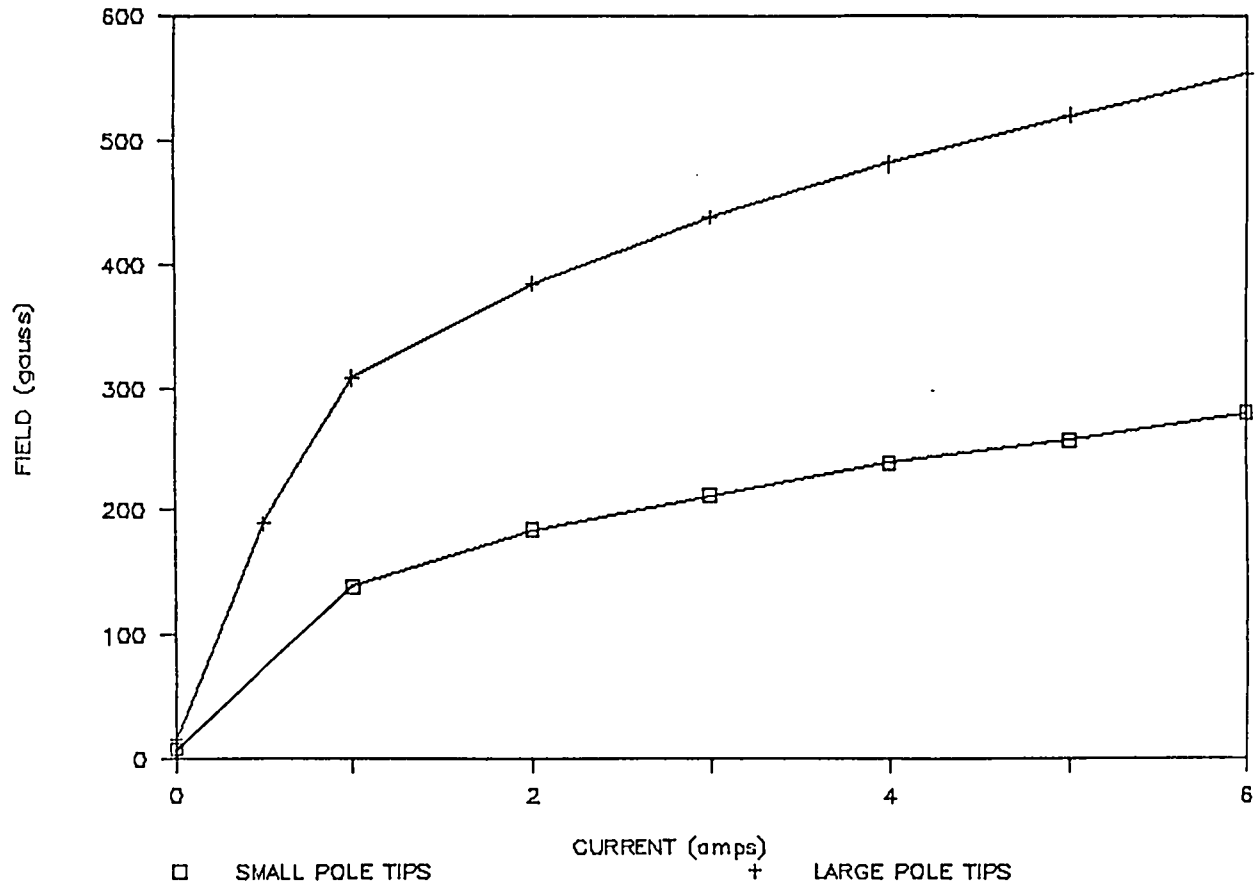
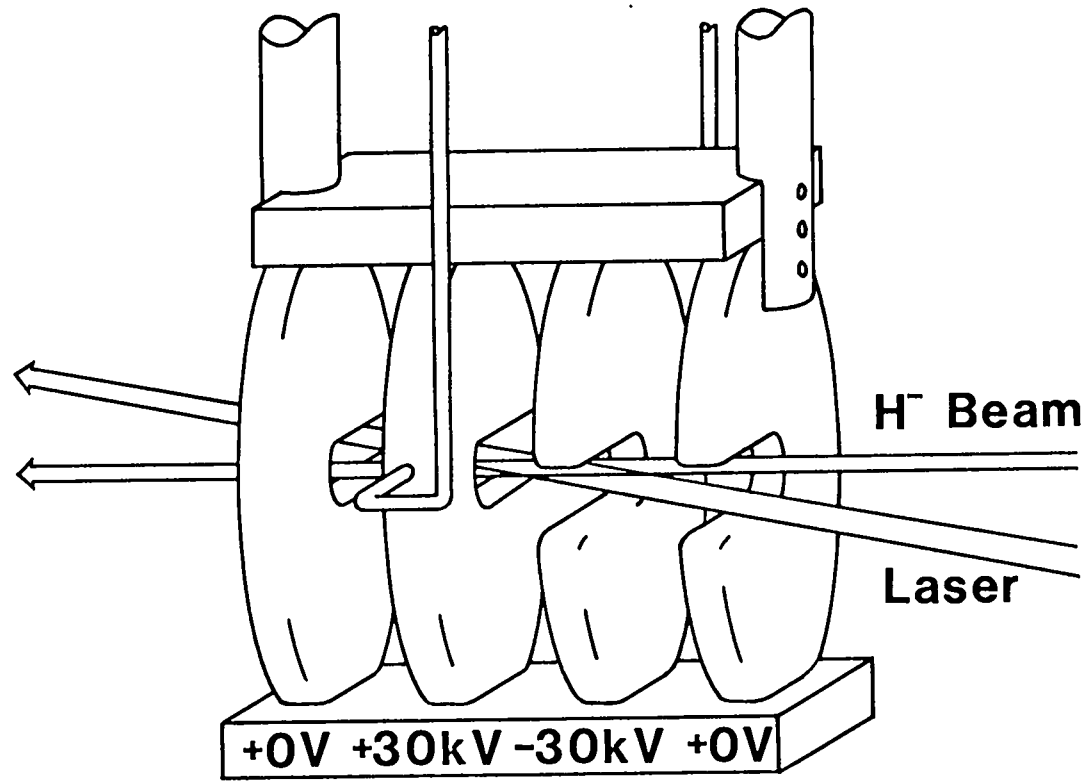


Figure 3.6 Magnetic field of magnets used in 1986.

carried a current of as much as 6 amps. With time and money both short we had Tom Feldman of Energy Engineering, 4616 McLeod Rd., Albuquerque, NM, design a heat pipe which ran through the center of the coil to carry off the heat. The heat pipe projected through a ferro-fluidic vacuum feedthrough on the top of the scattering chamber. Water was circulated through a jacket which surrounded the external portion of the heat pipe.

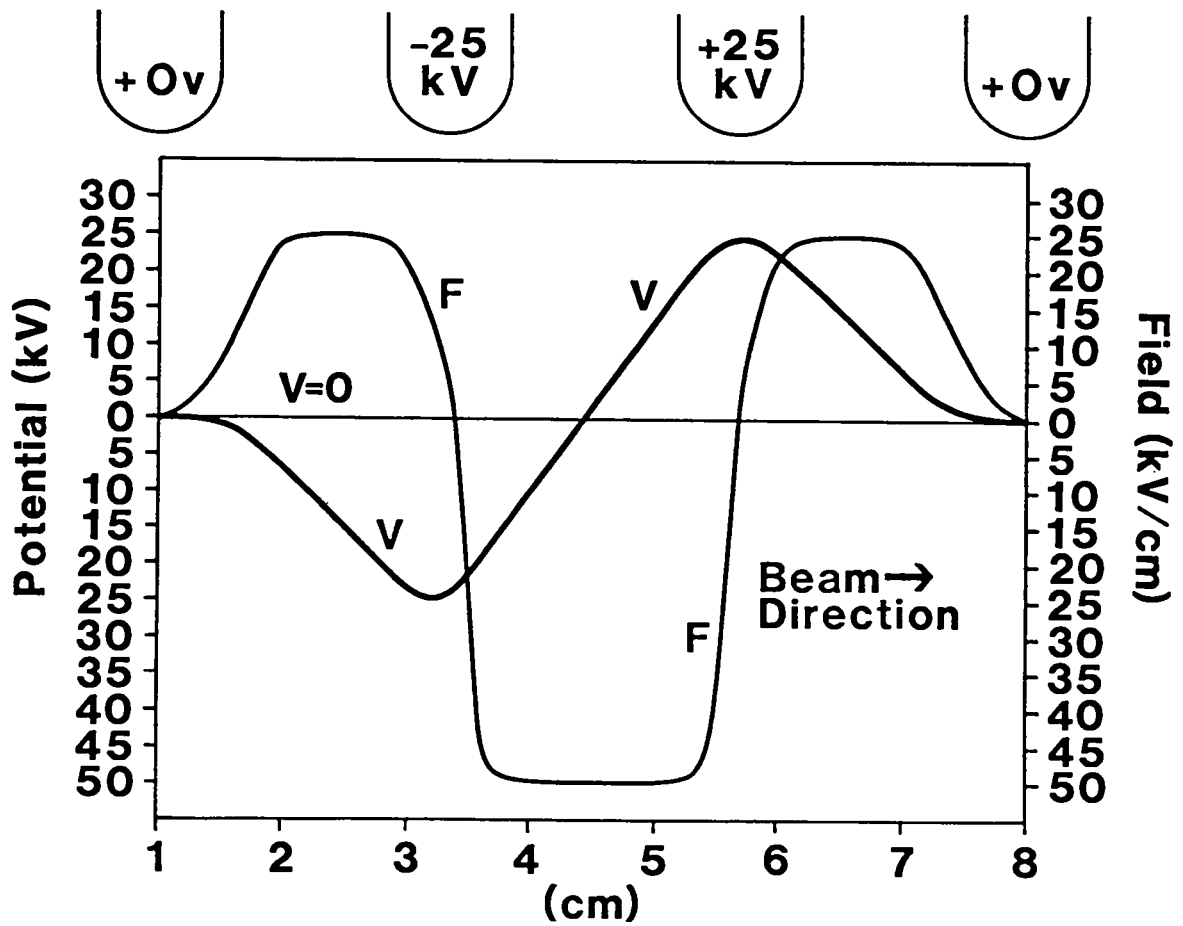
The system worked well up to 4 amps, but when the current was increased to 6 amps, we could see a steady rise in the background level as the heat caused outgassing from the insulation on the wire, which in turn increased the background through collisions with the gas.

The third method of generating a field was to impose directly an electric field in the laboratory frame using a "potential well," Figure 3.7. With the potential well we detected photodetached electrons that were tagged with a distinct energy depending on the place in the well where they were detached. The electron spectrometer designed for the experiment was then used downstream to look at these tagged electrons. Figure 3.8 shows how the potential well can tag a photodetachment electron with an energy distinct from the background electrons. An electron which existed in the beam in a free state before reaching the well passed through with no net change in energy. An electron which was freed through the



POTENTIAL WELL

Figure 3.7 Schematic of the interaction region with potential well



ENERGY TAGGING IN POTENTIAL WELL

Figure 3.8 A qualitative picture of energy tagging. The dark curve gives the additional energy acquired by an electron released at a given point. The lighter curve, F, gives electric field.

photodetachment process between the center plates could emerge with an additional energy which could be read from the potential curve in Figure 3.8. The additional energy would then give a unique trajectory in the spectrometer.

We had hoped to accomplish a field of 60 kV/cm using the well but never managed more than 50 kV/cm. When we first energized the well one of the power supplies self destructed at 20 kV/cm. It turned out that the protection circuitry was not adequate. We installed our own protection circuit which proved adequate up to 50 kV/cm once we wrapped an anticorona putty about the assembly.

Conceptually, the well is a workable idea but in practice there were other problems. The biggest problem seems to be the fact that our laser beam overlapped such a wide area within the well that we did not get the distinct tagging that we needed because the field changed substantially in the width of the laser beam. While the laser can be focused in the vertical dimension with little effect on the energy resolution, focusing in the horizontal dimension would destroy our angular resolution. In order to make use of the well for this experiment we would have to send the laser beam through a small aperture so that the interaction took place at a well defined location within the well. Another fix might be to scale up the well so that there is a uniform field over the width of the laser beam.

LASER POLARIZATION

The experiment required that we be able to polarize the light either normal to or parallel to the d.c. electric field. The laser light was polarized and there was a 1/2 wave plate in the laser that could be used to rotate the polarization, but a moment's thought leads us to the realization that once the light was reflected from five or six mirrors, three of which were rotated with respect to the rest, the initial polarization would be lost. We were forced to polarize the light inside the chamber as a final step before the interaction.

A schematic of our polarizer is shown in Figure 3.9. The effect of two polarizing plates, both at Brewster's angle, is to compensate one another for the spatial shift in the laser beam induced by a single plate and to improve the purity of polarization. The polarizer could be rotated 90° about the optical axis by means of a flipper attached to the wall of the scattering chamber. Both plates were coated so that the polarization was almost 100%.

Because the polarizer worked by reflecting light of the undesired polarization and transmitting the rest we could lose a substantial amount of power depending on the details. In the worst case the calorimeter which measured maximum power of 11 watts on the table with the laser

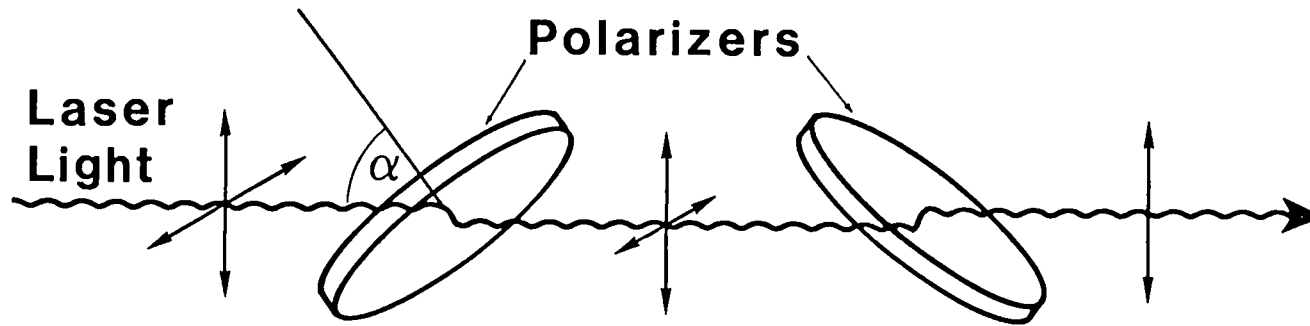


Figure 3.9

SCHEMATIC OF POLARIZER
 α is Brewster's Angle for $1.06\mu\text{m}$.

Q-switched read about 2.5 watts in the chamber during the experiment.

In 1985 the magnetic field imposed on the interaction region was normal to the laser, H^- plane so the motional electric field lay in that same plane and perpendicular to the H^- beam. Because near the Doppler free angle the laser beam appeared to the H^- to be near 90° the laser was effectively σ polarized no matter what the position of the polarizer.

In 1986, however, the magnetic field was imposed parallel to the laser beam. That gave an electric field normal to the H^- , laser plane. In this case, if the laser light was polarized normal to the H^- , laser plane, then it would be pure π polarized and if it was polarized in the plane with the laser beam effectively at 90° the light would be predominately σ polarized.

DETECTION OF PARTICLES

In 1985, with the laser in the Q-switched mode, we expected frequently to record more than one photodetachment as a result of the approximately 8 ns laser pulse. We could not distinguish separate events in such a brief period of time but the scintillator gave a larger pulse if more than one atom struck it in that time frame. In this case the signal was sent to an ADC, where we saw distinct peaks corresponding to one, two, three,

etc. atoms striking the scintillator. This information had to be decoded to determine the yield of a particular event.

In 1986, with the laser pulse spread over about 100 μ s, there was essentially no chance of more than one electron striking the scintillator within the recovery time of the device so that we could use the scintillator as a simple counter.

ELECTRON SPECTROMETER

The spectrometer was designed to be used in conjunction with the potential well. The substantial background of electrons produced in collisions with residual gas in the beam line could be reduced by arranging the photodetachment to occur in the potential well which tagged the signal electrons with an additional energy ranging from five to ten kV. Thus, a slightly different trajectory in the spectrometer allowed the signal electrons to be separated from the background.

The spectrometer was used as well with other experiments which are important to this discussion because they helped determine its energy resolution. In one experiment the H-minus beam was stripped in a thin foil (15, 30, or 45 micrograms/cm²) leaving a beam of neutral hydrogen with some population of excited states. Rydberg (high n) states were then field stripped in the

transformed electric field, F , of the spectrometer, where $F = \gamma\beta cB$, in SI units. Higher states ($n = 15$ and up in the case of an 800 MeV primary beam and $n = 26$ and up for 318 MeV), were stripped promptly and followed essentially the same trajectory in the magnet as the gas stripped electrons. Lower states were longer lived in the electric field, ionizing at some point well inside the spectrometer and, hence, following a trajectory of apparently higher energy particles. At 800 MeV states were seen as low as $n = 11$ and at 318 MeV $n = 14$. We saw, then, distinct peaks corresponding to specific Rydberg states as we varied the magnetic field strength.

In a variation of this experiment a weak magnetic field immediately downstream of the foil swept electrons and field stripped $n = 11$ and up. Then our laser was used to promote electrons from say, $n = 4$, to 11 or higher depending on the angle of intersection of the laser beam with the particle beam. We could then detect high states in the same manner as before.

We could also detect higher states by field-ionizing them in an electrostatic well which would label those electrons with an additional energy to separate them from background electrons in the spectrometer.

The principal design criterion for the spectrometer was that it be able to separate electrons tagged with 10 keV more energy than the background, gas-stripped

electrons. We assumed that our signal electron was photodetached or field ionized with negligible kinetic energy in the rest frame of the LAMPF beam. Considering an 800 MeV ($\beta = 0.842$) primary beam of H^- ions, a photodetached electron would have a kinetic energy of 436 keV. If we could tag that photodetached electron so that it had 446 keV, then the spectrometer had to be able to separate those two energies into two distinguishable peaks.

A 318 MeV ($\beta = 0.665$) primary beam yielded 176 keV photodetached electrons. In this case we wanted to be able to distinguish between 176 and 186 keV electrons.

If we consider the force equation,

$$\vec{F} = (qc)\vec{\beta} \times \vec{B}, \quad (33)$$

and assume a magnetic field which is everywhere homogeneous and normal to the trajectory of the electron we find that the radius of curvature,

$$\rho = |\vec{P}|/q|\vec{B}|. \quad (34)$$

From this a few simple conclusions can be made. If two particles with different momenta enter a magnetic field from the same initial drift trajectory they will be bent in circular orbits with different radii so that a bend of 180° will give the greatest separation between the

two particles (Figure 3.10). From $dp = \rho dP/P$ we find that, for a given momentum spread, a larger radius yields greater dispersion.

Clearly, then, we want to use the largest radius that is convenient but we note that for a particle beam of finite diameter (roughly one to two millimeters for our H minus beam) the particles we wish to detect are not focused as they leave the magnetic field. We would like to arrange a focus at some reasonable distance downstream where we can locate a detector.

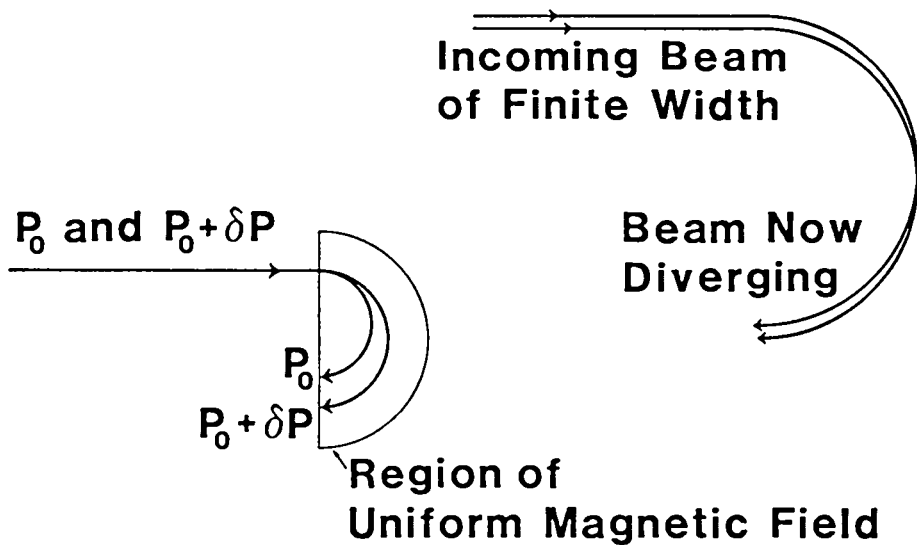


Figure 3.10. Simple Trajectories. A. Maximum separation occurs with a bend of 180° . B. Beam of finite width focuses at 90° and is then diverging.

We assume that the particle trajectory can be described by equations of the form (Steffan, 1965):

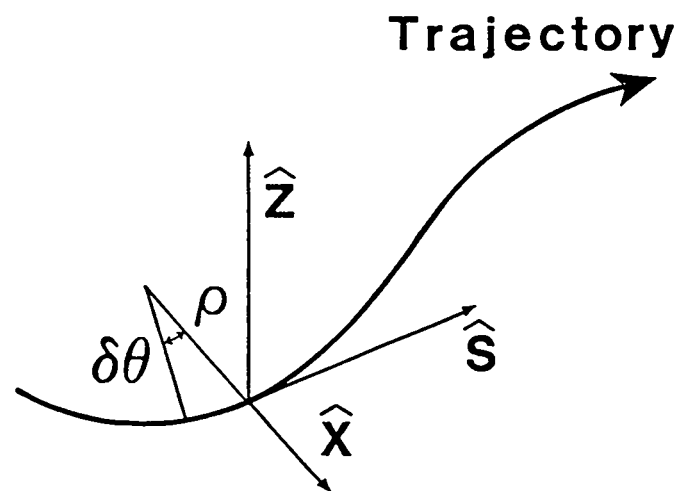
$$\frac{d^2u}{ds^2} + f(s)u = 0 \quad \text{with solutions:}$$

$$\begin{pmatrix} x \\ x' \end{pmatrix}_\ell = \begin{pmatrix} \cos \theta & \rho \sin \theta \\ -\frac{\sin \theta}{\rho} & \cos \theta \end{pmatrix} \begin{pmatrix} x \\ x' \end{pmatrix}_0 + \begin{pmatrix} \rho_0(1 - \cos \theta) \\ \sin \theta \end{pmatrix} \frac{\Delta P}{P_0} \quad (35a)$$

$$\begin{pmatrix} z \\ z' \end{pmatrix}_\ell = \begin{pmatrix} 1 & \rho \theta \\ 0 & 1 \end{pmatrix} \begin{pmatrix} z \\ z' \end{pmatrix}_0, \quad (35b)$$

where ρ is the radius of curvature of the trajectory, θ is the angle through which the trajectory is bent (Figure 3.11), x and x' are respectively, the halfwidth of the beam and its divergence, z and z' similarly; and $\Delta P/P_0$ is the momentum bite.

Consider, first, motion in the x -plane. We assume that the field is homogeneous throughout. The 'hard edged' model assumes further that the field starts abruptly at some point before the physical edge of the magnet - giving an effective length somewhat greater than the physical length. The effective length is dependent on the gap between the poles of the magnet. A standard rule-of-thumb adds to the physical length one half the gap width. Or, given the field map which we have after the



COORDINATE SYSTEM FOR CALCULATING TRAJECTORIES

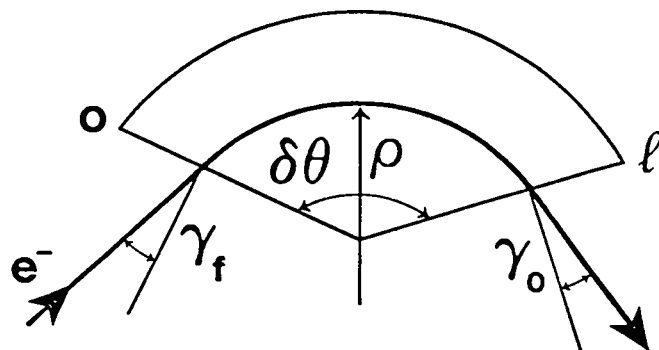


Figure 3.11

fact, the effective length can be calculated from

$$L_{\text{eff}} = \int B dl / B_{\text{max}} . \quad (36)$$

If we assume that $\theta = \pi$ then, from eq. 34a, $x_1(s) = -x_0 + 2\rho P/P_0$. We see that the initial width of the beam is recovered at the exit, if $dP/P = 0$, and we have maximum dispersion. But, as we have seen, the beam is diverging and will be relatively large at some downstream detector. By inclining the entry and exit faces of the magnet to the particle's trajectory we can focus the beam beyond the exit of the magnet. Simple geometric considerations give solutions for arbitrary entry and exit angles:

$$\begin{bmatrix} x \\ x' \end{bmatrix}_\ell = \begin{bmatrix} 1 & 0 \\ -\tan \gamma_f & 1 \\ \frac{\rho}{\rho} & 1 \end{bmatrix} \begin{bmatrix} \cos \theta & \rho \sin \theta \\ -\sin \theta & \cos \theta \\ \frac{\rho}{\rho} & \cos \theta \end{bmatrix} \begin{bmatrix} 1 & 0 \\ -\tan \gamma_0 & 1 \\ \frac{\rho}{\rho} & 1 \end{bmatrix} \begin{bmatrix} x \\ x' \end{bmatrix}_0 \quad (37a)$$

$$\begin{bmatrix} z \\ z' \end{bmatrix}_\ell = \begin{bmatrix} 1 & 0 \\ -\tan \gamma_f & 1 \\ \frac{\rho}{\rho} & 1 \end{bmatrix} \begin{bmatrix} 1 & \rho \theta \\ 0 & 1 \end{bmatrix} \begin{bmatrix} 1 & 0 \\ -\tan \gamma_0 & 1 \\ \frac{\rho}{\rho} & 1 \end{bmatrix} \begin{bmatrix} z \\ z' \end{bmatrix}_0 \quad (37b)$$

where γ_f, γ_0 refer to the entry and exit angles.

Setting the entry and exit angles equal and solving equation 37a with $\theta = \pi$, we find the focusing terms drop out.

A more careful examination shows that x' is a maximum for a bend of 90° . The equations of motion in x become:

$$\begin{aligned} \begin{bmatrix} x \\ x' \end{bmatrix}_\ell &= \begin{bmatrix} \tan \gamma & \rho \\ -\frac{1}{\rho} (1 + \tan^2 \gamma) & -\tan \gamma \end{bmatrix} \begin{bmatrix} x \\ x' \end{bmatrix}_0 \\ &+ \begin{bmatrix} -\rho \\ \tan \gamma - 1 \end{bmatrix} \frac{\Delta P}{P_0}. \end{aligned} \quad (38)$$

Solving for simultaneous focusing in both x and z we find $\theta = 4\gamma$ (Ritson, 1961). Taking entry and exit angles to be equal and the total bend 90° , $\gamma = 22.5^\circ$ degrees. The focal point can now be found from $f = x_\ell/x'_\ell$.

With this understanding of sector magnets, we need to consider the character of the particle beam itself. We made the assumption that the beam is 1 mm in diameter with a divergence of about 1 mrad and an intrinsic momentum spread of 0.1%.

The problem of a single magnet is easily tractable, but, if one considers more than one magnet in the problem, the algebra quickly becomes daunting. I used two computer programs, Transport and Turtle, which are written for much more complicated problems. Transport will solve for such values as entry and exit angles given constraints on the other variables in the problem. Turtle then can use the results of Transport to track a distribution of particles through a series of magnets and drifts.

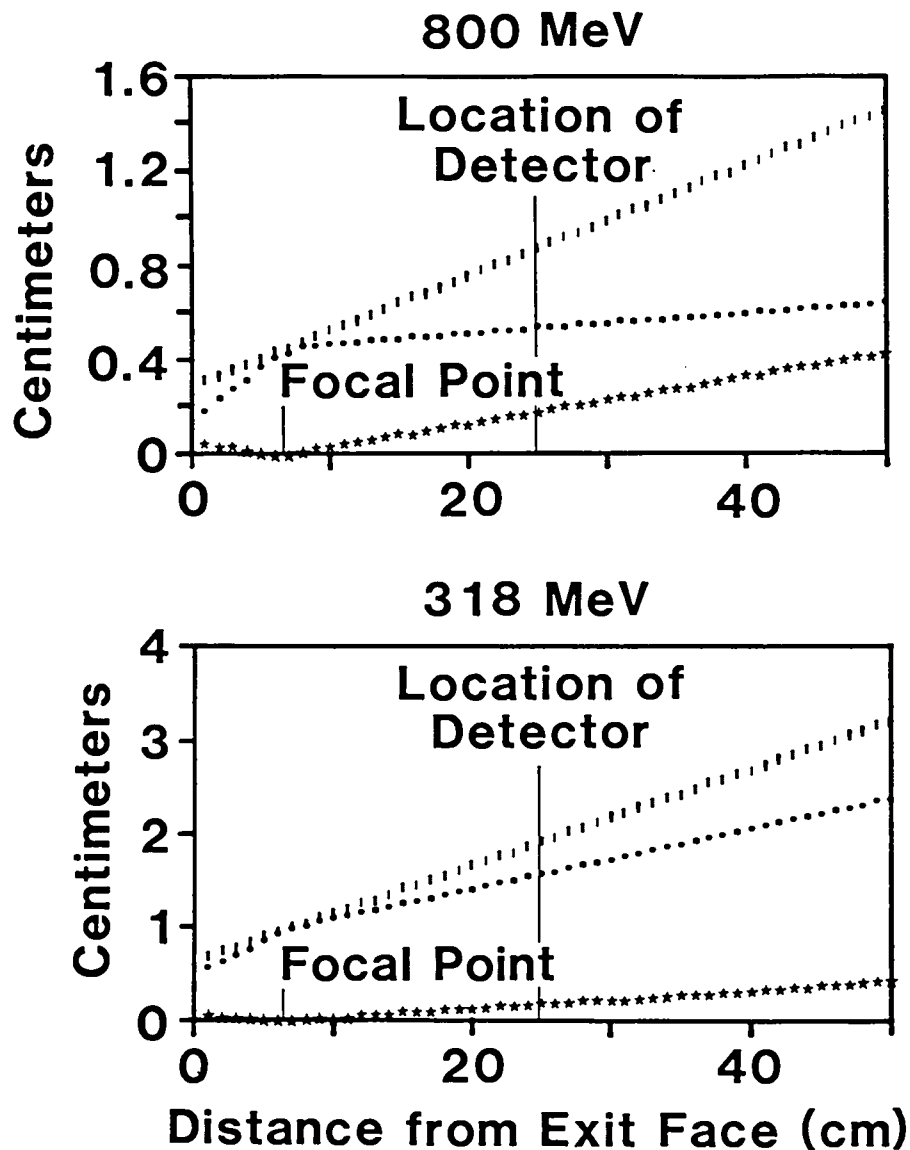
The focal plane of a sector magnet is inclined with respect to the central trajectory so that particles with

less momentum focus closer to the exit than those with more. We have two distinct packages of particles focusing at different points with different angular divergences. The most advantageous place to detect the signal package is not necessarily its focal point. Figure 3.12 shows that the extreme edges of the two beams continue to grow further apart as we move downstream. We can detect the signal electrons downstream of the focal point to gain dispersion.

The spectrometer is a sector magnet with entry and exit faces inclined at 22.5° to the design trajectory, Figure 3.13. The radius of curvature is 20 cm with an effective path length of approximately 34 cm. The pole tips and return yoke are machined from 10/06 iron. We needed 300 amp-turns to generate the magnetic field of 135 gauss which is required at a primary beam energy of 800 MeV. We used 30 turns of rectangular wire driven with a 0-to-15 amp, 0-to-60 volt power supply.

The magnet fits around a Y-shaped beam pipe with a rectangular cross section. The gap between the pole tips is two inches. The detector side of the Y is capped with a set of flanges which hold 0.5 mil Havar foil over a window 0.3×1.0 inches. Approximately 1 cm beyond the aperture is a scintillator attached directly to a photomultiplier tube. The drift between the exit of the magnet and the detector is 25 cm.

Design Parameters for Detector Location



- Axis Separation
- Edge Separation
- * Width of Beam

Figure 3.12 Design parameters for detector location.

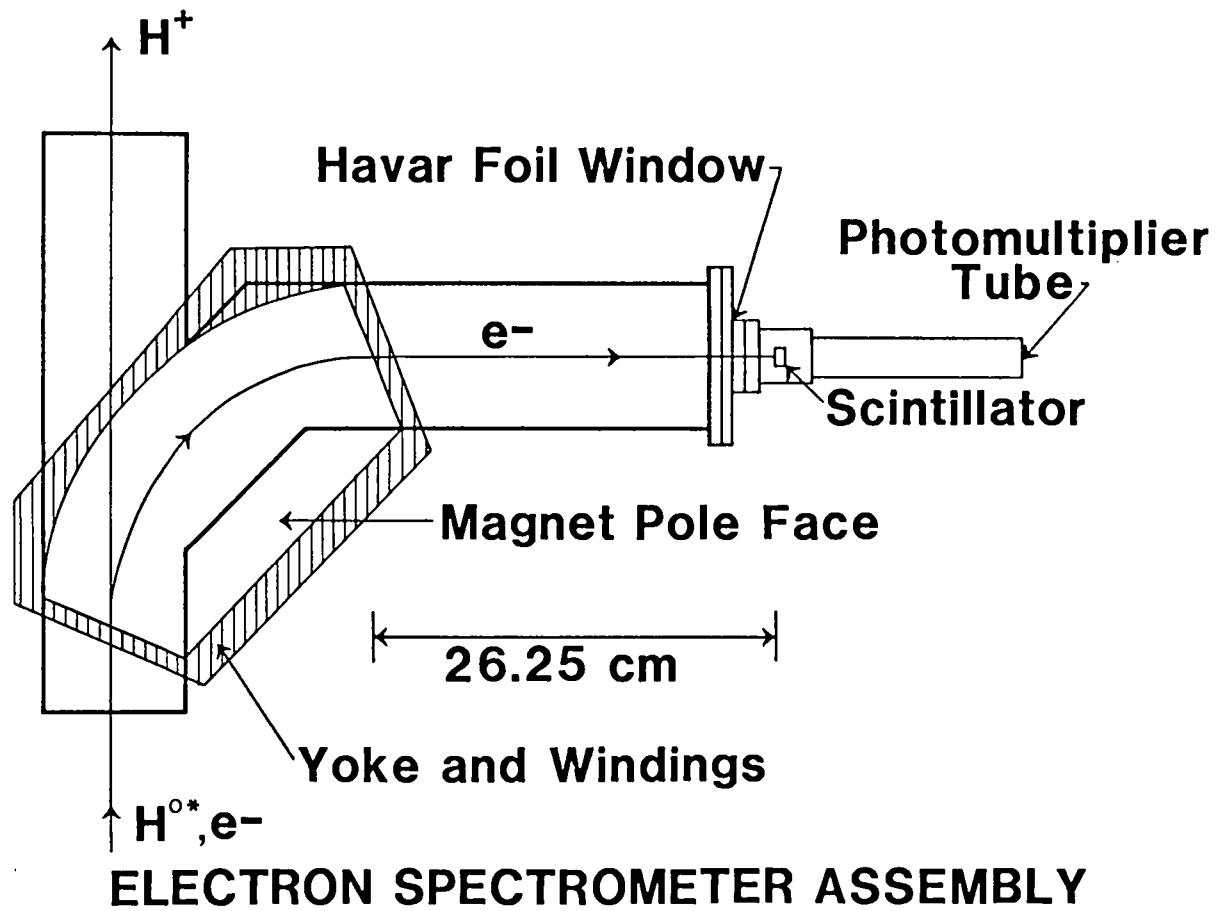


Figure 3.13

Initial plans called for the use of a silicon detector mounted in the vacuum to gain energy resolution. A cooled SiLi detector is capable of energy resolution of a few tens of electron volts. The resolution is inversely proportional to the size of the detector so we thought to use one as small as possible mounted so that it could be moved vertically. We could then find the signal by sweeping horizontally with the magnetic field and by moving the detector itself in the vertical direction. Aside from the fact that we started too late to get the required apparatus delivered in time, the major drawback to using a SiLi detector was the slow conversion time inherent both in the detector itself and in the analog to digital conversion necessary for energy resolution.

We did purchase a room temperature detector which, in principle, would resolve 8 to 10 keV - not significantly better than we expected from the magnet alone.

If the magnet did its job, a scintillator used simply to count the selected particles with no energy resolution would work. The scintillator has a very fast recovery time and there would be no need for A to D conversion.

We used a scintillator 1 cm in diameter and 0.5 cm thick coupled directly to a photomultiplier tube. We made a series of slits to cover the scintillator, ranging in size from 1/32 inch (0.8 mm) to 3/32 inch (2.4 mm) wide.

The Turtle program predicted a beam diameter of less than 0.1 mm at the focus.

Our initial runs were made with the smallest slit but, eventually, we removed the slit altogether with satisfactory results. Unfortunately, we did not find time to do a study of the effect of slit sizes.

The first test of the spectrometer was to detect electrons stripped from the H^- beam by a thin (15 micrograms/cm²) foil. The foil could be biased so that we could tag the stripped electrons with ± 5 kV or 0kV. Figure 3.14 shows the result of the test. FWHM of the central peak implies a resolution of approximately 1.3%. Note that the low energy peak is essentially unresolved. This may be attributed to the fact that multiple collisions of gas-stripped electrons gave an energy distribution with a distinct maximum value with a tail on the low energy side. Thus electrons tagged with an energy above the gas-stripped maximum stand alone above the background which is seen in the resolved +5 kV peak.

The real test came when we looked for high Rydberg states in H^0 . Neutral hydrogen left in $n = 4$ after being stripped in the foil was laser promoted to some higher state which was field stripped in the spectrometer's motional electric field. Several peaks were seen at a given magnetic field, but to see the full series the field had to be readjusted to bring other peaks into focus. At

EFFECT OF ENERGY TAGGING ON POSITION OF ELECTRON PEAK IN SPECTROMETER

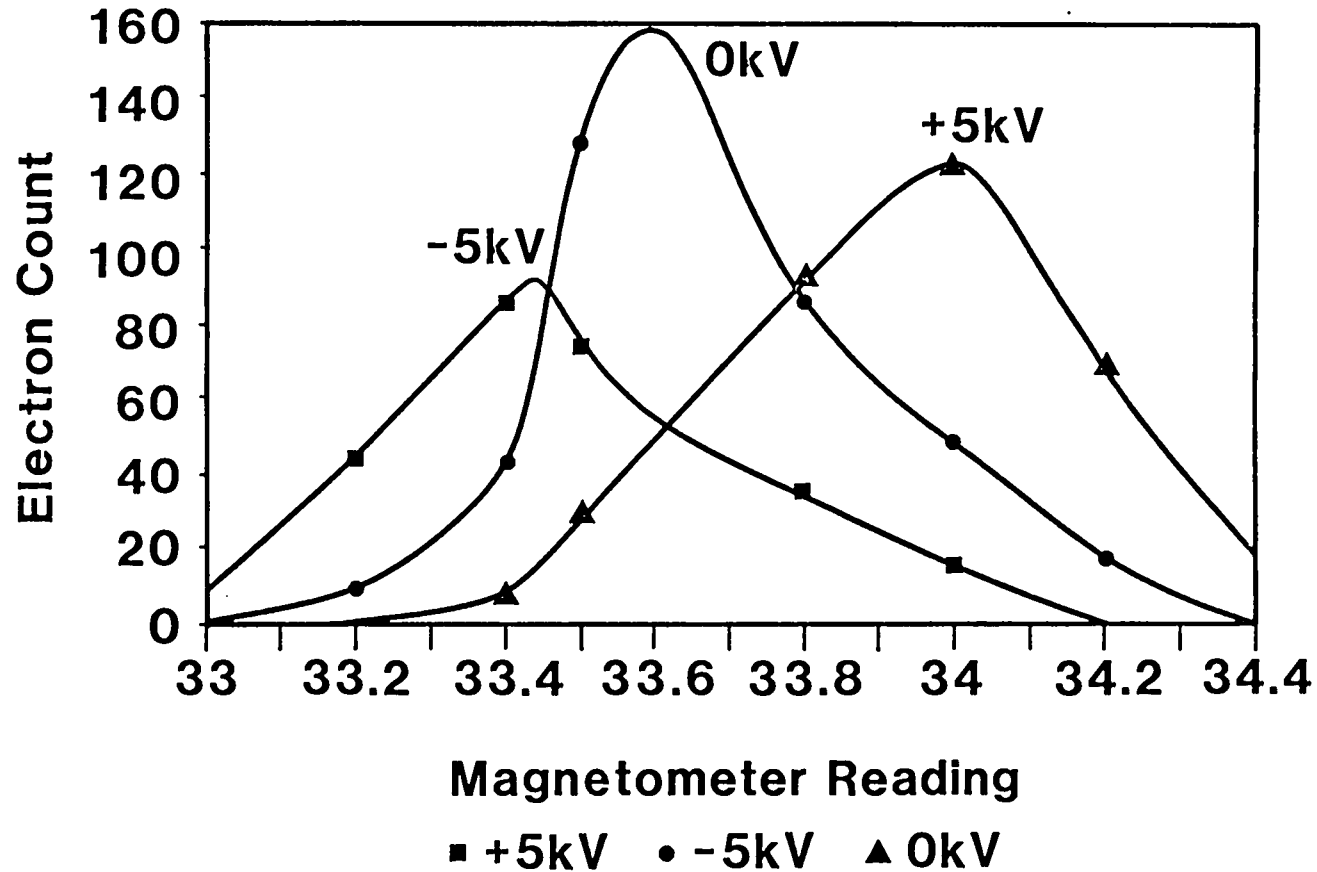


Figure 3.14 Effect of energy tagging on position of electron peak in spectrometer.

800 MeV we saw only a narrow range of Rydberg states. States with $n < 11$ were not stripped in the motional electric field, while states of $n > 15$ striped so promptly they were superimposed on the background and were not resolvable as distinct peaks. At 318 MeV the picture improved greatly. Even though the motional field was reduced due to the small field needed to bend the particles and the reduced relativistic factors, we could see $n = 13$ through 25. The reduction in field allowed a greater separation of Rydberg peaks which resulted in greater resolution. Figure 3.15 is an example of Rydberg data taken with the spectrometer. The peaks have a width of approximately 1 meV which we take to be our experimental resolution since the intrinsic line width of the transitions is much smaller than that observed.

Using the simplest considerations, we were able to construct an electron spectrometer with a momentum resolution of 1.5%. It is possible that we could gain some improvement by optimizing the size of the slit in front of the spectrometer. Additional improvements may come with a more careful design along the lines of Crewe et al., (1971) who designed a spectrometer for use in a scanning electron microscope and whose work was adapted for use for more conventional beta spectroscopy by Sellin (1986).

HYDROGEN SERIES

N= 4 TO 19, 20, 21, 22

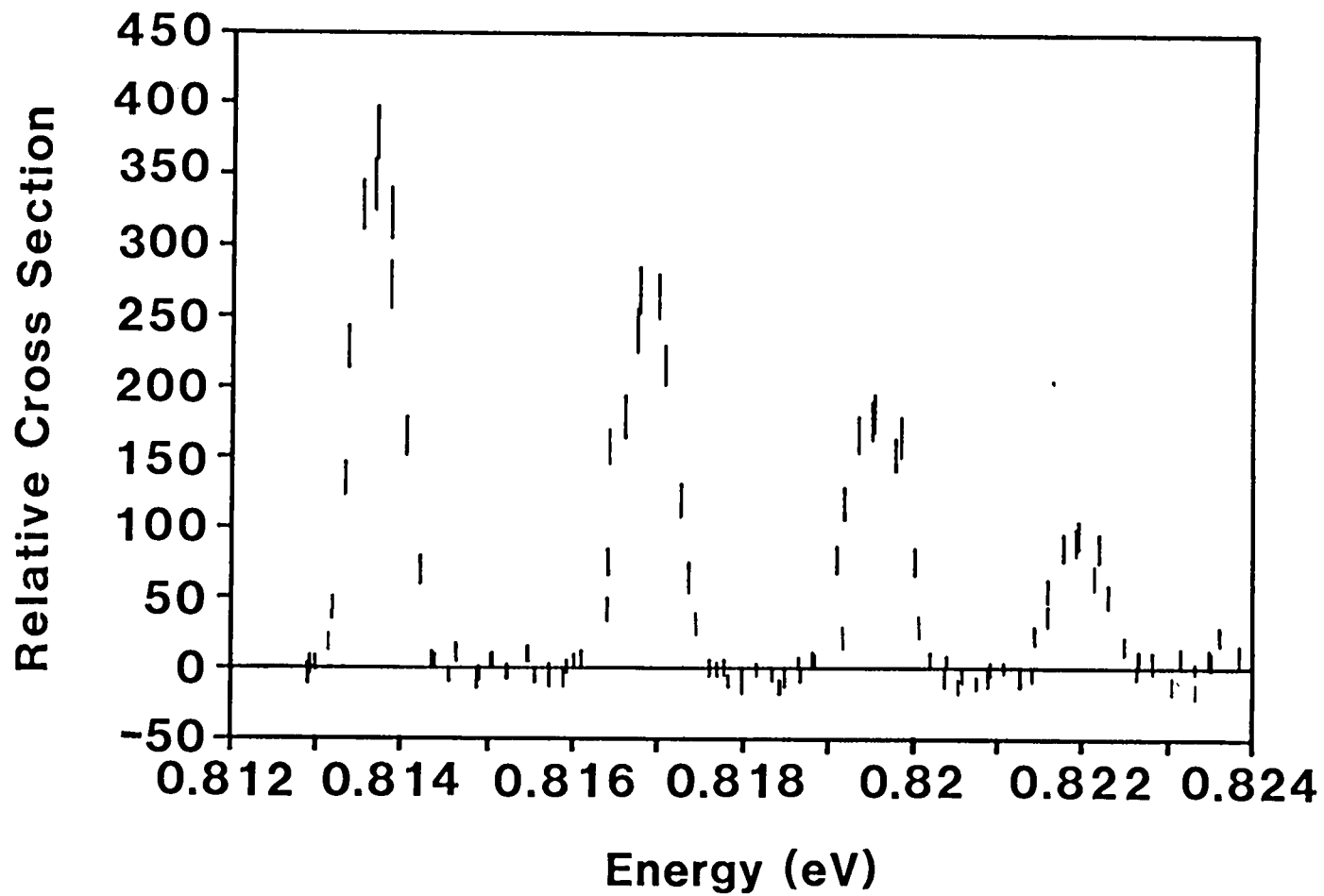


Figure 3.15 Hydrogen series.

TUNE UP

Before we could begin to take data we had to tune up the beam so that we had maximum overlap between the ion beam and the laser beam. With the laser at an angle where we expected a large photodetachment signal we had CCR personnel scan the H^- up and down using a steering magnet upstream of our experiment while we took data. Thus we probed the extent of the laser beam and could determine what setting for the steering magnet gave the best overlap.

Once we had the best setting we could run a phosphor into the beam, which could be viewed with a remote TV. We then had a visual fix on where the beam was so that it could periodically be checked.

Before running, CCR attempted to maximize the signal on our ion chamber by adjusting the appropriate focusing and steering magnets and the stripper aperture. We monitored the ion chamber signal on the oscilloscope looking for a characteristic shape that indicated the beam was properly tuned on the stripper aperture upstream.

Unfortunately, all these adjustments proved to be temporary and required constant monitoring and readjustment.

A TYPICAL RUN

Before a run we set the spider to a given starting angle by running the stepper motor from the panel until the encoder showed the appropriate setting. We selected steps per angle for the run, typically 20 to 50. The NIM scaler was set for the number of counts from the ion chamber which determined how long we counted at each angle. The longer we counted the better the statistics but the greater chance that something might change during the course of the run which could take an hour or more.

The laser power was read from the calorimeter in the chamber.

The run was then started by typing the appropriate commands into the computer which in turn issued a start command when it was prepared to take data. The Q system is set up for a maximum of 100 angles for a run. When we took small steps per angle we often continued a scan for two or even three runs.

The data was recorded on a tape and a file was written to the hard disk when the run was completed. A plot of the data could then be displayed and printed on the line printer. The data file was then read from the Microvax to a Zenith 150 microcomputer where it was formatted into Lotus 123.

TIMING AND ELECTRONICS

The experiment was run and data was taken by a Microvax minicomputer. Two blocks of electronics provided an interface between the experiment and the computer. CAMAC modules such as scalars and ADC's provided a direct interface for data taking. NIM modules were used primarily for timing and running the experiment.

As mentioned earlier, in 1986 we used the laser in a non-Q-switched mode which simplified timing considerably. I will describe here the simplified setup. The earlier setup was much the same with the complication that timing had be of the order of nanoseconds rather than microseconds.

Refer to Figure 3.16 for the discussion that follows.

We recieved a timing signal (TS) from CCR about 100 μ s before arrival of a pulse of H^- ions. This signal started the sequence which fired the laser and recorded data from the laser firing. TS started a delay which resulted in firing the laser about 100 μ s into the 700 μ s long pulse of ions. TS also started a delay which opened a timing gate in a Camac ADC to allow the signal from the laser photodiode to be read and digitized for recording on the data tape.

TS was also sent to a coincidence circuit (called the Ready circuit) where it became one of several conditions which had to be satisfied to enable the computer to take

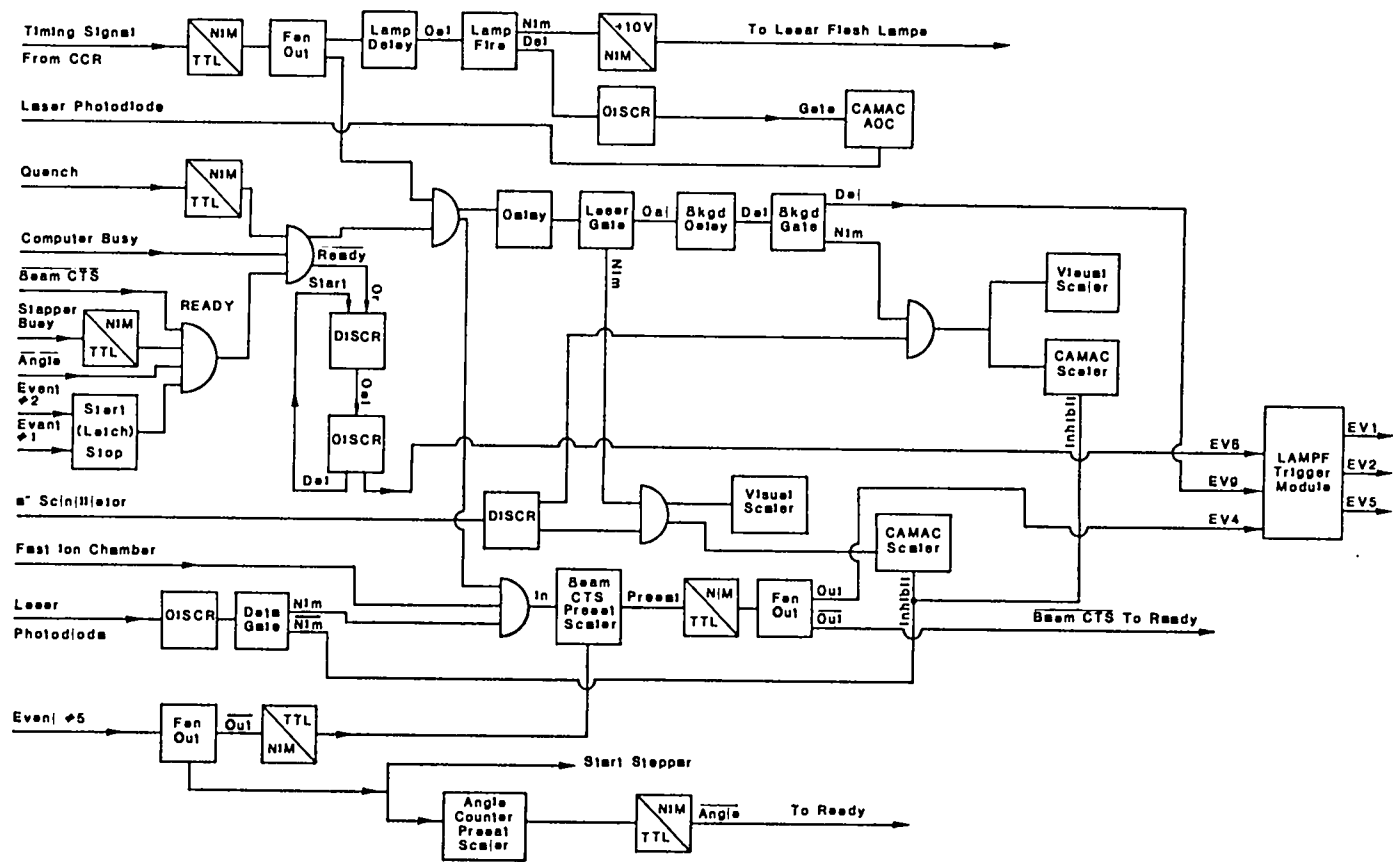


Figure 3.16 Block diagram of electronics.

data from the impending H minus-laser collision. "Quench" was another signal from CCR. It served as a veto if the H⁻ pulse would be of severely reduced intensity. "Computer busy" signaled that the computer was tied up with processing an earlier event and was not ready to take data. "Beam counts" stopped data taking at a particular angle once a predetermined current of H⁻ flowed through the experiment. "Stepper busy" did not allow the recording sequence to begin if the stepper motor was still in the process of rotating the spider. "Angle" stopped data taking when the system had taken data at a predetermined number of angles. Event #2 was a signal from the Microvax which began a run and event #1 stopped a run.

If the coincidence conditions were all met then a timing sequence was begun which resulted in recording the number of particles striking the detector in two blocks of time. Centered on the 100 microsecond laser pulse was an 80 microsecond data gate during which time a CAMAC scaler was enabled to count the signals in our detector. Some 50 microseconds after the laser pulse another gate opened to read the signal not associated with the laser. This background was subtracted from the earlier signal during analysis. Figure 3.17 summarizes the timing for a particular laser event.

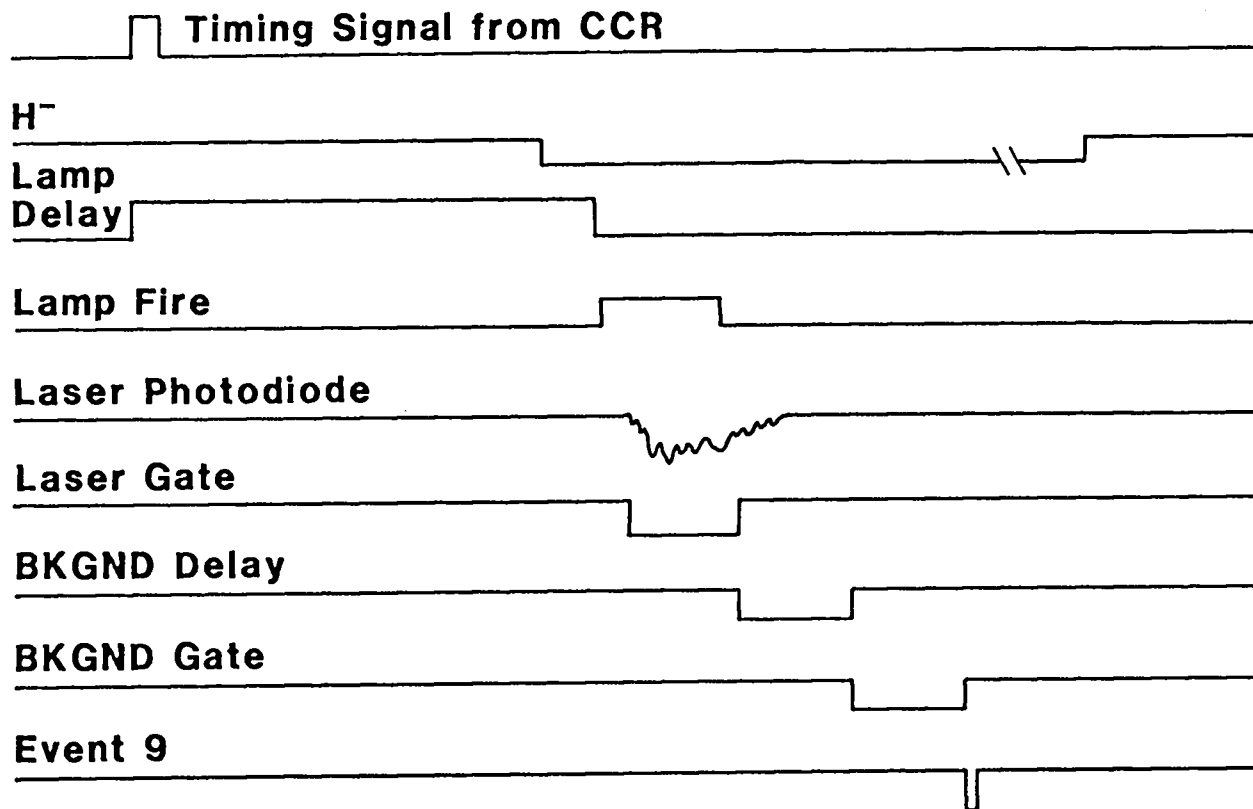


Figure 3.17 Timing scheme. An initial signal from CCR starts the sequence, triggering a delay which in turn fires the laser flash lamps during the passage of the ion pulse. "Laser gate" allows data to be taken during the laser pulse. After an appropriate delay "bkgnd gate" allows a reading of the detector during the ion pulse but well after the laser pulse. Event 9 signals the computer that data should be read and recorded.

During the experiment the background signal was set both before and after the laser signal at different times. The ion pulse amplitude often displayed a constant negative slope between a sharp leading and trailing edge so that a background gate of the same width as the data gate would read either too much or too little. With the laser off we adjusted the background gate to give the same signal as the data gate. Even this was not fool proof as the shape of the ion pulse might easily change over time. This can be seen in some of the data where the signal below threshold is substantially above zero.

Figure 3.18 shows two photographs of the ion pulse with the timing gates superimposed. The top photograph shows three distinct pulse shapes all of which required a different relationship between the data gate and the background gate and yet those different shapes all occurred in less than one second. The second photo shows the more typical case. The width of the gates was approximately 80 μ secs.

The "Events" referred to in Figure 3.16 were computer events for certain important conditions during the run. Events #1 and #2 have been defined. Event #5 sent the signal which rotated the spider to a new angle. Event #8 occurred every ten seconds and enabled the computer to read information from devices such as the calorimeter, the vacuum gauge, and the magnetometer on the electron spectrometer.

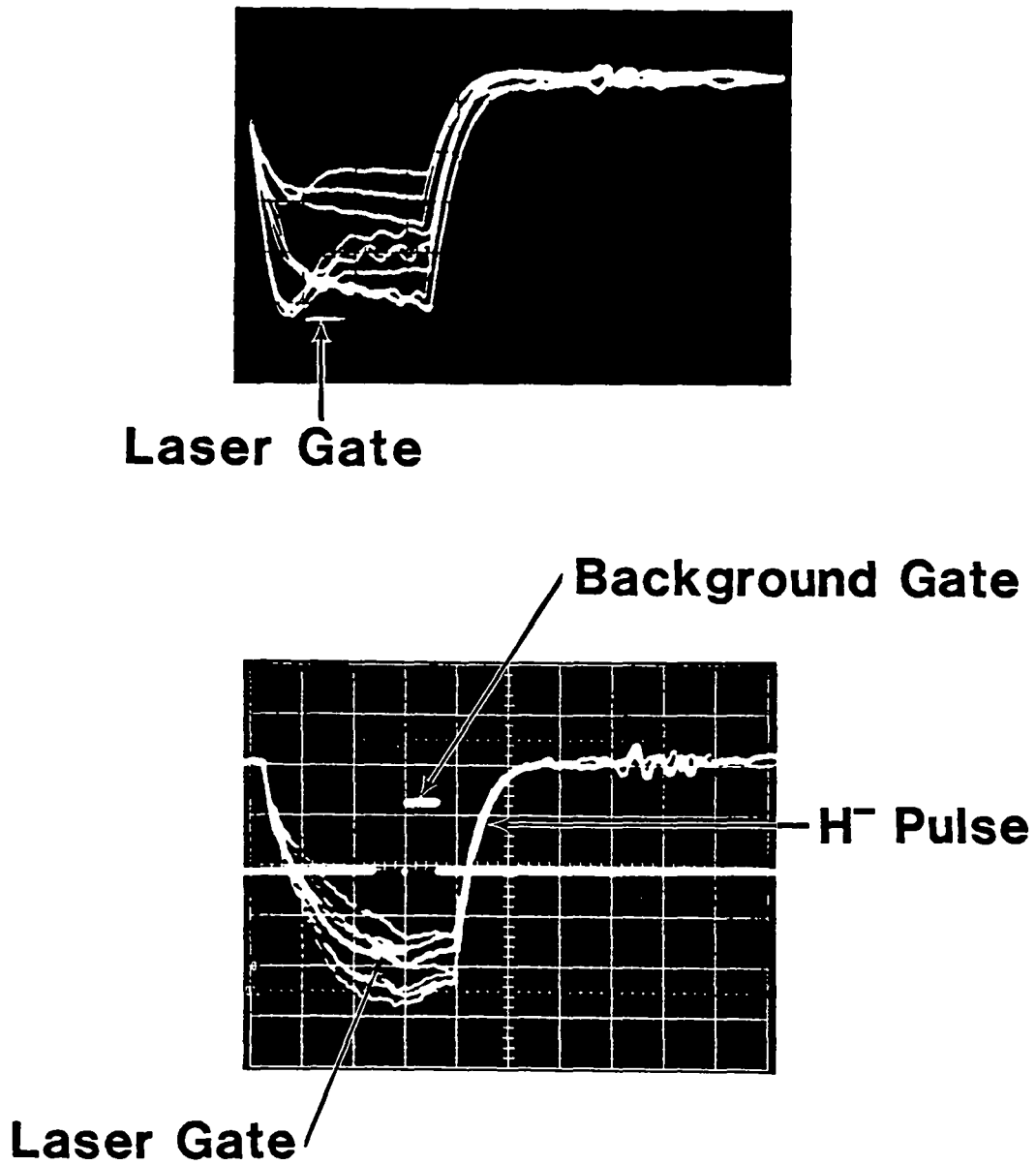


Figure 3.18 Examples of H minus ion pulse with laser and background gates

CHAPTER 4: DATA AND ANALYSIS

The data discussed here are the result of a number of experiments spread over two years. Several different experimental setups under differing conditions were used. In 1985 all of the data were taken at a primary beam energy of 500 MeV. We explored the H^- cross section using σ polarized light in large motional electric fields. In 1986 we used two primary beam energies, 800 MeV and 318 MeV and we looked at both σ and π polarization. We used the vertical bender detection scheme in 1985 and for the 1986 800 MeV runs. We used an electron spectrometer for the 318 MeV runs.

Because of the various methods used the discussion can be confusing. Table 1 provides an overview of what was done when, and how it was done.

In our analysis we have thought of the condition when the current in the magnet which provides the motional electric field is zero as "zero field." This is not strictly true since there is hysteresis in the magnet. At zero current there is still some residual magnetic field which in turn transforms into magnetic and electric fields in the rest frame of the ion.

"Zero field" data always provided important parameters of the apparatus. Because the determination of these parameters, encoder zero and steps per degree, is a

TABLE 1

OVERVIEW OF EXPERIMENTS

BEAM ENERGY	EXPERIMENT	DETECTION SCHEME	APPENDIX
1985	500 MeV "ZERO FIELD"	VERTICAL BENDERS	1
	PURE SIGMA POLARIZATION HIGH MOTIONAL ELECTRIC FIELDS 0 - 1.3 MV/cm	VERTICAL BENDERS	2
1986	800 MeV "ZERO FIELD"	VERTICAL BENDERS	3
	PURE SIGMA OR PI POLARIZATION MODERATE MOTIONAL ELECTRIC FIELDS 0 - 160 kV/cm	VERTICAL BENDERS	4
318 MeV	ZERO FIELD	ELECTRON SPECTROMETER	3
	PURE PI POLARIZATION LOW ELECTROSTATIC FIELDS 0 - 50 kV/cm	ELECTRON SPECTROMETER	5

requirement common to the rest of the data, I will discuss that aspect of analysis separately.

The rest of the analysis will be divided into two groups with appropriate subdivisions. We will look at the 1985 data first with consideration of the "zero field" data and then of the field data which were all taken with σ polarization. Then the 1986 data will be divided into three subtopics: "zero field," σ polarization field data, and finally π polarization field data (the ripples). There are few 1986 σ polarization runs. They serve primarily to confirm the polarization dependence of the ripple phenomenon.

DATA REDUCTION AND CURVE FITTING

The 1985 data was partially analyzed by the LAMPF Q system during the runs. The Q system is a software framework supplied by LAMPF which can interface our computer system with the experiment both for remote control and for data taking. The output included the encoder value of each angle, the corresponding energy calculated using the appropriate parameters contained in a parameter file, and a calculated cross-section which used the same parameter file. The parameter file contained the values for β , encoder zero and steps per degree. If these parameters were not correct during the run then we must use the replay feature of Q to rerun the data and

recalculate the energy and cross section. In fact, we do not know the encoder zero before beginning a series of runs because, as explained below, we must use experimental information to determine the zero.

In 1986 there was no online analysis of the data due primarily to the fact that a new computer and new version of the Q system were installed and we did not have time to rewrite the online analysis code. Raw data were written to a file on the hard disc of the Micro-Vax. These data were then read from the Micro-Vax to a Zenith IBM PC compatible computer where it was put into spreadsheet format using Lotus 123. The Lotus worksheet was then used to calculate cross sections from raw data and to make cuts on the data. The data prepared in Lotus was then read into a file that was compatible with the fitting program.

Lotus proved to be an excellent format for examining the effects of different cuts on the data and for recalculating the cross sections using different parameters. However, using Lotus required that I or a helper spend a great deal of time with each data file. It may have been more efficient in the long run to use Lotus only for preliminary examination and then write a set of programs which could run from a batch file sequentially operating on all data files essentially without human interference. Conversely, using Lotus on each file forced

one to look closely at the data, a process which might be ignored using batch processing.

The cross section is calculated using the formula,

$$\sigma = GR \frac{\beta \sin \alpha}{IJ(1 + \beta \cos \alpha)} , \quad (39)$$

where G is a geometric factor depending on the overlap of the laser and particle beams, R is the rate of photodetachment, I and J are the photon and ion currents, respectively, (Bryant et al., 1971). Since we are unable to determine accurately the overlap, G becomes an arbitrary constant and we measure relative, not absolute, cross sections. Unlike a typical experiment in nuclear or particle physics we are easily able to look at the total cross section rather than a differential one. Because the transverse momentum imparted during the interaction of photon with ion is completely negligible we are able to detect all of the products of the reaction with one small scintillator.

The zero field data were analyzed to establish an encoder zero and the power law obeyed by the Armstrong characterization of the cross section above threshold. The data were first fit using a simplex fitting routine (Caceci and Cacheris, 1985) which fed its results into a covariant matrix calculation which computed the standard deviations of the fitted parameters (Whitman, 1982).

A simplex is a geometric figure with one dimension more than the number of parameters to be fit. In the simplest case to visualize imagine that we wish to fit a function with two free parameters to some data set. We wish to minimize χ^2 , with

$$\chi^2 = \sum \frac{[x_i - \bar{x}_i(a,b)]^2}{\sigma_i^2}, \quad (40)$$

where the x_i are data points, $\bar{x}_i(a,b)$ are the fitted points and σ is the error associated with x_i . The $\bar{x}_i(a,b)$ are shown explicitly to be functions of the two free parameters. In χ^2, a, b space the simplex is a triangle. Now visualize a surface, $\chi^2 = \text{fn}(a,b)$, within this space for which we want to find a point which is the absolute minimum of χ^2 . The simplex program takes the initial guesses for the parameters, computes χ^2 then finds two other nearby points on the surface. These three points form the vertices of a triangle. One vertex will have a greater value of χ^2 than the other two. If the triangle is now rotated about the side opposite the vertex with maximum χ^2 that vertex will most likely have moved downhill, which is the goal. By testing the vertices again for maximum χ^2 the program now selects another side about which to rotate - successively flipping the simplex downhill. The program also can test whether a larger or

smaller figure will lead to improvement. Eventually, the simplex becomes trapped in a minimum at which point the program calculates the standard deviation of the resulting parameters and finally stops.

In higher dimensional space the simplex becomes harder to visualize although the principle is the same. The function fitted to the zero field data was the Armstrong formula:

$$\sigma = \frac{A(E - E_0)^P E_0^{1/2}}{E^3} + B \quad (41)$$

Here are four parameters: A, an arbitrary amplitude; B, a background which in theory should be zero; P, the power describing the behavior of the cross section above threshold; and E_0 , the threshold.

Only the values of P and E_0 are of interest. Unfortunately, we are unable to say anything about the absolute value of E_0 . Our only opportunity to do so would have been during the 318 MeV runs when we used the potential well and we could achieve a true zero field condition. At the time, though, our interest was primarily on the ripple phenomenon. We would have had to look at some known feature which lies nearby in energy on both sides of the beam in order to have a very precise energy calibration for the apparatus. One of the transitions in the $n = 4$ hydrogen series would have been ideal. These transitions were viewed only at 318 MeV in

1986 and then on only one side of the beam. We used the fitted value of E_0 only as an approximate calibration. The value of P , however, is an important experimental result which we shall see approximately confirms the prediction made by Eugene Wigner in 1946.

It should be noted that successful fitting of the data is something of an art. In principle, of course, the simplex program rolls downhill until finding the minimum. In reality, the surface being fit might have local minima which can trap the simplex or the true minimum might just be very shallow making convergence difficult. I found that by graphing unsuccessful tries I could make better guesses as to where to start the process and, by iteration, eventually converge to a true minimum.

DETERMINATION OF ENCODER ZERO AND STEPS PER DEGREE

There are three possible methods for determining the parameter steps per degree, S , and two for determining the encoder zero, EZ . I will discuss each in the context of the actual experiment.

In 1985, before the run began, we measured S using a theodolite before the vacuum chamber was closed up. Unfortunately, before we took the data presented here, the steel belt which drives the encoder broke, invalidating the theodolite measurement. During the run the measured S remained the best value available. The encoder zero was

determined by looking at the position of the H^- threshold on both sides of the beam. Zero degrees is, by definition, located exactly between those two values such that it will correspond to head-on with the ion beam.

For the 1985 data these two very approximate values were used in the final analysis for reasons to be discussed.

In 1986 we did not attempt to measure S using a theodolite. Instead we relied on our ability to measure the location of a known feature such as the H^- threshold to determine both EZ and S . The best technique would be to locate a sharply peaked feature such as a hydrogen resonance. During the 318 MeV phase of the 1986 runs we did look at both the $n = 3$ and 4 series of hydrogen on one side of the beam. This procedure is discussed in some detail in the section on the electron spectrometer. The location, in energy, of these resonances is known several orders of magnitude better than our resolution so that the spacing between them serves as an excellent measure of the number of steps per degree and, in fact, allows us to determine β . The angular location of the $n = 4$ to $n = 14$ transition is within 3.35° of the H^- threshold so that we have a local calibration that should minimise the slight non-linearity that we know exists in the stepper-spider-encoder system.

We fit the Doppler equation

$$E_{\text{cm}} = \gamma E_L (1 + \beta \cos \alpha) , \quad (1)$$

where α was expressed in terms of encoder values:

$$\alpha = \left[\frac{\text{Encoder} - \text{EZ}}{S} \right] , \quad (42)$$

β and S were free parameters, E_{cm} the well-known energy value for the one of the hydrogen resonances, and Encoder was the fitted location of the resonances. The result of the fit gave $S = 574.98(5)$, and $\beta = 0.662786(86)$.

Since we did not look at the $n = 4$ series on the other side of the beam, we were not able to use this technique to determine the location of EZ. The only thing left at this point is to use the location of the H^- threshold - an indistinct feature which cannot be located as precisely as could a narrow hydrogen resonance.

To further complicate matters we did not look at threshold on both sides of the beam during the 318 MeV run so we must combine information from the 800 MeV run with the 318 MeV data. It turns out that the 318 MeV value for S is not consistent with the 800 MeV data. Using the best location of EZ from 800 with the S from 318, the location of the threshold indicates that the β of the ion beam

during the 800 run must have been of the order of 0.858 (corresponds to beam energy of 887 MeV!).

Now, it must be remarked that, since we are operating near the Doppler free angle, we are not very sensitive to beta. Therefore, it is not surprising that our fitted β might be imprecise, although this result seems unreasonable.

The inescapable conclusion is that during the change over from 800 to 318 MeV we must have done something to change the steps-per-degree calibration. This is not a completely unreasonable assumption given the fact that during the change we removed the heavy electromagnet assembly from the spider table.

In the end, we have used the location of EZ determined from the 800 data with both 800 and 318. We have used S_{318} with only the 318 MeV data and used an S_{800} for the 800 MeV data. The approximate zero determined during the 1986 run was 100336 encoder steps and the result of the fitting was 100359.

To determine S_{800} we find threshold on both sides of the beam. We assume that the beam energy is exactly 800 MeV, and we assume that threshold, E_0 , is at exactly 0.7542 eV (Pekeris, 1958). From this we can find the angle between the ion beam and the laser which corresponds to 0.7542 eV at 800 MeV, -140.6° . Dividing the number of

encoder steps between the two threshold values by twice the angle we have $S_{800} = 576.4$.

To summarize the situation, the encoder zero used for the 1985 data was -4891 (the system was rotated 180° from normal) and the steps per degree was 577.48. Neither of the values is exactly correct but a change would consume a great deal of time with little effect on the power law or on the qualitative results from the 1985 field data. In 1986 a single value for encoder zero, 100359, was determined from observing the location of the H^- threshold. Two values for steps per degree were used, one for the 800 MeV data and one for the 318 MeV data, 576.4 and 575.0, respectively.

ANALYSIS OF 1985 DATA

Analysis of this data was somewhat hampered by the computer system. The online analysis code which was appended to the Q system had grown through the history of this series of experiments. Several authors contributed elegantly to the code, but, as those authors moved on to other projects, the workings of the code became increasingly opaque to those who followed. In addition, to change any of the parameters required replaying the run. Replay is a feature of Q wherein the data tape is played back as though the experiment were actually being run over again - a time consuming process. The upshot is

that as we looked at the 1985 data we felt that it did not warrant that investment of time.

1985 "Zero Field" Data

The electromagnet used in 1985 had a field at zero current of about 150 gauss. This transforms to 52 kV/cm at 500 MeV. This "zero field" is of the order of the low field runs in 1986! Nevertheless this provided the basis for the 1985 analysis and, considering that 52 kV/cm is approximately 10^{-5} atomic units, we can consider it to be approximately zero field.

Table 2 shows the result of fits of "zero field" data. All data files were cut off at approximately 0.805 eV and fit to equation 41. The files were then cut off closer and closer to threshold and fit again in order to determine the trend towards the power obeyed by the cross section at threshold. Recall that the Wigner prediction does not tell us how far above threshold the power of 1.5 should apply.

Several things are obvious from the data. There appears to be a systematic discrepancy between the east and west side runs. We see that the east side runs give consistently a lower power than the west when the anomalous run 6163 on the west is taken out of consideration. This is particularly obvious in the

ideogram¹, Figure 4.1. I have been unable to explain the discrepancy and must leave it to some unknown systematic error. We will see in the 1986 data that this discrepancy does not exist.

The 1986 data was taken with finer energy increments than the bulk of the 1985 data. In the tables of 1985 data, runs taken with energy increments of 1.4 meV are marked with asterisks. Other runs were taken with increments of 7 meV. In contrast the bulk of the 1986 data was taken with steps of 1.7 meV or less. The result is that statistical fluctuations in the coarser data will have greater weight making the data less consistent.

It is obvious from Table 2 that the encoder zero and the steps per degree in use are not correct. East and west sides show different values for threshold. As mentioned earlier, these parameters were not revised. The error in encoder zero is a linear shift and has no effect on the resulting power. The error in steps per degree is not linear but, considered over the small energy range that we look at it can be considered to be approximately

¹An ideogram is a convenient method to examine the consistency of a set of data. The ordinate is an arbitrary run number. The abscissa is the value of the fitted parameter. Each point is displayed with the appropriate error bar. The curve is the sum of a Gaussian probability function calculated for each point. The area under each curve is $1/\sigma$ rather than $1/\sigma^2$ so that systematic errors are emphasized. Consistent data will show a singly peaked symmetric curve.

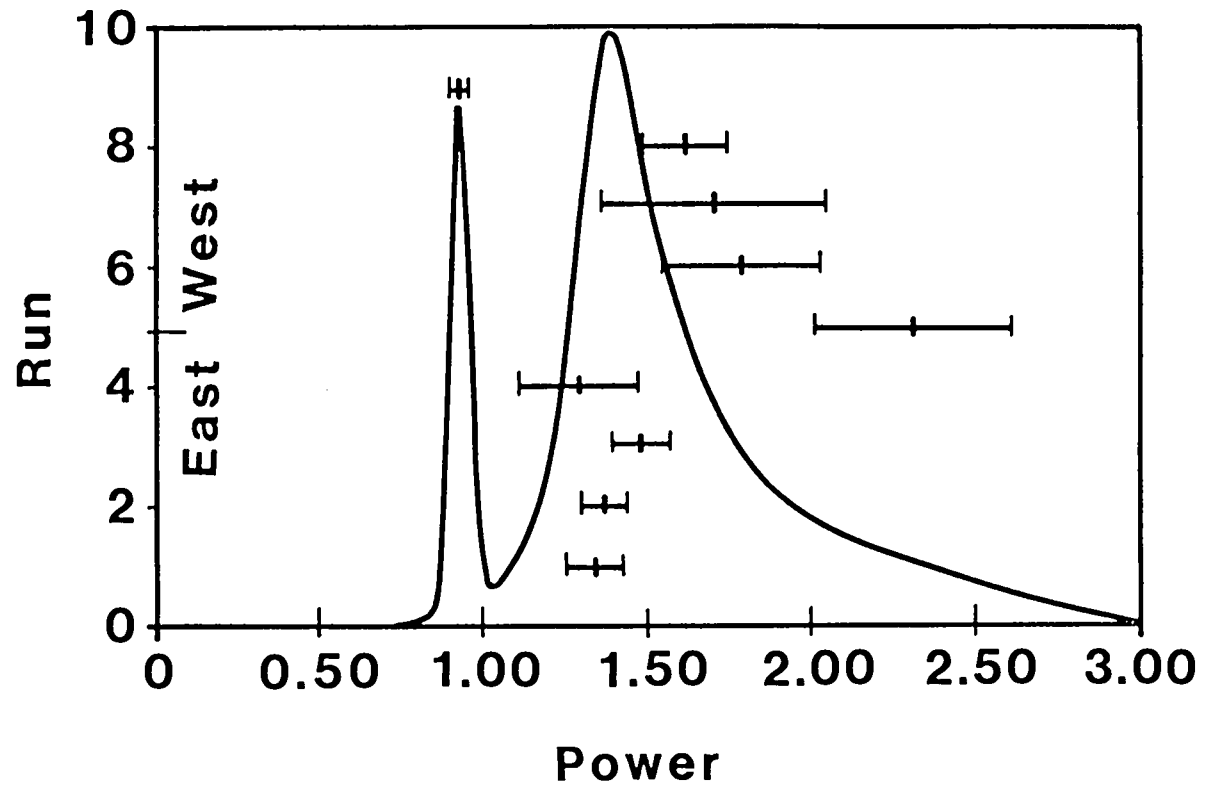


Figure 4.1
IDEOGRAM 1985 ZERO FIELD DATA

TABLE 2
(Continued on next page)
1985 DATA
SUMMARY OF ZERO FIELD FITS WITH SUCCESSIVELY SMALLER EMAX

WEST	EMAX=0.805eV							EMAX=0.788eV						
	EO	STD DEV	POWER	STD DEV	AMPL	BKGND	REDUCED CHI SQ	EO	STD DEV	POWER	STD DEV	AMPL	BKGND	REDUCED CHI SQ
RUN														
6126	0.7454	0.0036	2.29	0.3	16004	-0.04	0.64	0.7589	0.0028	1.37	0.21	1526	0.45	0.46
6127	0.7505	0.0029	1.77	0.24	3479	-0.008	1.04	0.7599	0.0009	0.83	0.07	178	0.06	0.25
6134	0.7509	0.0074	1.69	0.34	1593	-0.002	0.34	0.7521	0.0071	1.66	0.48	1625	-0.01	0.13
6135	0.7536	0.0026	1.6	0.13	1598	-0.04	0.14	0.7529	0.0029	1.61	0.21	1544	-0.04	0.06
*6163	0.7539	0.0004	0.92	0.03	746	0.08	1.5	0.7492	0.0015	1.22	0.08	1523	0.07	1.3
AVERAGE	0.7538	0.000391	0.971	0.0289				0.7516	0.001186	1.287	0.069			
=====														
EAST	EMAX=0.803							EMAX=0.791						
6149	0.7657	0.0015	1.33	0.09	1764	-0.09	0.76	0.7652	0.0023	1.297	0.2	1492	-0.11	0.76
*615051	0.7616	0.0007	1.36	0.07	2346	0.08	1.2	0.7638	0.0008	1.13	0.07	1181	0.17	1.2
*6162	0.7609	0.001	1.47	0.09	2975	0.08	0.86	0.7648	0.0009	1.21	0.08	1472	0.26	0.84
6143	0.7685	0.0014	1.28	0.18	2013	0.0006	0.87	0.7701	0.0019	1.22	0.18	1710	0.28	0.71
AVERAGE	0.7627	0.000500	1.376	0.0459				0.7647	0.000553	1.176	0.0485			
=====														
EAST + WEST AVERAGE	0.7572	0.000308	1.086	0.0244				0.7624	0.000501	1.213	0.0397			

TABLE 2 CONTINUED
1985 DATA
SUMMARY OF ZERO FIELD FITS WITH SUCCESSIVELY SMALLER EMAX

WEST	EMAX=0.782eV							EMAX=0.771eV						
	EO	STD DEV	POWER	STD DEV	AMPL	BKGND	REDUCED CHI SQ	EO	STD DEV	POWER	STD DEV	AMPL	BKGND	REDUCED CHI SQ
6126	0.7551	0.0038	1.46	0.32	1589	0.41	0.2	0.7563	0.0066	1.42	0.96	1524	0.42	0.21
6127	0.7534	0.0054	1.48	0.44	1536	0.03	0.45	0.7584	0.0018	1.38	0.38	1677	0.07	0.08
6134	0.7568	0.0045	1.56	0.41	1609	0.015	0.07	0.7560	0.0091	1.59	1.43	1735	0.007	0.05
6135	0.755	0.0028	1.58	0.25	1632	-0.02	0.05	0.7531	0.0026	1.63	0.36	1598	-0.03	0.01
*6163	0.7497	0.001	1.39	0.1	3601	0.06	1.1	0.7486	0.0016	1.58	0.23	7004	0.06	1.1
AVERAGE	0.7508	0.00088	1.428	0.0855				0.7531	0.0011	1.545	0.1685			
=====														
EAST	EMAX=0.780							EMAX=0.769						
6149	0.7570	0.0064	1.49	0.63	1514	-0.28	0.34							
*615051	0.7632	0.001	1.2	0.13	1477	0.17	0.45	0.7609	0.003	1.33	0.9	1575	0.08	1.1
*6162	0.7647	0.0011	1.22	0.15	1510	0.26	0.56	0.7558	0.0068	1.55	1.22	1512	0.08	0.27
6143	0.7675	0.0025	1.24	0.42	1379	0.27	0.43							
AVERAGE	0.7641	0.00071	1.216	0.0945				0.7600	0.0027	1.407	0.7242			
=====														
EAST + WEST AVERAGE	0.7589	0.00055	1.332	0.0634				0.7540	0.001	1.538	0.1641			

linear. Hence a change in these parameters would lead to no substantial qualitative change in our results.

Figure 4.2 shows the trend of the power with data cut off closer and closer to threshold for data from each side separately and for both sides combined. We see the discrepancy between east and west here. The combined plot is essentially the same as the west side because the values are weighted averages and the weights assigned to the west side runs are generally larger.

These data imply that the power law changes in the region between threshold and 0.8 eV, but I am reluctant to draw any conclusions from this data particularly in comparison to the 1986 data. These data are not inconsistent with a power of 1.5 at threshold.

The 1985 zero field runs with fitted curves are presented in Appendix I.

1985 σ Polarization Field Data

These data were analyzed in 1986 by fitting with the Armstrong formula, equation 41, even though it should not be a good descriptor of the physics. Now that we have in hand the theory of Rau and Wong the data will be reanalyzed and published elsewhere. For the time, the Armstrong fits allow us to take a systematic look at the data.

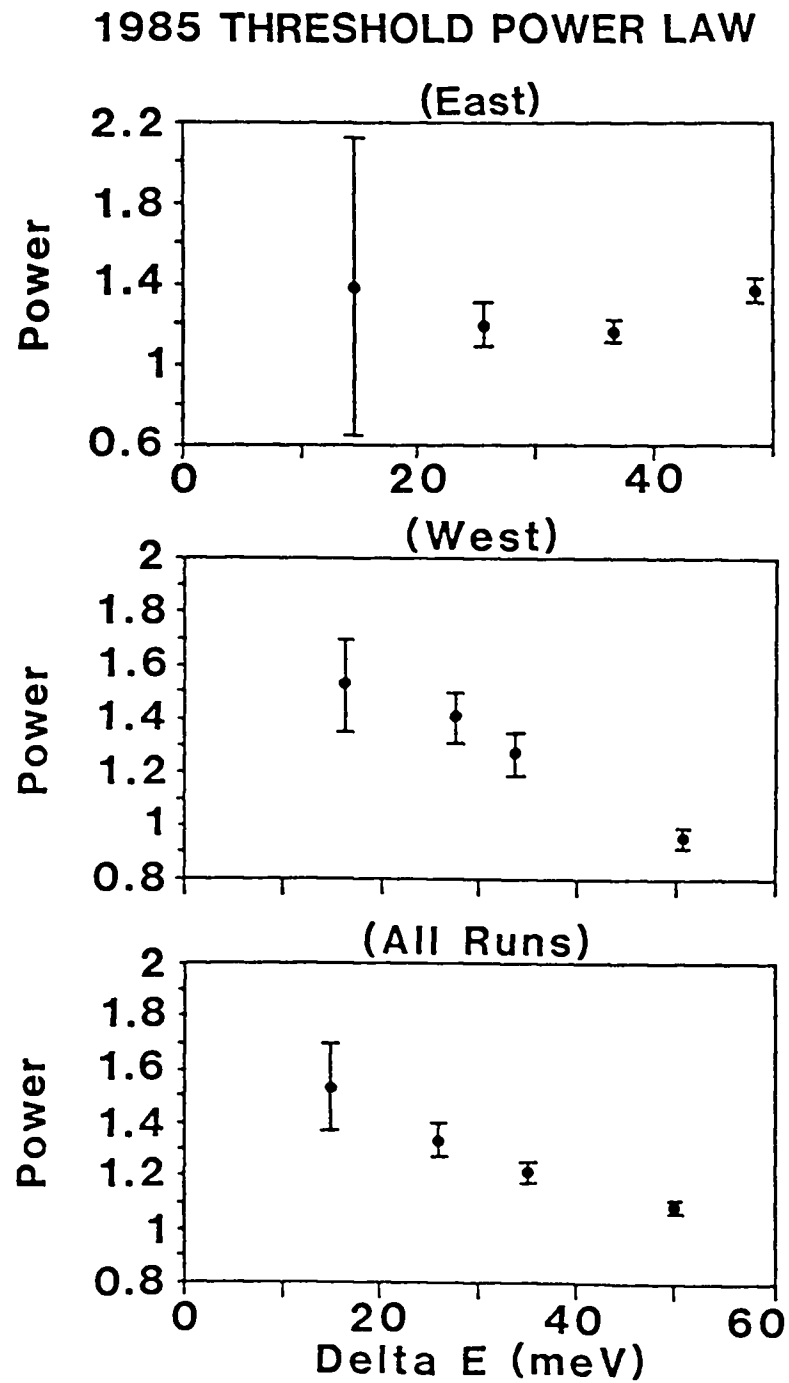


Figure 4.2 1985 threshold power law. Delta E is the distance in energy above threshold that the data sets were cut off.

Table 3 displays the results for all 1985 data. As expected we see a lowering of threshold and an increase in power. The classical threshold for each field value is given at the top of the each column.

In Figure 4.3 we see a series of data runs showing the progressive change in the cross section as the field is increased.

The fitted powers are not consistent within each field value although the 1.32 MV/cm runs do show an unusual consistency if we ignore runs 6138 and 6144 which are anomalous with respect to the other other runs in the series. The power of all three 1 MV/cm runs is not consistent with the trend of the data. Figure 4.4 graphs the change in power and threshold as the field is increased. The apparent change in direction of the curves is attributed primarily to three runs which seem inconsistent. At 1.18 Mv/cm there are only two data points and there both runs do not follow the trend. At 1.32 MV/cm run 6138E skews the weighted average strongly but it is so much different from the rest that we really must question its validity.

All of the 1985 field runs are presented in Appendix 2.

ANALYSIS OF 1986 DATA

Once we had the best values for encoder zero and steps per degree we could refit the zero field data using the

TABLE 3
1985 DATA
SUMMARY OF ALL RUNS (cutoff approximately 0.805 eV)

ELECTRIC FIELD (MV/cm)		0	0.35	0.68	1	1.18	1.32										
CLASSICAL																	
THRESHOLD (eV)		0.7542	0.7307	0.7144	0.7003	0.6927	0.6871										
RUN #	THRESHOLD (std dev)	POWER (std dev)	RUN #	THRESHOLD (std dev)	POWER (std dev)	RUN #	THRESHOLD (std dev)	POWER (std dev)	RUN #	THRESHOLD (std dev)	POWER (std dev)	RUN #	THRESHOLD (std dev)	POWER (std dev)	RUN #	THRESHOLD (std dev)	POWER (std dev)
6149E	0.76571	1.33	6148E	0.7578	2.05	6141E	0.7116	3.21	6140E	0.6618	5.11	6145E	0.692	3.01	6138E	0.7632	1.65
	0.0015	0.09		0.0104	0.78		0.0204	1.07		0.0303	1.5		0.0118	0.52		0.0012	0.16
*615051E	0.7616	1.36	*6161E	0.737	2.43	6147E	0.6551	6.54	6146E	0.6735	4.03	6130W	0.7115	2.15	6144E	0.6245	5.35
	0.0007	0.07		0.0034	0.21		0.059	3.35		0.0145	0.74		0.0089	0.41		0.0187	0.81
*6162E	0.7609	1.47	6142E	0.7648	1.38	*615960E	0.6911	3.31	6131W	0.6346	5.14				*615253E	0.6596	3.04
	0.001	0.09		0.0052	0.41		0.0049	0.23		0.0332	1.43					0.0051	0.18
6143E	0.7685	1.28	6133W	0.742	1.86	6132W	0.6566	4.18							*615455E	0.6384	3.99
	0.0014	0.18		0.0034	0.24		0.0243	1.04								0.0068	0.25
6126W	0.7454	2.29													6128W	0.6467	3.95
	0.0036	0.3														0.0196	0.72
6127W	0.7505	1.77													6129W	0.6664	3.83
	0.0029	0.24														0.0302	1.21
6134W	0.7509	1.69													6136W	0.6434	3.87
	0.0074	0.34														0.0106	0.38
6135W	0.7537	1.6															
	0.0026	0.13															
*6163W	0.7539	0.92															
	0.0004	0.03															
*THESE RUNS WERE TAKEN WITH 40 STEPS PER ANGLE THE REST WITH 200 STEPS PER ANGLE																	
WTD AVG	0.7571	1.1		0.7445	2.08		0.6907	3.36		0.6664	4.4006		0.7044	2.48		0.7521	2.76
STD DEV	0.0003	0.02		0.0021	0.14		0.0047	0.22		0.0122	0.6		0.0071	0.32		0.0011	0.1
AVERAGES WITH 6163, 6138, 6144 NOT INCLUDED																	
WTD AVG	0.7618	1.43		0.7445	2.08		0.6907	3.36		0.6664	4.4		0.7044	2.48		0.6509	3.45
STD DEV	0.0005	0.04		0.0021	0.14		0.0047	0.22		0.0122	0.6		0.0071	0.32		0.0037	0.13

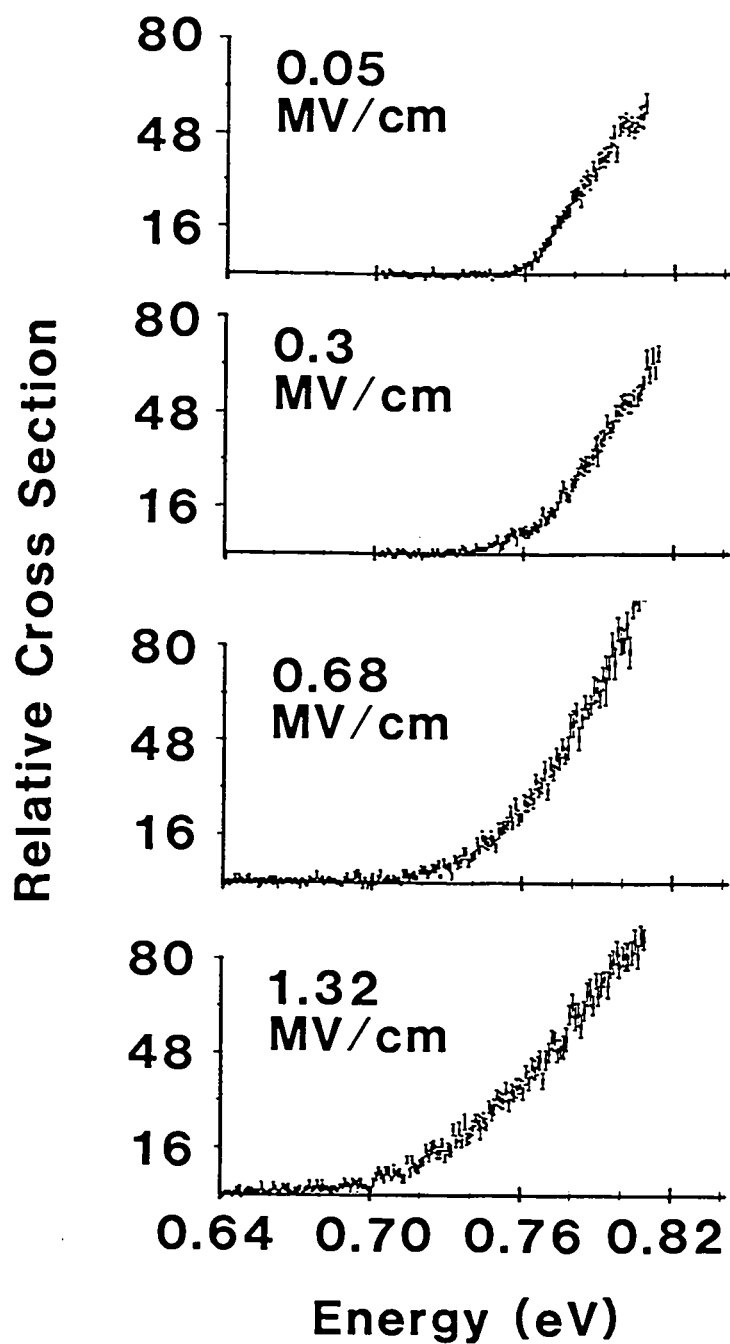
1985 σ POLARIZATION FIELD DATA

Figure 4.3 Series of sigma polarization runs at different fields.

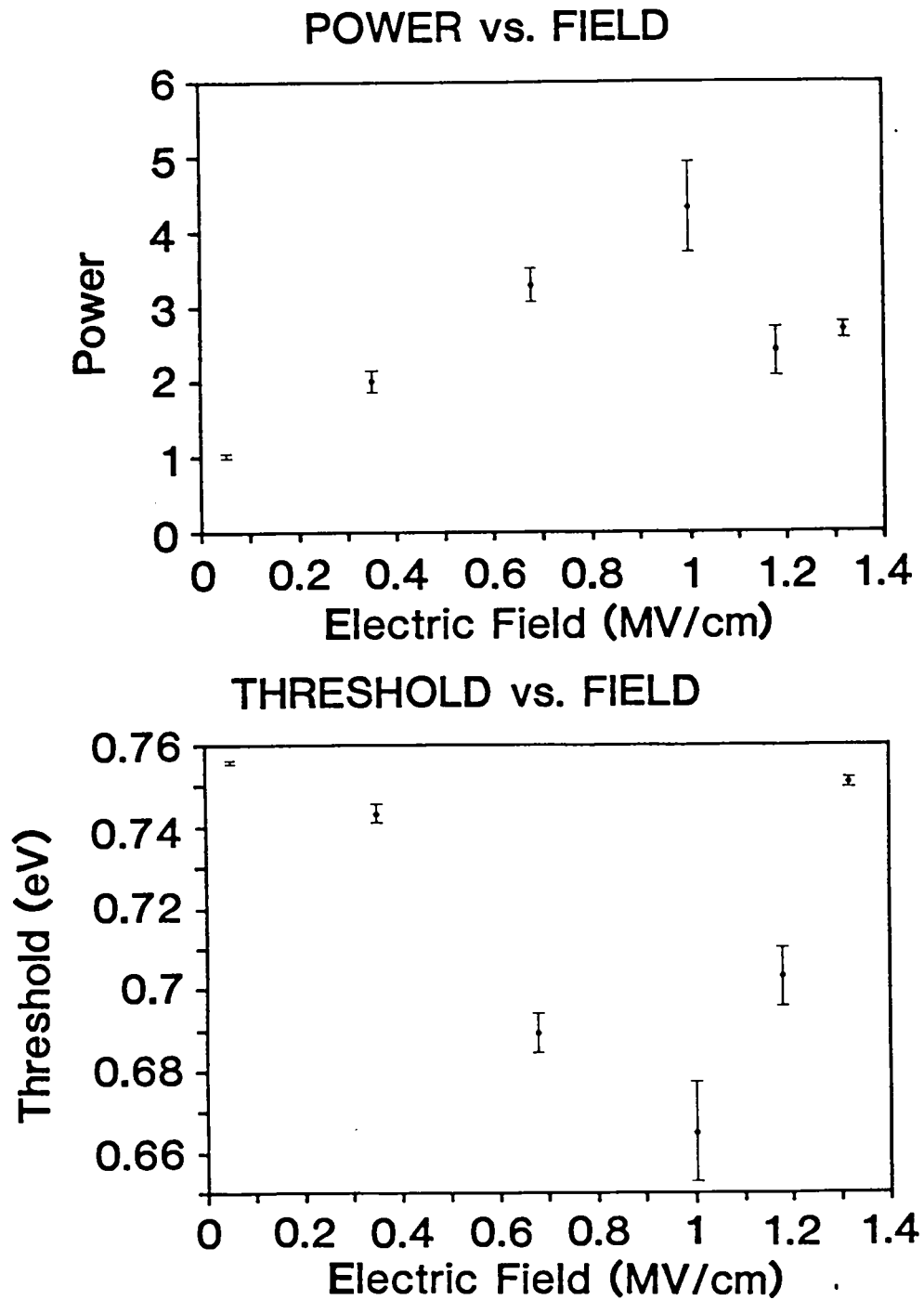


Figure 4.4 Effect of electric field on power and threshold.

new numbers and find the power dependence of the cross section function.

The length of time data is taken during the run is directly determined by the ion current. The data are therefore, already normalized to beam current. Furthermore, as discussed in Chapter 3, examination of the laser normalization data leads us to believe that it is unreliable. Laser normalization is left out of the calculation making the explicit assumption that less error is introduced by leaving it out than by including it.

Occasional data points for background and ion current fall several standard deviations outside the average. All runs were filtered to eliminate data points which corresponded to either background or ion current values more than 3σ away from the mean. In a normal distribution one would expect one point out of 370 to be that far away from the mean. In our data we often find two or three points out of one hundred are cut.

The error assigned to each data point is the square root of the sum of the counts taken while the data gate was open and the counts taken while the background gate was open.

After we installed the larger pole tips on the magnet we found that we occasionally rotated the assembly far enough for the halo of the ion beam to scrape the magnet. This gave enormous signals which were eliminated from the

data by cutting all data with energy less than 0.705 eV for runs 297 and later. This effect can be seen in the plot of runs 326,327,328 in Appendix 3 where the beam tune must have been such that the problem occurred at a larger angle.

The value of the electric field which appears on all of the 1986 data is the value at the angle corresponding to the zero field threshold of 0.7542 eV.

1986 "Zero Field" Data

Most of this "zero field" data is not strictly taken at zero field, just as in 1985. The 1986 magnet had a smaller residual field. Using the small pole tips the residual electric field was approximately 2.4 kV/cm which would shift the classical photodetachment threshold downward by 0.1 mV, not enough to affect our experiment. Using the large pole tips the field was approximately 4.8 kV/cm which gives a shift of the order of 0.5 mV. Again this shift is less than our experimental resolution but certainly large enough to be considered in the next generation of experiments. These fields are of the order of 10^{-6} atomic units so they are a better approximation to zero field than the data sets from 1985.

All runs were cut off at the same energy value for an initial look at the power law. With a maximum energy value of 0.80 eV the average fitted power was 1.455(33).

By successively truncating the data sets closer and closer to threshold we see a consistency that was not there in the 1985 data. Figure 4.5 shows the results of this analysis. The plot labeled "all runs" includes the two truly zero field runs taken at 318 MeV when the potential well was in place. These two runs yield lower values for the power than expected, both are 1.41(8). This is not inconsistent with the Wigner prediction of 1.5.

Table 4 displays the results of the zero field fits and Figure 4.6 is an ideogram which shows that the data is very consistent. The 1986 zero field data is all presented in Appendix 3. All of these data files have been arbitrarily normalized to make them easily comparable. The apparent lack of error bars is due to the fact that each data point is the result of several thousand counts. Then an error taken as \sqrt{n} is of the order of a few percent and is too small to be obvious with the plotting package used to produce the graphs.

Runs 319 and 320 were intended to be high statistics looks at threshold to help find the power law. Unfortunately, we did not take enough data before reaching threshold so that the fitting program has a great deal of difficulty finding a good fit.

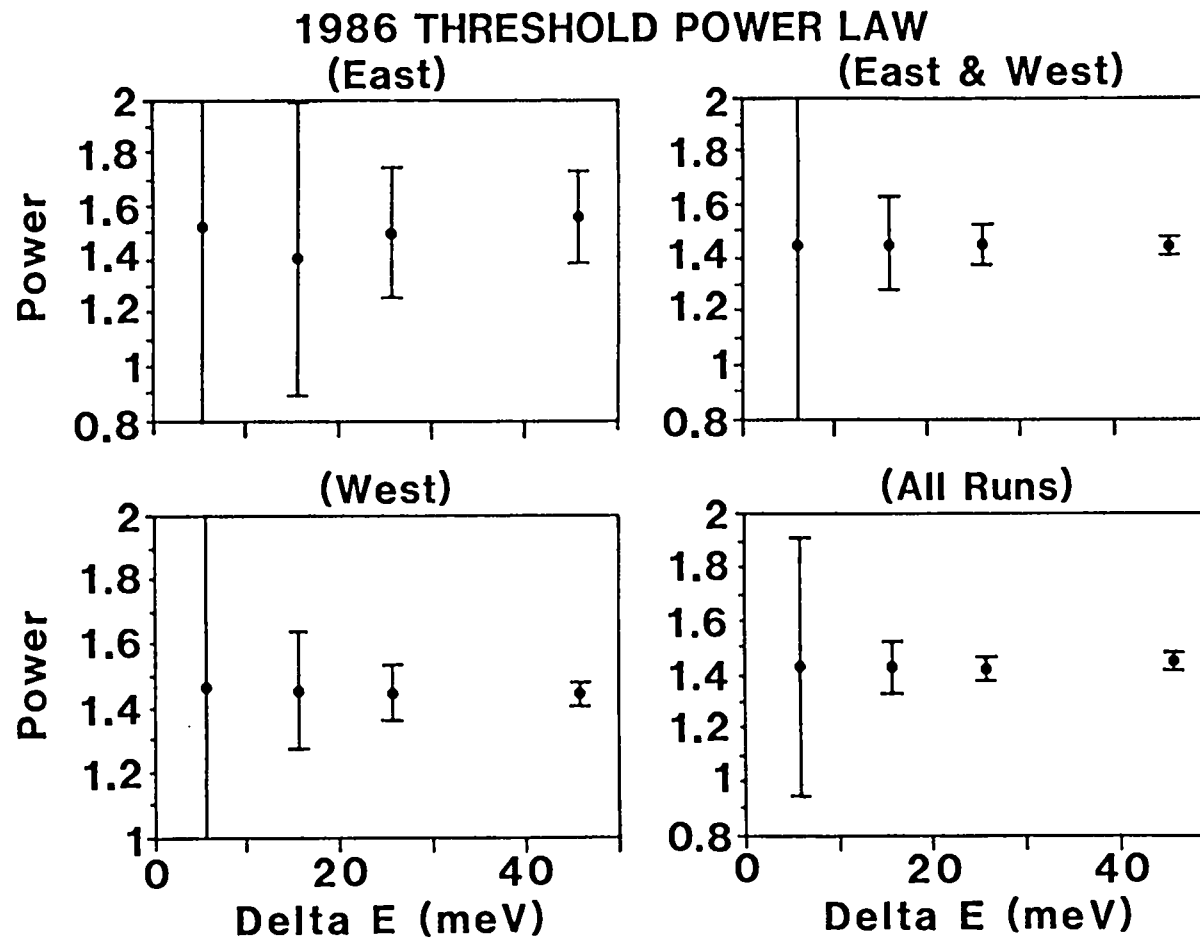


Figure 4.5 1986 threshold power law. Delta E is the distance in energy above threshold that the data sets were cut off. "All runs" includes the two true zero field runs taken at 318 MeV using the potential well.

TABLE 4
 (Continued on next page)
 1986 DATA

SUMMARY OF ZERO FIELD FITS WITH SUCCESSIVELY SMALLER EMAX
 ENCODER ZERO 100359 STEPS PER DEGREE 576.4

RUN	EMAX=0.8eV							EMAX=0.78eV								
	EO	STD DEV	POWER	STD DEV	AMPL	BKGND	REDUCED	CHI SQ	EO	STD DEV	POWER	STD DEV	AMPL	BKGND	REDUCED	CHI SQ
202	0.754	0.0015	1.43	0.087	71025	90	0.11		0.7545	0.0029	1.41	0.3	71082	90	0.15	
210	0.7544	0.001	1.51	0.062	94042	140	0.16		0.7544	0.0015	1.51	0.16	94035	140	0.12	
226227	0.7542	0.0012	1.38	0.0715	55031	280	0.33		0.7542	0.0013	1.38	0.13	55059	280	0.13	
281282	0.7533	0.0124	1.44	0.0757	102934	306	1.15		0.7542	0.0019	1.42	0.2	102085	307	1.2	
302303	0.7570	0.0016	1.43	0.113	47453	46	0.33		0.7575	0.0027	1.43	0.32	49110	46	0.36	
317318	0.7440	0.0028	1.59	0.139	42993	82	0.63		0.7452	0.0039	1.57	0.31	43103	82	0.63	
319									0.7544	0.0055	1.79	0.58	115001	40	0.46	
320									0.7473	0.0105	1.84	0.67	104930	29	0.5	
WEST AVG	0.7541	0.000612	1.451	0.0334					0.7541	0.0008	1.451	0.079				
230E									0.7534	0.0026	1.49	0.262	45053	580	0.16	
246247E	0.7579	0.0026	1.54	0.174	31825	91	0.13		0.7568	0.0054	1.56	0.625	32007	91	0.13	
EAST AVG	0.7579	0.0026	1.543	0.174					0.7540	0.002342	1.498	0.2416				
EAST+WEST																
AVERAGE	0.7543	0.000596	1.455	0.0328	(excluding 473, 474)				0.7541	0.000073	1.46	0.0754				
473 (318 MeV)									0.7529	0.00078	1.41	0.078	566065	380	8.5	
474 (318 MeV)									0.7529	0.00078	1.406	0.078	450071	350	8.8	
ALL RUNS	0.7543	0.000596	1.455	0.0328					0.7533	0.000439	1.423	0.0445				

TABLE 4 CONTINUED

1986 DATA

SUMMARY OF ZERO FIELD FITS WITH SUCCESSIVELY SMALLER EMAX

ENCODER ZERO 100359

STEPS PER DEGREE 576.4

RUN	EMAX=0.77eV							EMAX=0.76eV						
	EO	STD DEV	POWER	STD DEV	AMPL	BKGND	REDUCED CHI SQ	EO	STD DEV	POWER	STD DEV	AMPL	BKGND	REDUCED CHI SQ
202	0.7533	0.006	0.15	0.963	68292	101	0.12	0.7535	0.0834	1.42	23	60330	101	0.15
210	0.7547	0.0021	1.5	0.342	100596	134	0.11	0.7561	0.0044	1.4	2.09	99973	134	0.11
226227	0.7547	0.0017	1.37	0.285	55081	280	0.11	0.7532	0.0054	1.44	1.79	55056	280	0.11
281282	0.7515	0.0039	1.49	0.555	109990	290	1.3							
302303	0.7577	0.0045	1.41	0.913	46885	46	0.35	0.7503	0.006	1.4	1.58			
317318	0.7443	0.0058	1.54	0.617	37055	80	0.67	0.7434	0.0108	1.58	1.691	37864	81	0.69
319	0.7541	0.0096	1.8	1.74	115062	40	0.43							
320	0.7515	0.0065	1.74	0.899	101286	39	0.4							
WEST AVG	0.7541	0.001132	1.458	0.1808				0.7531	0.0029	1.458	0.8793			
230E	0.7552	0.0035	1.43	0.579	45049	580	0.16	0.7528	0.013	1.52	4.22	45733	579	0.17
246247E	0.7572	0.0091	1.54	1.8	31397	91	0.13							
EAST AVG	0.7554	0.003266	1.439	0.5511				0.7528	0.013	1.524	4.22			
EAST+WEST														
AVERAGE	0.7542	0.0011	1.46	0.1718				0.7530	0.0028	1.46	0.8608			
473 (318 MeV)	0.7526	0.0011	1.42	0.17	566006	380	8.5	0.7526	0.0025	1.42	0.828	900019	400	5.9
474 (318 MeV)	0.7526	0.00114	1.416	0.17	450056	350	8.4	0.7525	0.0025	1.42	0.828	450062	350	7.3
ALL RUNS	0.7532	0.000636	1.429	0.0984				0.7527	0.001493	1.432	0.4841			

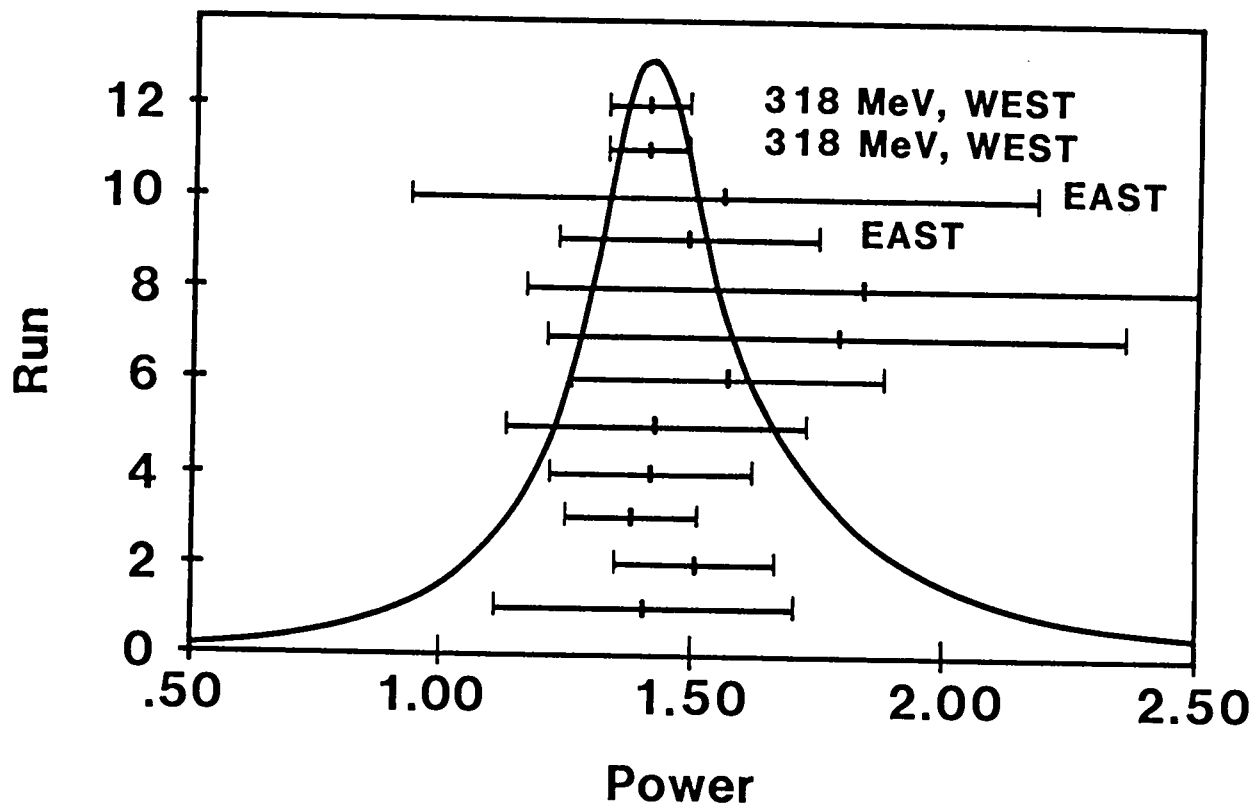


Figure 4.6
IDEOGRAM 1986 ZERO FIELD DATA

1986 σ Polarization Field Data

The eight data runs in this category serve primarily to verify the polarization dependence of the ripple phenomenon that we will look at next. The electric field strengths were not great enough to cause the obvious shifts in apparent threshold that can be seen in the 1985 σ data.

I fit these runs with the Armstrong formula, equation 41, but the results are not any more consistent than the 1985 results. This could well be due to the fact that equation 41 is not the proper form to describe this phenomenon. In fact, the fits give results which we know cannot be correct. The higher field runs fit with a threshold value higher than the low field runs.

Appendix 4 contains the 1986 σ data with fits to equation 41. Table 5 is a summary of the 1986 σ data.

1986 π Polarization Field Data

Now, given our best values for encoder zero and steps per degree we were ready to look at the ripple data. Figure 4.7 gives a quick view of the π data compared to the σ data.

The analysis of the ripple data was aimed at characterizing the location of the minima of the ripples. Fitting to the Reinhardt theory was impractical on two counts. There exists only one free parameter, an

TABLE 5
 1986 DATA
 SUMMARY OF SIGMA POLARIZATION RUNS

ELECTRIC FIELD (kV/cm)	RUN	THRESHOLD (std dev)	POWER (std dev)
56	225	0.7555 0.0009	1.42 0.04
56	233	0.7429 0.0024	1.71 0.17
72	285286	0.7438 0.0007	1.48 0.03
92	315316	0.7404 0.0029	1.7 0.05
114.3	313314	0.7424 0.0028	1.74 0.07
130.1	312	0.7643 0.0013	1.24 0.02
143.4	310	0.7577 0.0014	1.35 0.02
143.4	326327328	0.7626 0.0018	1.39 0.03

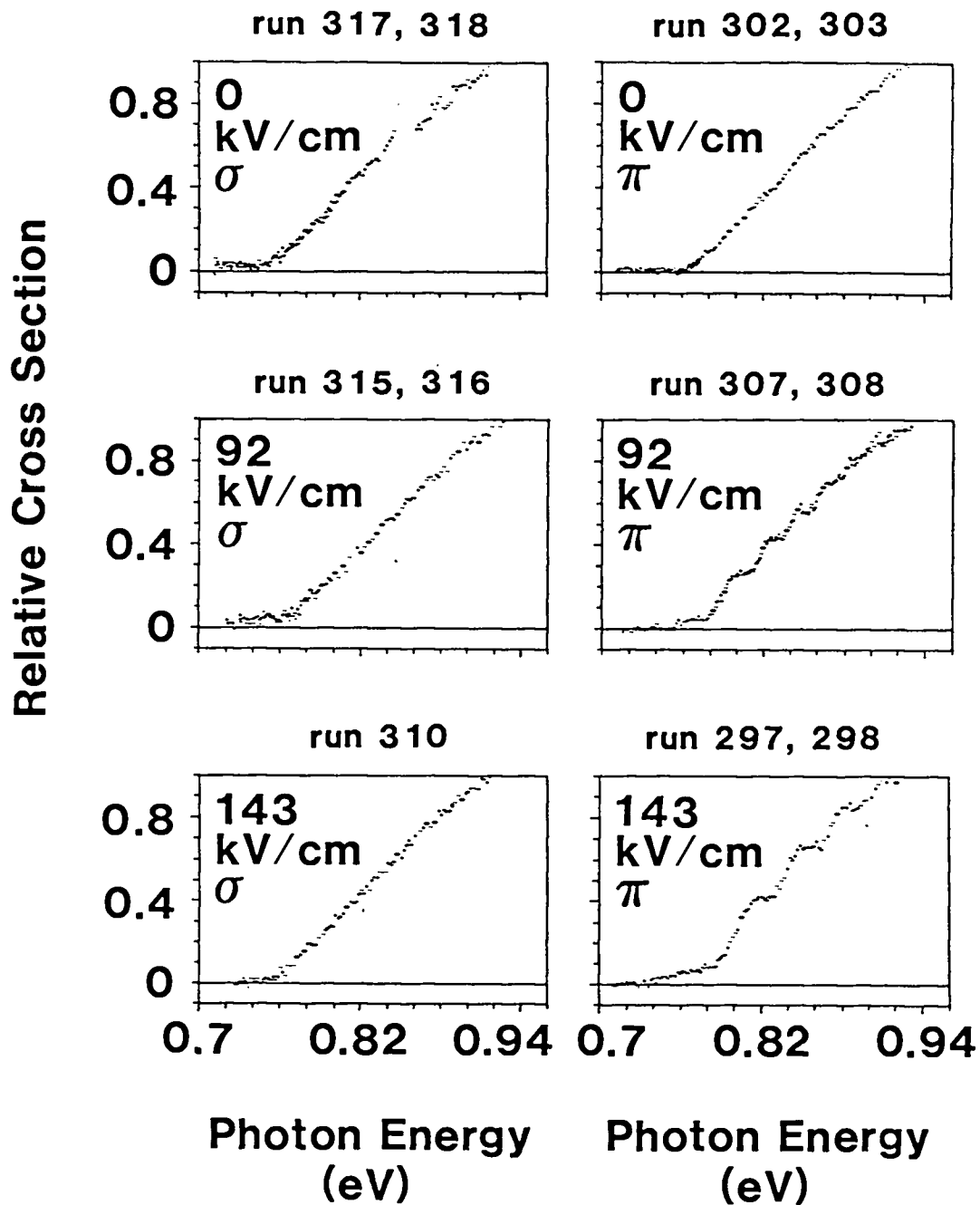


Figure 4.7 Overview of 1986 data comparing sigma and pi polarization at different fields.

amplitude factor, which would have no physical content since our experiment measures only relative cross section and not absolute. Secondly, each calculation of the theoretical function takes about 13.5 hours of CPU time on our Micro-Vax II. The calculation for a constant field takes only a few minutes but to model our experiment we must recalculate the relevant complex matrices at each angle since the value of the electric field changes with angle. Figure 4.8 shows curves generated with Reinhardt's computer program, modified to model our experiment, superimposed on our data.

Since the ripples are a phenomenon superimposed on the zero field cross section it seems reasonable to subtract the zero field form from the ripple data to expose the ripple structure. This subtraction makes more apparent the exact location of the minima and maxima of the ripple structure. Figure 4.9 shows an example of the method.

The theory of Rau and Wong (1987) leads us to expect that the oscillations should be symmetric about the zero field curve but this does not appear to be the case in our data as it is presented here. This is at least partly an artifact of the method used to normalize the data with respect to the calculated zero field curve. The data are normalized so that the maximum point is the same value as the maximum point of the zero field curve and so that the

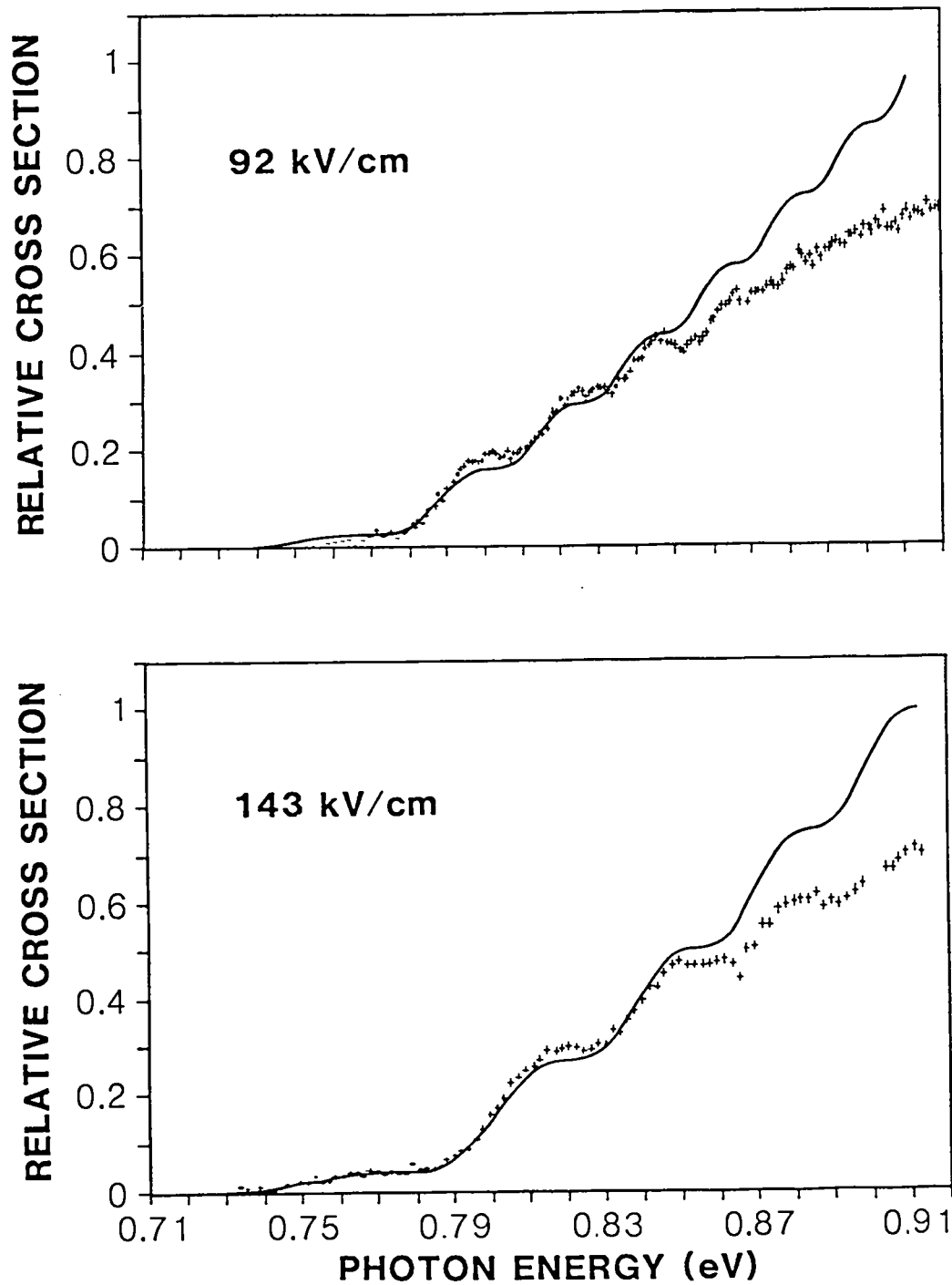


Figure 4.8 Relative cross sections for pi polarization compared with the theory of W. P. Reinhardt.

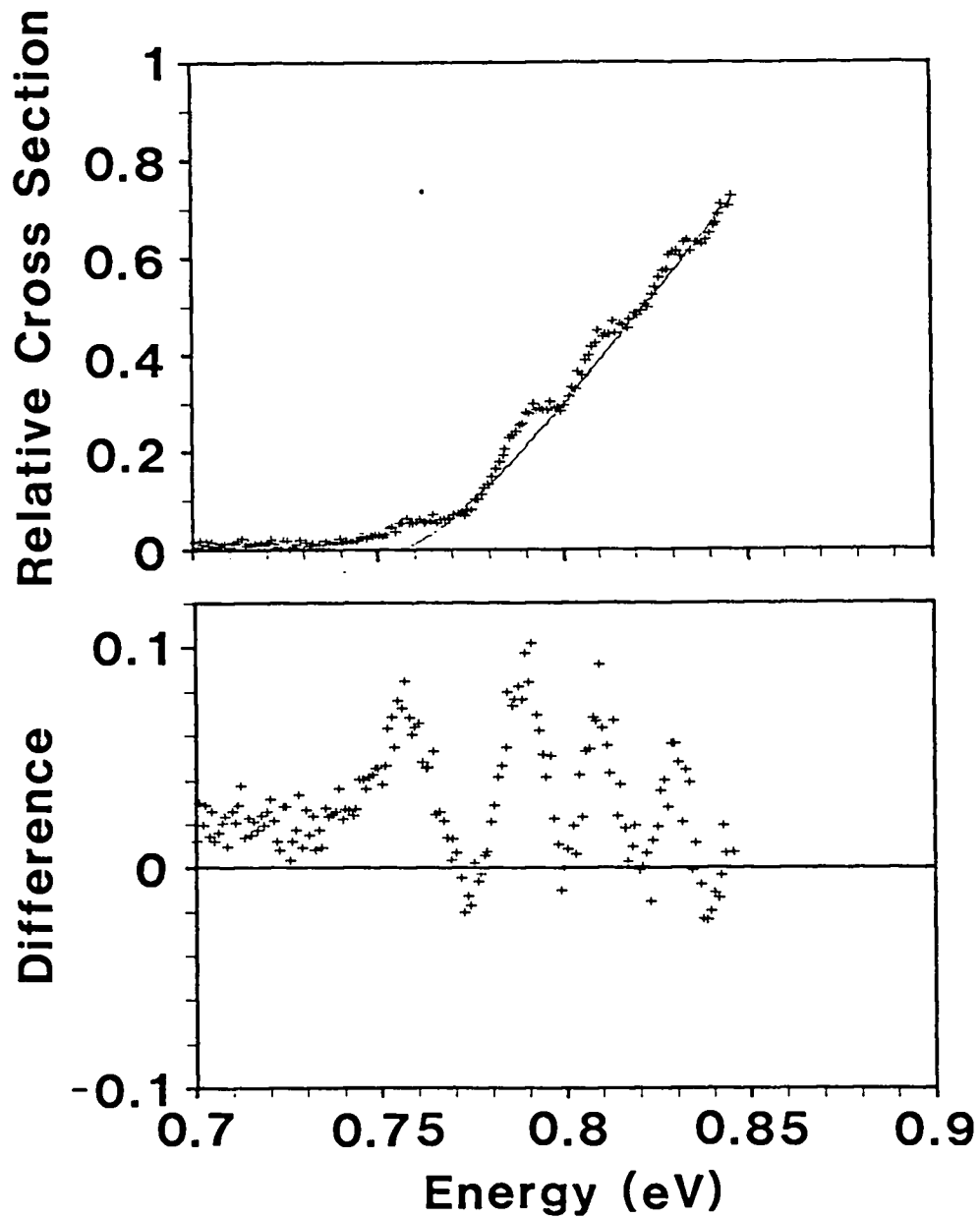
42 kV/cm π POLARIZATION

Figure 4.9 Example of the subtraction method.

maximum cross section value is proportional to the maximum energy.

Figure 4.10 shows the 143 kV/cm cross section from Figure 4.8 now compared to the theory of Rau and Wong. In this case the data have been normalized to the theory which gives an absolute cross section. All of the π polarization data is presented in Appendix 5.

Once the subtraction was done we used the standard ocular interpolation method to determine the location of minima. Additionally, we attempted to fit the minima individually with a gaussian. The gaussian shape is not a good descriptor of the shape of the ripples but it fit most of them easily, giving reasonable values for the minima with a useful error. About one half the fits converged and they are generally in very good agreement with the eye. Both the gaussian minima and those determined by eye are included in the data presented in Table 6.

Table 6 also includes values, labeled a' and n , calculated from the data. The a' values may be compared to the simple theory of Bryant et al. (1987) where the energy of the minima are given by equation 21. The a' values were calculated using

$$a'_s = \frac{(E_{\min} - 0.7542\text{eV})}{-(eF)^{2/3} \left[\frac{\hbar^2}{2m} \right]^{1/3}} . \quad (43)$$

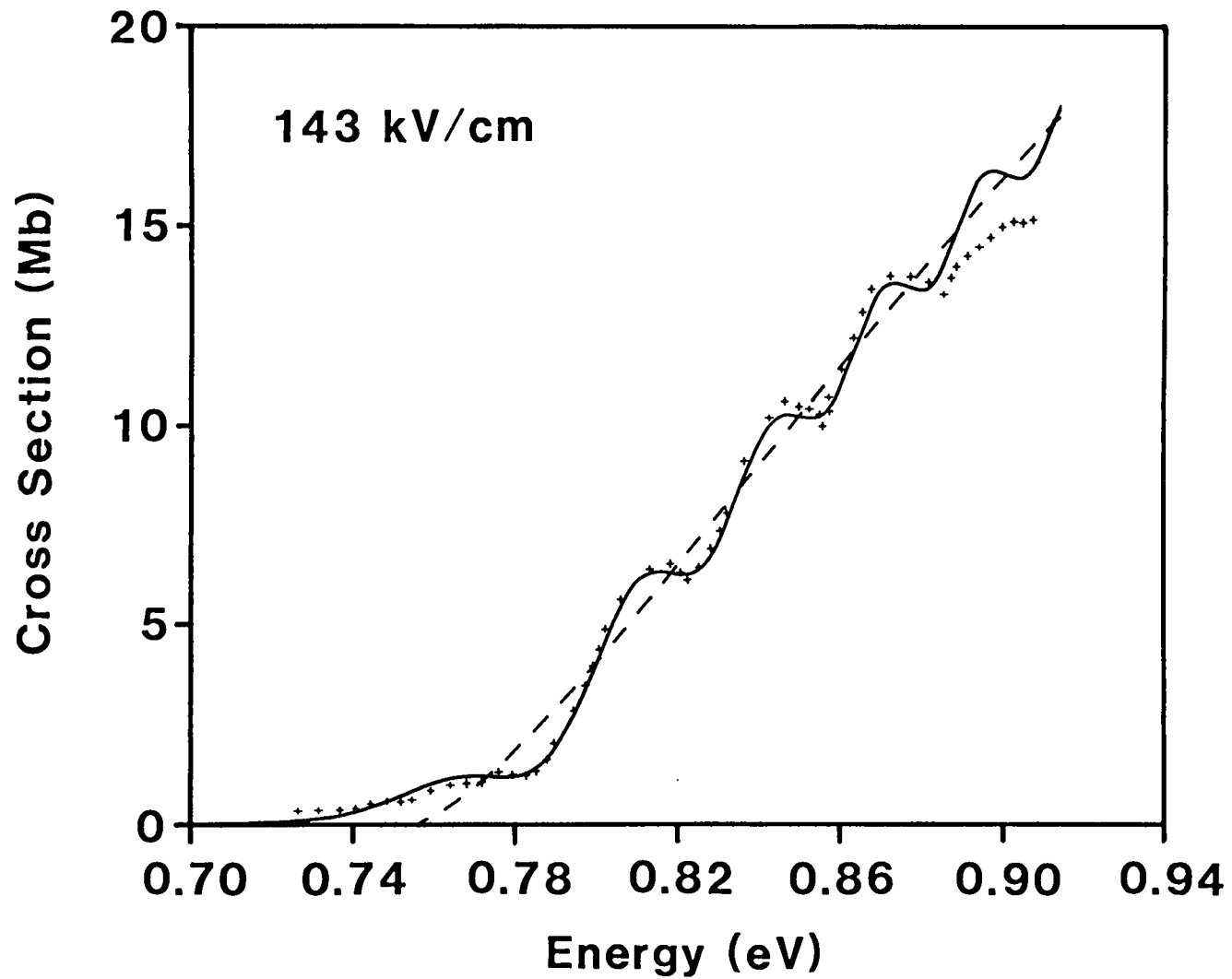


Figure 4.10 Relative cross section for pi polarization compared with the theory of Rau and Wong.

TABLE 6A

RIPPLE SUMMARY

Shows location of minima determined by eye and by fitting. Includes minima of Reinhardt's theoretical cross section (run numbers labeled kv/cm) as well as a's to compare with Airy function zeros and n values to compare with Rau and Wong's minima. One atomic unit of electric field equals 5.1×10^{-9} V/cm.

RUN	FITTED			FIELD			RUN	FITTED			FIELD		
	MIN1MA	MIN1MA	ERROR	(AU X10-5)	A'S	N		MIN1MA	MIN1MA	ERROR	(AU X10-5)	A'S	N
(eV)							(eV)						
207000	0.7726	0.7729	0.0005	1.11	1.709	0.474	241000	0.8421			1.18	7.827	4.647
207000	0.7942			1.13	3.664	1.488	241000	0.8537			1.19	8.803	5.543
207000	0.8095			1.15	5.018	2.385	249250	0.7758			1.11	2.002	0.601
208209	0.769	0.7703	0.0005	1.10	1.378	0.343	249250	0.7968			1.13	3.896	1.632
208209	0.792	0.7942	0.0005	1.13	3.467	1.370	249250	0.8184	0.8125	0.0002	1.16	5.795	2.960
208209	0.8104	0.8113	0.0003	1.15	5.097	2.442	249250	0.8279			1.17	6.616	3.611
208209	0.8256	0.8246	0.0005	1.16	6.418	3.450	252253	0.7754			1.28	1.789	0.508
211000	0.7696			0.83	1.736	0.485	252253	0.8007	0.8015	0.0005	1.31	3.862	1.611
211000	0.785			0.84	3.438	1.353	252253	0.82	0.82	0.0003	1.33	5.402	2.664
211000	0.7971			0.85	4.752	2.198	252253	0.8368			1.35	6.716	3.693
212213	0.7687	0.7675	0.0003	0.83	1.636	0.444	252253	0.85			1.37	7.732	4.563
212213	0.7986	0.7984	0.0003	0.85	4.914	2.311	260261	0.7761			1.11	2.030	0.613
212213	0.8106	0.8117	0.0003	0.86	6.196	3.273	260261	0.7982			1.14	4.021	1.711
212213	0.8219	0.8217	0.0003	0.87	7.388	4.261	260261	0.8289			1.17	6.702	3.681
212213	0.8334			0.88	8.585	5.338	260261	0.8458			1.19	8.140	4.928
212213	0.8434			0.89	9.615	6.327	262263	0.7746			1.11	1.892	0.552
212213	0.8519			0.89	10.48	7.202	262263	0.7957			1.13	3.798	1.571
214215	0.772	0.7678	0.0004	1.11	1.654	0.451	262263	0.8126			1.15	5.290	2.582
214215	0.7925	0.7925	0.0003	1.13	3.512	1.397	262263	0.828			1.17	6.624	3.618
214215	0.8094	0.8096	0.0003	1.15	5.009	2.379	270712	0.7741			1.28	1.681	0.462
214215	0.8257	0.8255	0.0006	1.16	6.426	3.457	270712	0.7979			1.31	3.636	1.471
241000	0.7745			1.11	1.883	0.548	270712	0.8146			1.33	4.975	2.354
241000	0.7938			1.13	3.628	1.466	270712	0.8322			1.35	6.359	3.402
241000	0.8141			1.15	5.421	2.678	270712	0.8461			1.37	7.433	4.301
241000	0.8293			1.17	6.736	3.710	270712	0.8638			1.39	8.781	5.521

TABLE 6A CONTINUED

RUN	FITTED			FIELD			RUN	FITTED			FIELD			RUN	FIELD			
	MIN1MA (eV)	MIN1MA	ERROR	(AU X10-5)	A'S	N		MIN1MA (eV)	MIN1MA	ERROR	(AU X10-5)	a'	N		MIN1MA (eV)	(AU X10-5)	a'	N
270712	0.8784			1.40	9.875	6.585	304056	0.8485	0.8483	0.0004	2.44	5.180	2.502	92kV/cm	0.783	1.86	1.90	0.555
287288	0.7733	0.7724	0.0002	1.44	1.491	0.386	304056	0.8728	0.8238	0.0003	2.49	6.432	3.461	92kV/cm	0.811	1.91	3.68	1.499
287288	0.7984	0.8002	0.0002	1.47	3.396	1.328	304056	0.8959	0.898	0.0004	2.54	7.596	4.442	92kV/cm	0.835	1.95	5.16	2.491
287288	0.8195	0.82	0.0004	1.50	4.954	2.340	307308	0.7779	0.7726	0.0045	1.82	1.581	0.422	92kV/cm	0.855	1.98	6.37	3.419
287288	0.8384			1.53	6.319	3.370	307308	0.8094	0.8094	0.0005	1.88	3.607	1.453	92kV/cm	0.875	2.01	7.56	4.419
289901	0.7786			1.69	1.709	0.474	307308	0.8338	0.8356	0.0005	1.92	5.128	2.464	92kV/cm	0.894	2.04	8.67	5.420
289901	0.8066			1.74	3.607	1.454	307308	0.8538	0.856	0.0006	1.95	6.367	3.410	114kV/cm	0.788	2.28	1.94	0.576
289901	0.8248			1.77	4.808	2.237	307308	0.8719	0.8742	0.0005	1.97	7.453	4.317	114kV/cm	0.82	2.39	3.67	1.494
289901	0.8483			1.80	6.323	3.374	329330	0.7737	0.7691	0.0004	1.12	1.795	0.510	114kV/cm	0.848	2.45	5.15	2.480
289901	0.861			1.82	7.128	4.038	329330	0.7941			1.15	3.627	1.466	114kV/cm	0.873	2.5	6.43	3.465
297298	0.7883			2.91	1.669	0.457	329330	0.8115	0.8072	0.017	1.16	5.152	2.482	114kV/cm	0.895	2.54	7.54	4.400
297298	0.8302			3.02	3.630	1.467	329330	0.8287	0.8305	0.0008	1.18	6.631	3.624	130kV/c	0.79	2.63	1.87	0.544
297298	0.8641			3.11	5.147	2.478	329330	0.843	0.8404	0.0005	1.20	7.843	4.661	130kV/c	0.827	2.72	3.72	1.525
297298	0.8927			3.18	6.391	3.429	331332	0.772			1.12	1.642	0.446	130kV/c	0.857	2.79	5.17	2.496
299300	0.789	0.7785	0.005	2.64	1.818	0.520	331332	0.7951			1.15	3.716	1.520	130kV/c	0.884	2.85	6.43	3.467
299300	0.828	0.8273	0.0022	2.74	3.761	1.547	331332	0.8131			1.17	5.293	2.584	130kV/c	0.909	2.90	7.58	4.434
299300	0.86	0.862	0.0005	2.81	5.302	2.590	331332	0.8286			1.18	6.622	3.616	143kV/cm	0.793	2.90	1.90	0.556
299300	0.888	0.8883	0.0007	2.87	6.611	3.607	331332	0.8416			1.2	7.723	4.555	143kV/cm	0.832	3.00	3.72	1.525
299300	0.919	0.9168	0.0013	2.94	8.013	4.814	333334	0.7923			3.35	1.696	0.469	143kV/cm	0.864	3.08	5.16	2.491
299300	0.941	0.9405	0.0008	2.98	9.002	5.731	333334	0.8389			3.5	3.666	1.489	143kV/cm	0.893	3.15	6.43	3.462
299300	0.965	0.9686	0.0008	3.03	10.04	6.757	333334	0.8741			3.6	5.093	2.439	164kV/cm	0.797	3.37	1.89	0.554
299300	0.989	0.9901	0.0017	3.08	11.06	7.814	333334	0.911			3.7	6.541	3.550	164kV/cm	0.839	3.50	3.66	1.488
299300	1.008	1.0087	0.0015	3.11	11.88	8.697	333334	0.9426			3.78	7.748	4.576	164kV/cm	0.875	3.61	5.12	2.458
304056	0.78	0.7815	0.0008	2.3	1.477	0.381	333334	0.9713			3.85	8.818	5.556	164kV/cm	0.907	3.69	6.37	3.415
304056	0.82	0.8194	0.0002	2.4	3.663	1.487	333334	0.9954			3.90	9.701	6.412					

TABLE 6B

This is the same data displayed in Table 6a sorted by n and a'.
The electric field is given in atomic units X 10⁻⁵.

MINIMA FITTED FIELD							MINIMA FITTED FIELD						
N	A'	RUN	(eV)	MINIMA ERROR	FIELD		N	A'	RUN	(eV)	MINIMA ERROR	FIELD	
0.343	1.378	208209	0.769	0.7703	0.0005	1.10	1.328	3.396	287288	0.7984	0.8002	0.0002	1.47
0.381	1.477	304056	0.78	0.7815	0.0008	2.3	1.353	3.438	211000	0.785			0.84
0.386	1.491	287288	0.7733	0.7724	0.0002	1.44	1.370	3.467	208209	0.792	0.7942	0.0005	1.13
0.422	1.581	307308	0.7779	0.7726	0.0045	1.82	1.397	3.512	214215	0.7925	0.7925	0.0003	1.13
0.444	1.636	212213	0.7687	0.7675	0.0003	0.83	1.453	3.607	307308	0.8094	0.8094	0.0005	1.88
0.446	1.642	331332	0.772			1.12	1.454	3.607	289901	0.8066			1.74
0.451	1.654	214215	0.772	0.7678	0.0004	1.11	1.466	3.627	329330	0.7941			1.15
0.457	1.669	297298	0.7883			2.91	1.466	3.628	241000	0.7938			1.13
0.462	1.681	270712	0.7741			1.28	1.467	3.630	297298	0.8302			3.02
0.469	1.696	333334	0.7923			3.35	1.471	3.636	270712	0.7979			1.31
0.474	1.709	207000	0.7726	0.7729	0.0005	1.11	1.487	3.663	304056	0.82	0.8194	0.0002	2.4
0.474	1.709	289901	0.7786			1.69	1.488	3.664	207000	0.7942			1.13
0.485	1.736	211000	0.7696			0.83	1.489	3.666	333334	0.8389			3.5
0.508	1.789	252253	0.7754			1.28	1.491	3.669	164kV/c	0.839			3.50
0.510	1.795	329330	0.7737	0.7691	0.0004	1.12	1.507	3.695	114kV/c	0.82			2.36
0.520	1.818	299300	0.789	0.7785	0.005	2.64	1.520	3.716	331332	0.7951			1.15
0.544	1.873	130kV/c	0.79			2.63	1.523	3.721	92kV/cm	0.811			1.87
0.548	1.883	241000	0.7745			1.11	1.525	3.725	130kV/c	0.827			2.72
0.552	1.892	262263	0.7746			1.11	1.525	3.725	143kV/c	0.832			3.00
0.555	1.899	164kV/c	0.797			3.37	1.547	3.761	299300	0.828	0.8273	0.0022	2.74
0.556	1.901	143kV/c	0.793			2.90	1.571	3.798	262263	0.7957			1.13
0.564	1.920	92kV/cm	0.783			1.83	1.611	3.862	252253	0.8007	0.8015	0.0005	1.31
0.571	1.936	114kV/c	0.788			2.29	1.632	3.896	249250	0.7968			1.13
0.601	2.002	249250	0.7758			1.11	1.711	4.021	260261	0.7982			1.14
0.613	2.030	260261	0.7761			1.11	2.198	4.752	211000	0.7971			0.85

TABLE 6B CONTINUED

MINIMA FITTED				FIELD		MINIMA FITTED				FIELD		MINIMA FITTED				FIELD				
N	A' RUN	(eV)	MINIMA ERROR			N	A' RUN	(eV)	MINIMA ERROR			N	A' RUN	(eV)	MINIMA ERROR					
2.237	4.808	289901	0.8248		1.77	3.374	6.323	289901	0.8483		1.80	4.434	7.586	130kV/c	0.909		2.90			
2.311	4.914	212213	0.7986	0.7984	0.0003	0.85	3.402	6.359	270712	0.8322		1.35	4.440	7.594	114kV/c	0.895		2.51		
2.340	4.954	287288	0.8195	0.82	0.0004	1.50	3.410	6.367	307308	0.8538	0.856	0.0006	1.95	4.442	7.596	304056	0.8959	0.898	0.0004	2.54
2.354	4.975	270712	0.8146		1.33	3.422	6.383	164kV/c	0.907		3.69	4.478	7.637	92kV/cm	0.875		1.98			
2.379	5.009	214215	0.8094	0.8096	0.0003	1.15	3.429	6.391	297298	0.8927		3.18	4.555	7.723	331332	0.8416		1.2		
2.385	5.018	207000	0.8095		1.15	3.450	6.418	208209	0.8256	0.8246	0.0005	1.16	4.563	7.732	252253	0.85		1.37		
2.439	5.093	333334	0.8741		3.6	3.457	6.426	214215	0.8257	0.8255	0.0006	1.16	4.576	7.748	333334	0.9426		3.78		
2.442	5.097	208209	0.8104	0.8113	0.0003	1.15	3.461	6.432	304056	0.8728	0.8238	0.0003	2.49	4.647	7.827	241000	0.8421		1.18	
2.463	5.127	164kV/c	0.875		3.60	3.462	6.433	143kV/c	0.893		3.15	4.661	7.843	329330	0.843	0.8404	0.0005	1.20		
2.464	5.128	307308	0.8338	0.8356	0.0005	1.92	3.467	6.439	130kV/c	0.884		2.85	4.814	8.013	299300	0.919	0.9168	0.0013	2.94	
2.478	5.147	297298	0.8641		3.11	3.468	6.440	92kV/cm	0.855		1.95	4.928	8.140	260261	0.8458		1.19			
2.482	5.152	329330	0.8115	0.8072	0.017	1.16	3.499	6.479	114kV/c	0.873		2.47	5.338	8.585	212213	0.8334		0.88		
2.491	5.165	143kV/c	0.864		3.08	3.550	6.541	333334	0.911		3.7	5.496	8.753	92kV/cm	0.894		2.01			
2.496	5.172	130kV/c	0.857		2.79	3.607	6.611	299300	0.888	0.8883	0.0007	2.87	5.521	8.781	270712	0.8638		1.39		
2.502	5.180	304056	0.8485	0.8483	0.0004	2.44	3.611	6.616	249250	0.8279		1.17	5.543	8.803	241000	0.8537		1.19		
2.505	5.184	114kV/c	0.848		2.42	3.616	6.622	331332	0.8286		1.18	5.556	8.818	333334	0.9713		3.85			
2.531	5.220	92kV/cm	0.835		1.91	3.618	6.624	262263	0.828		1.17	5.731	9.002	299300	0.941	0.9405	0.0008	2.98		
2.582	5.290	262263	0.8126		1.15	3.624	6.631	329330	0.8287	0.8305	0.0008	1.18	6.327	9.615	212213	0.8434		0.89		
2.584	5.293	331332	0.8131		1.17	3.681	6.702	260261	0.8289		1.17	6.412	9.701	333334	0.9954		3.90			
2.590	5.302	299300	0.86	0.862	0.0005	2.81	3.693	6.716	252253	0.8368		1.35	6.585	9.875	270712	0.8784		1.40		
2.664	5.402	252253	0.82	0.82	0.0003	1.33	3.710	6.736	241000	0.8293		1.17	6.757	10.04	299300	0.965	0.9686	0.0008	3.03	
2.678	5.421	241000	0.8141		1.15	4.038	7.128	289901	0.861		1.82	7.202	10.48	212213	0.8519		0.89			
2.960	5.795	249250	0.8184	0.8125	0.0002	1.16	4.261	7.388	212213	0.8219	0.8217	0.0003	0.87	7.814	11.06	299300	0.989	0.9901	0.0017	3.08
3.273	6.196	212213	0.8106	0.8117	0.0003	0.86	4.301	7.433	270712	0.8461		1.37	8.697	11.88	299300	1.008	1.0087	0.0015	3.11	
3.370	6.319	287288	0.8384		1.53	4.317	7.453	307308	0.8719	0.8742	0.0005	1.97								

We include also a calculation of n from

$$n = \frac{(E_{\min} - 0.7542\text{eV})^{3/2}}{3\pi F}, \quad (44)$$

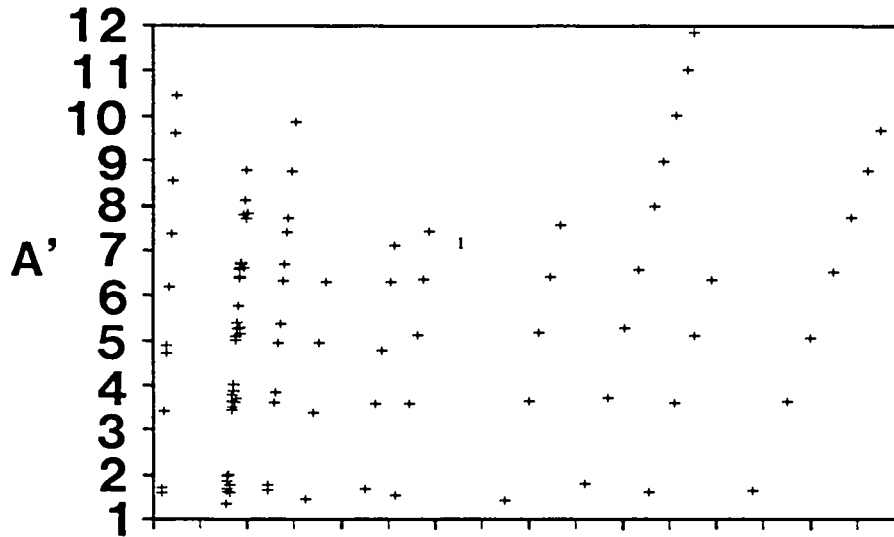
based on Rau and Wong's statement, equation 15, for the maxima. The threshold value of 0.7542 eV must be converted to atomic units. We have assumed that the minima correspond to half integer values to make the comparison. The results are quite consistent with this premise.

Figure 4.11 plots the values of $|a'|$ and n versus electric field. Figure 4.12 plots the n values versus energy. We have a consistent picture of a given oscillation associated with a particular value of a' or n ; the energy location changes as the electric field is changed but the order of the oscillation remains the same. Table 7 gives the average values for a' and n for each order of oscillation. The n values in particular are in very good agreement with theory.

Rau and Wong have predicted that the amplitude of the oscillations about the zero field curve will be proportional to $F^{1/3}$. I measured the peak to valley amplitude for the $n = 1/2$ and $n = 3/2$ minima. The results are plotted in Figure 4.13, along with a curve fitted to the equation

SUMMARY OF RIPPLE MINIMA

A' vs. Electric Field



N vs. Electric Field

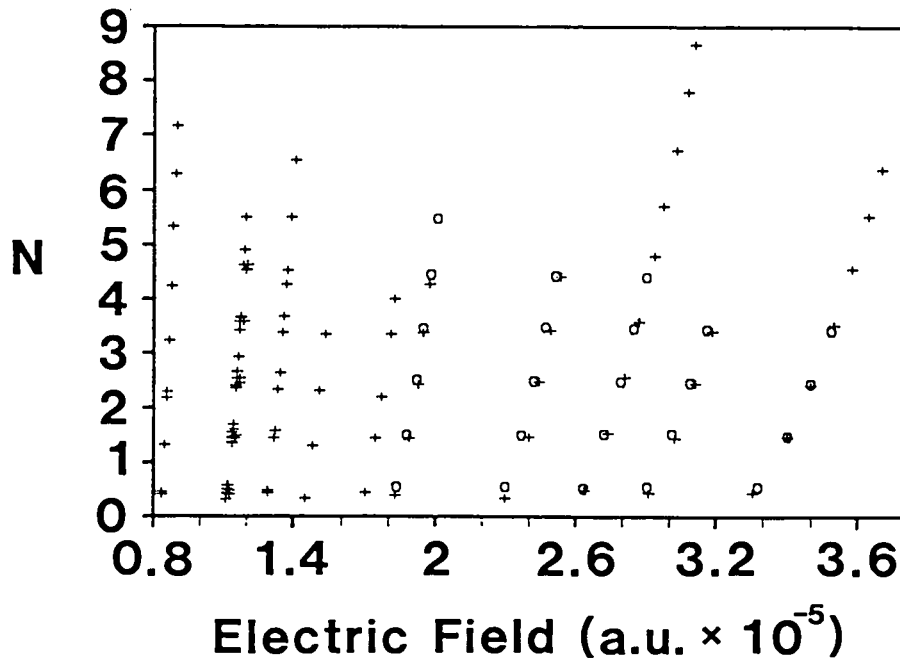


Figure 4.11 Summary of ripple minima vs. electric field. Circles mark location of minima from Reinhardt's theory.

SUMMARY OF RIPPLE MINIMA N vs. Energy of Minima

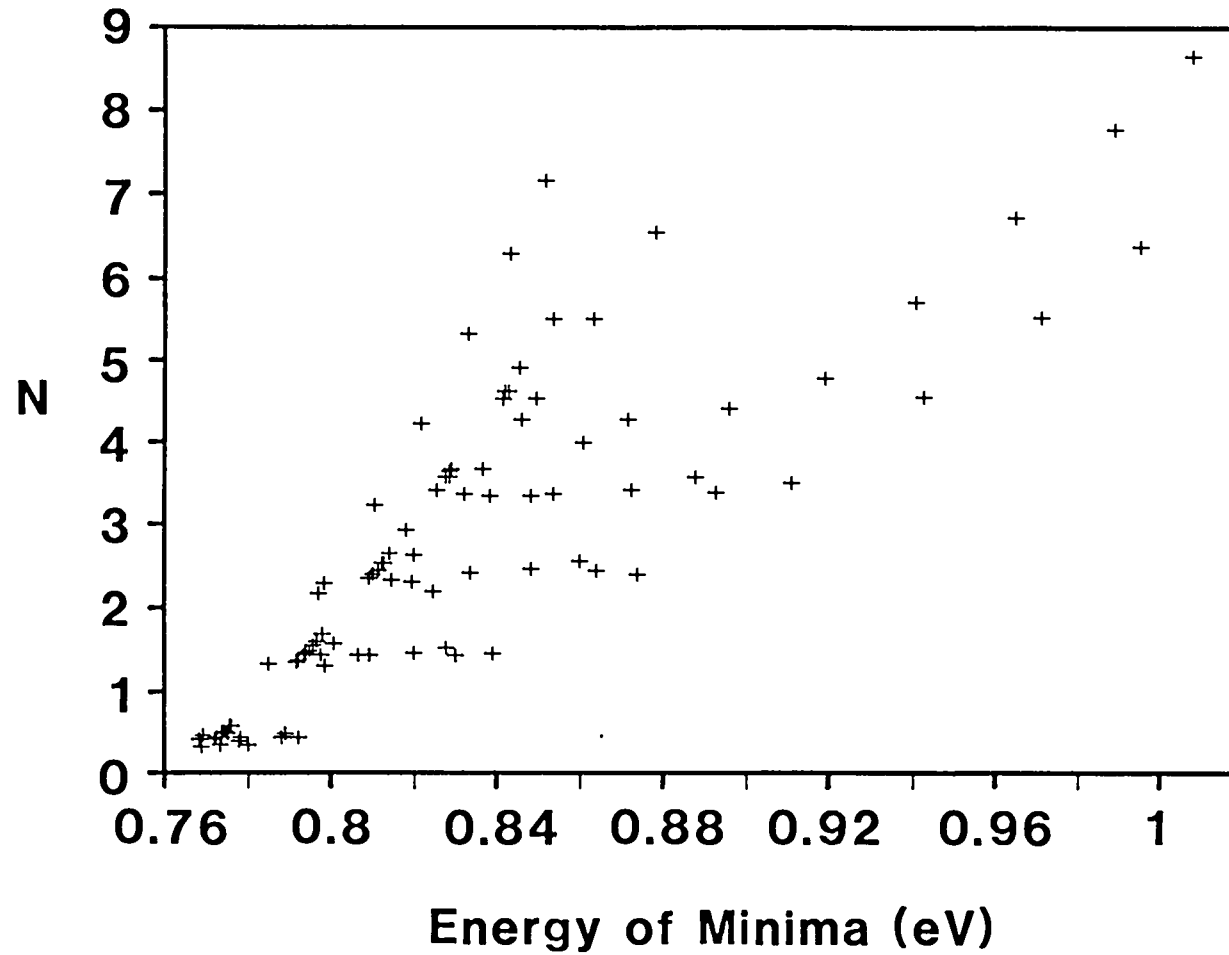


Figure 4.12 Summary of ripple minima, n vs. energy of minima.

TABLE 7
 AVERAGE VALUES FOR A' AND FOR N

A'	STD DEV	TRUE A'	N	STD DEV
-1.75	0.16	-1.02	0.49	0.07
-3.67	0.13	-3.25	1.49	0.08
-5.15	0.21	-4.82	2.48	0.08
-6.49	0.14	-6.16	3.51	0.12
-7.66	0.24	-7.37	4.5	0.22
-8.79	0.12	-8.49	5.53	0.11
-9.81	0.16	-9.54	6.52	0.17
-10.78	0.29	-10.53	7.51	0.31
-11.88		-11.48	8.7	

SUMMARY OF AMPLITUDES

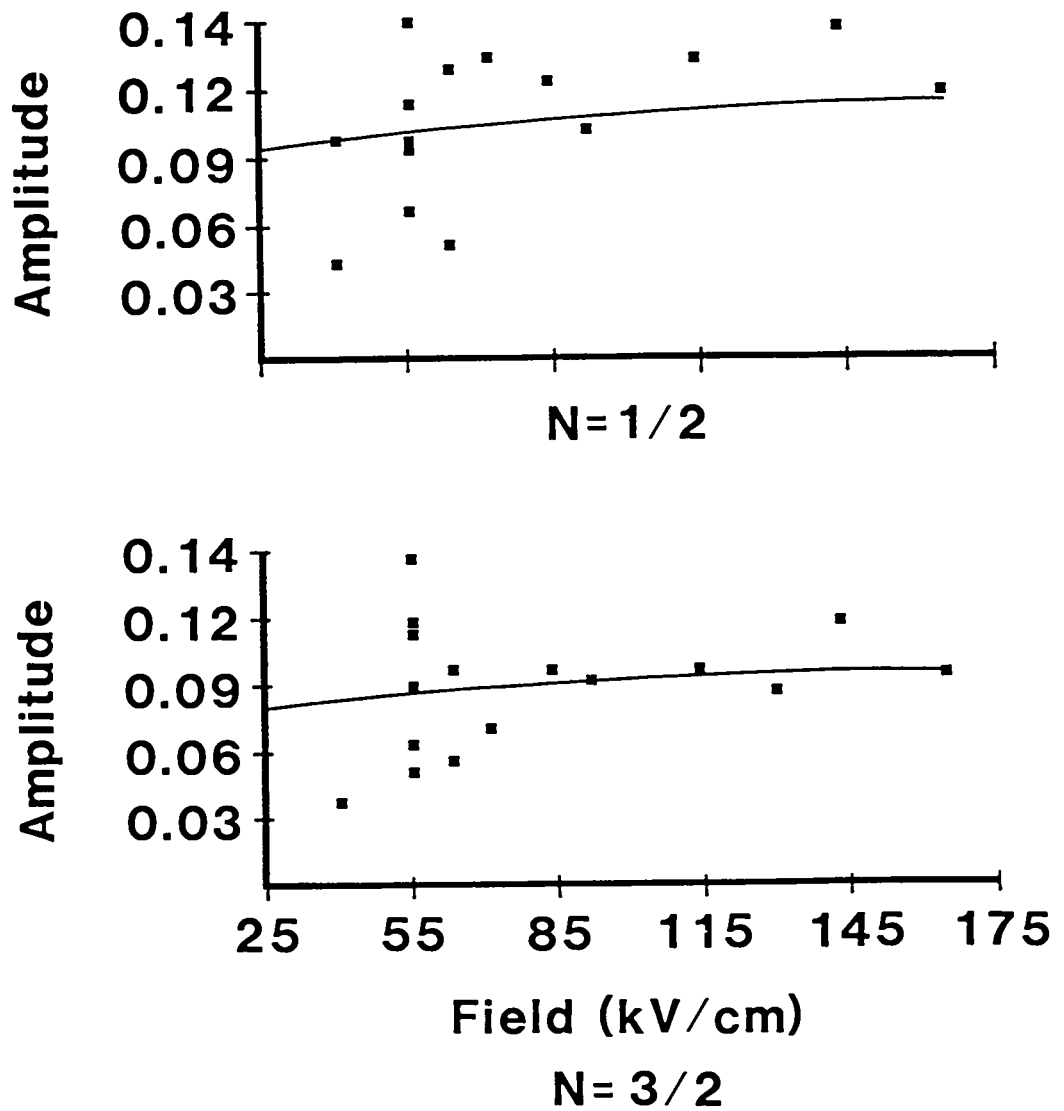


Figure 4.13 Summary of Amplitudes.

$$A = A_0 \left[\frac{F}{F_0} \right]^P . \quad (45)$$

where A_0 and P are free parameters and F_0 was the lowest field value in the data set.

The data points were all given equal errors. The result of the fit is $P = 0.340$ for $n = 1/2$ and $P = 0.333$ for $n = 3/2$. No error is given for these values because the fitting program had difficulty and I have not yet followed up on it. The result is consistent with Rau and Wong's prediction.

There were three useful field runs taken with the potential well and the electron spectrometer. These runs give confirmation to the premise that the ripple effect is due solely to the electrostatic field. None of these runs is a good example of the phenomenon. One has only one distinguishable minimum. The other two have two minima. Table 8 gives the results from these runs.

There was some question during the runs whether or not we truly accomplished a field of the stated magnitude on the interaction region. The fact that the minima do not yield the a' and n values expected may be evidence of this. By assuming an n of $1/2$ or $3/2$, as appropriate, we have calculated the electric field implied. It is clearly much less than the nominal field. The inconsistency between the fields calculated for $n = 1/2$ and $n = 3/2$ is probably due to the fact that the $n = 3/2$ minima are so indistinct that our values for them are in error.

TABLE 8

RIPPLE MINIMA FROM DATA TAKEN WITH POTENTIAL WELL

RUN	FIELD (kV/cm)	MINIMUM (eV)	A'	N	CALCULATED FIELD (kV/cm)
468	40	0.7668	-1.48	0.38	11
469	40	0.7676	-1.58	0.42	12
469	40	0.7771	-2.70	0.94	9
477	50	0.7679	-1.39	0.35	12
477	50	0.7782	-2.43	0.80	9

Using the simple theory from Chapter 2 we can get a determination of our experimental resolution. For the case shown in Figure 4.6b the energy above threshold where the ripples fade is ~ 0.12 eV. The field is ~ 95 kV/cm, giving time = 2.4×10^{-13} sec.

The coherence time corresponds through the Heisenberg Uncertainty Principle to an energy resolution of 1.4 meV, which is consistent with the resolution of our experiment.

ERRORS

All of the errors cited with data presented in this paper are statistical. We must consider, however, systematic errors.

We are fortunate that the angle between the laser beam and the H^- beam with all three beam energies considered

here is close to the Doppler free angle. Examining the Doppler formula, equation 1, we see that it depends on two variables, α and β . On taking the total derivative of the equation we find that, when $\cos\alpha = -\beta$, the term which depends on β drops out and dE depends only on α . In other words the momentum spread of the H^- beam becomes unimportant.

We are concerned with $d\alpha$ which depends on the divergence of both the laser and the H^- beam. These uncertainties contribute to our energy resolution, smearing out narrow peaks such as the $n = 4$, H^0 transitions discussed in Chapter 3, where we found the width of an intrinsically much narrower peak to be ≈ 1 meV.

We discussed the possible error introduced by misalignment of the laser and the mirrors. All we can do here is to make an educated guess. It is unlikely that this contributes a shift of more than 1 meV.

Because we seek only a relative cross section we can be somewhat cavalier about errors from the ion chamber and the photodiode.

The source of error which potentially could have the most serious impact on our results is the measurement of steps per degree, S . Finding S was an iterative process. I fit the data using an initial encoder zero, EZ , and S . The result of that implied a different EZ and S . After several iterations the difference between one set of

values and the previous set became negligible. The main criterion was to use an EZ and S such that when all the data sets were fit and the fitted parameters averaged, the resulting value for the threshold was as close as possible to 0.7542 eV. Use of other values for S near the one used in the end did not yield significantly different values for the power law.

CHAPTER 5: CONCLUSIONS

We have examined the H^- photodetachment cross section in electric fields using both π and σ polarized laser light. With π polarized light we have data taken with fields from zero to 164 kV/cm. With σ polarized light our data was taken at fields ranging from 52 kV/cm (the putative zero field data from 1985) to 1.32 MV/cm.

In our analysis we lead up to conclusions about the Wigner threshold law which applies in the zero field case. The 1985 "zero field" data imply a changing power in the region between threshold and 0.8 eV. This may be due to the fact that it was not truly zero field or to an actual inconsistency in the data. We expect the power to increase with field, however. Here we see a decrease. In 1986, although most of the data were taken with a small residual electric field of about 10^{-6} atomic units, we conclude that the data are consistent with the Wigner law at least as far as 46 meV above threshold.

We are intrigued that the two runs taken with no residual field present yield a power below that predicted by Wigner. The result 1.41(8) for both runs suggest the need for a more careful study.

The σ polarization data give a qualitative confirmation of the expectations described in Chapter 2. The cross section is non-zero at the zero field threshold.

The cross section decays, apparently exponentially, below the zero field threshold and it appears to tend to the zero field cross section well above threshold. Any definitive statement awaits a more careful study.

The π polarization data are consistent with all three of the theories described in Chapter 2. The theory of W. P. Reinhardt does not conform well to the overall shape of the cross section above about 0.85 eV, although he has predicted the approximate location of minima well.

The theory of Rau and Wong, by describing the cross section in a field as a modulation on the zero field cross section, does follow the general shape of the data as it begins to turn down at about 0.85 eV. Their specific prediction for the maxima of oscillations must be very close to correct. We find the positions of minima to be well described by half integer values of n from equation 43 and, by inference, believe the maxima to be well described by integer values of n .

In a rather crude fashion we confirm the prediction that the amplitude of the oscillations is proportional to $F^{1/3}$. For the first two orders of oscillation we find the amplitudes to be proportional to $F^{(0.34)}$ and $F^{(0.33)}$ respectively.

We confirm two other qualitative statements by Rau and Wong. In an electric field the cross section is

finite and positive at the zero field threshold and it decreases rapidly and monotonically below threshold.

We emphasise the fact that our analysis of field data and the theories which describe them tell us nothing about the H^- ion itself. We have confirmed a textbook quantum mechanics problem which has no particular dependence on the binding energy of the ion itself. Reinhardt (1985) assumes a generalized symmetric initial state and a final state of an electron in an electrostatic field. We need only input the value of the zero field threshold. Rau and Wong (1987) include the zero field H^- cross section only after the details of the process have been worked out. Bryant et al. (1987) use only the zero field threshold energy as input for their prediction of minima. Bryant (1987), with his "atomic interferometer," adds the zero field cross section in the same manner as Rau and Wong.

In future experiments we should look for deviations from Rau and Wong's theory in the region just below and just above the zero field threshold. It is here that the cross section should be most sensitive to the details of the H^- binding potential. We see no obvious deviations in our data but a very careful study with this in mind would give confirmation or details for small changes in the theory.

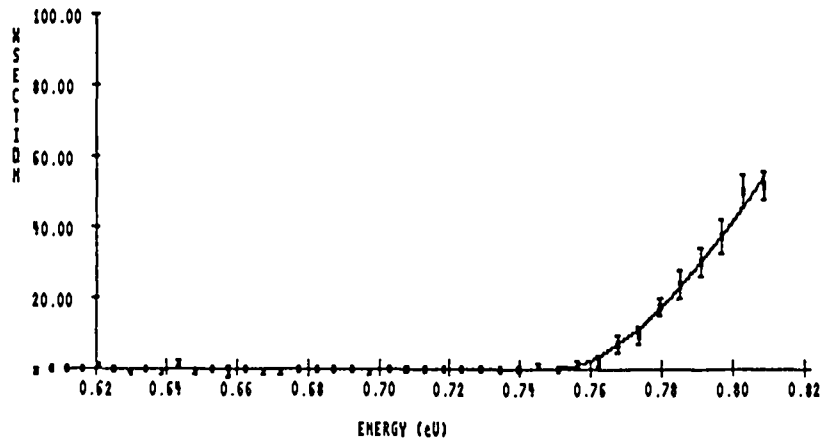
In future experiments I hope we will be able to maintain better control over the energy calibration of the

system. Taking the time to measure steps per degree with a theodolite before the experiment and finding some feature such as the H^0 $n = 4$ series on both sides of the beam during the run will be indispensable for the next generation of experiments. We should never again rely on an indistinct feature such as the H^- threshold for our calibration.

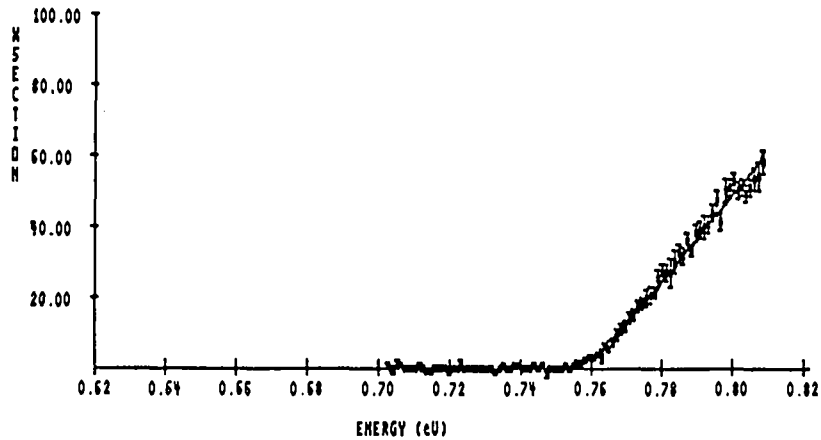
We have more than once taken data that did not include enough of the uninteresting region on both sides of the feature of interest. In this case the two runs intended to give a definitive result for the power dependence of the zero field cross section did not include enough data below threshold for a good fit. Had this been included they look as though they would have accomplished the job quite well.

APPENDIX 1

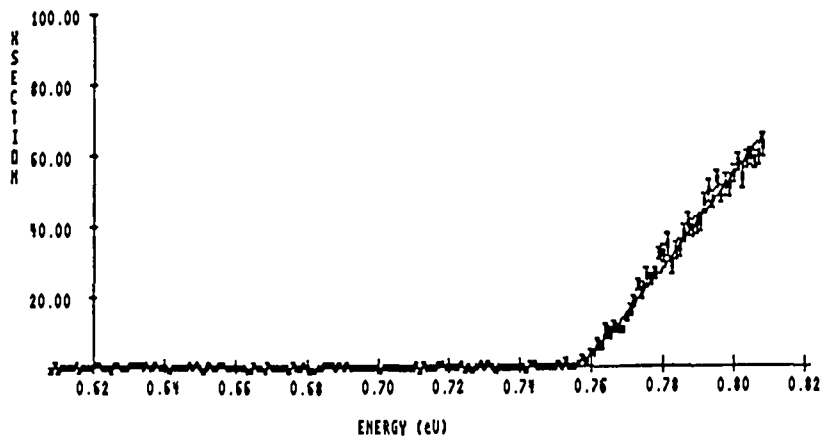
1985 "ZERO FIELD" DATA



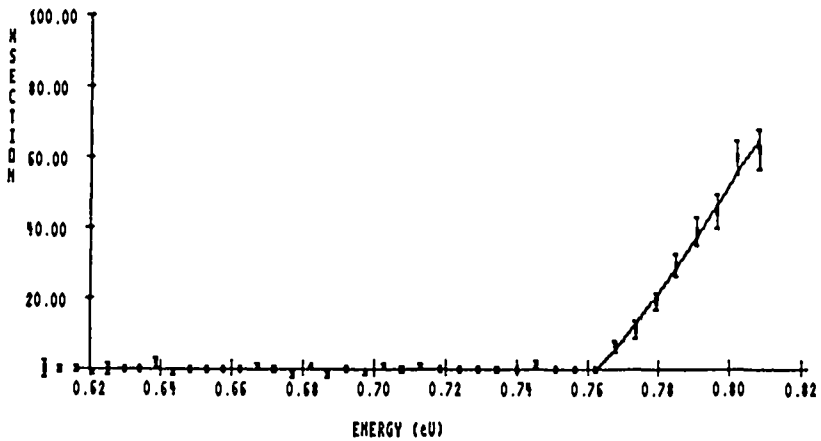
a:6149



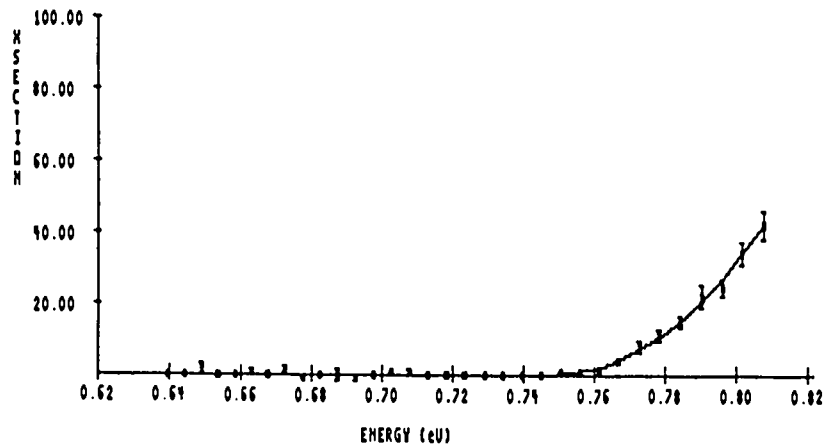
a:6162



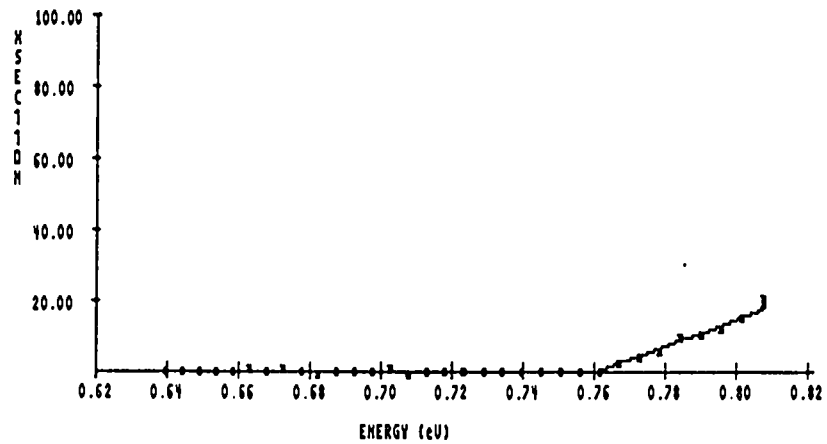
a:615051



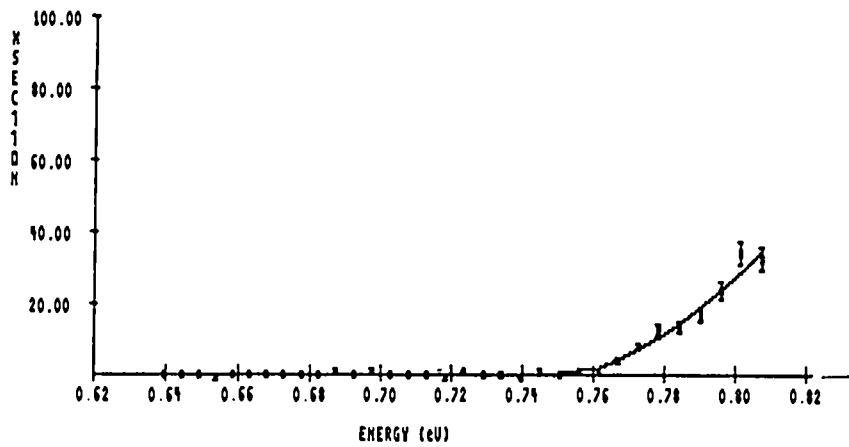
a:6193



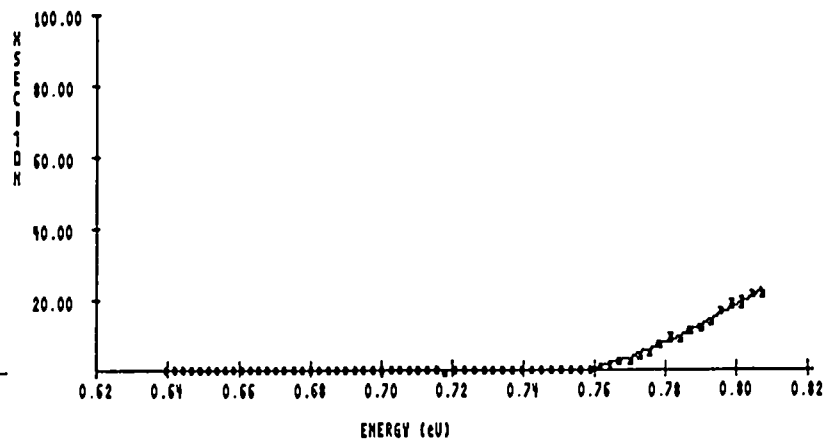
a:6126



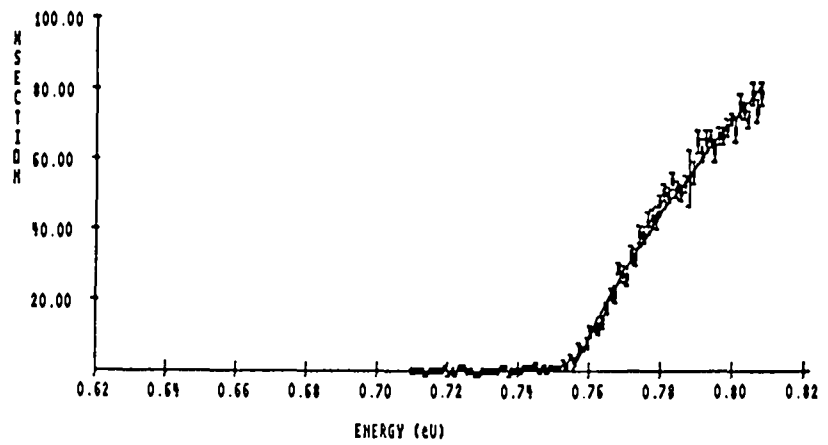
a:6134



a:6127



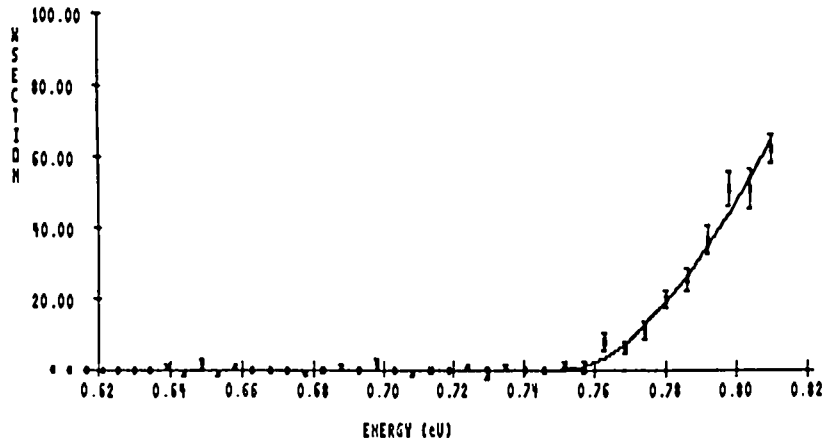
a:6135



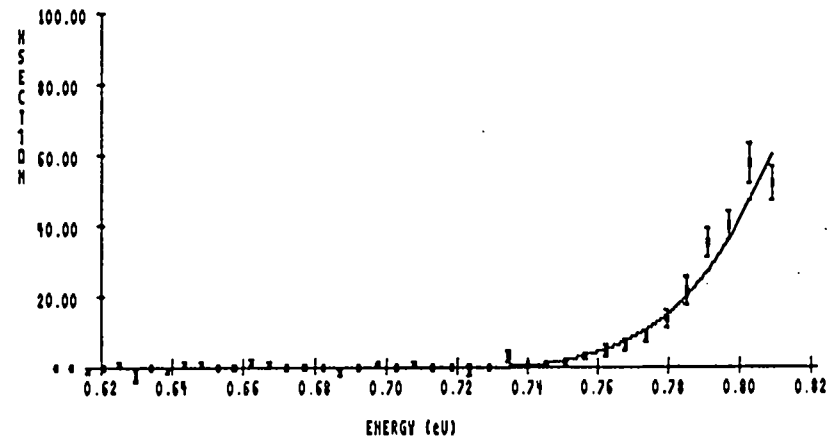
a:6163

APPENDIX 2

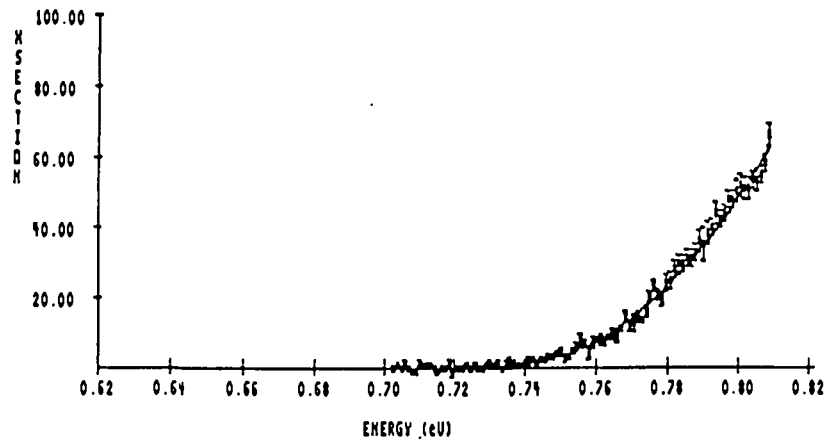
1985 SIGMA POLARIZATION FIELD DATA



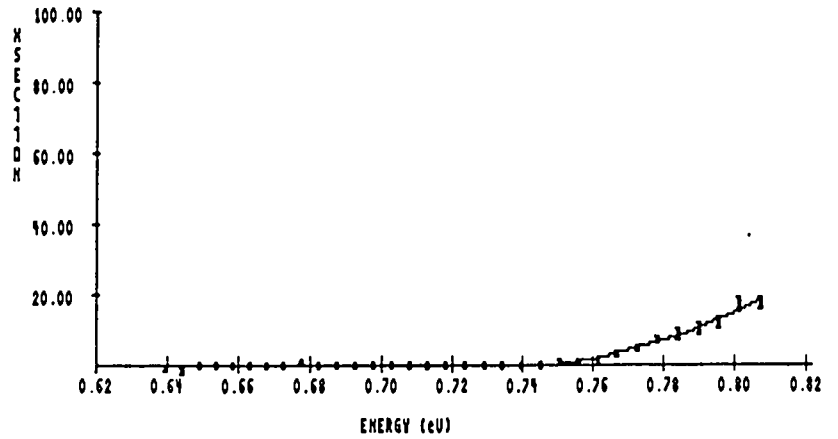
a:6148



a:6192

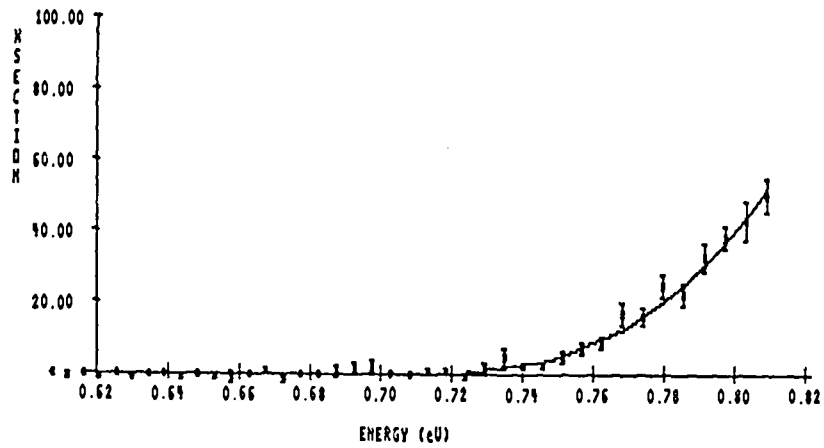


a:6161

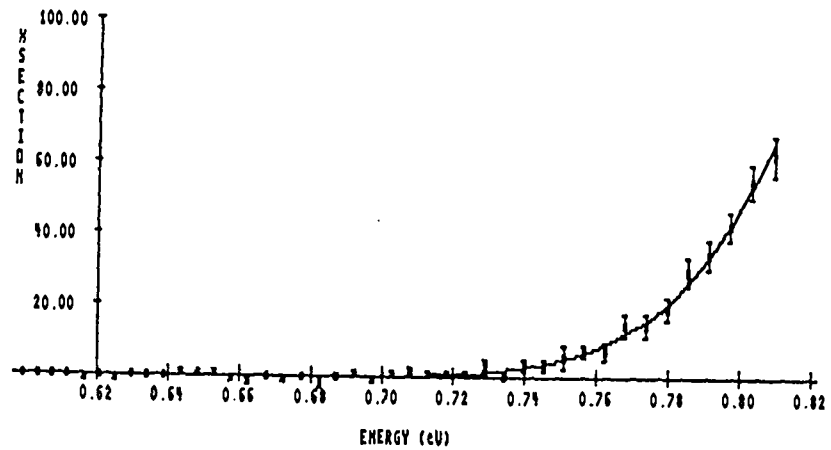


a:6133

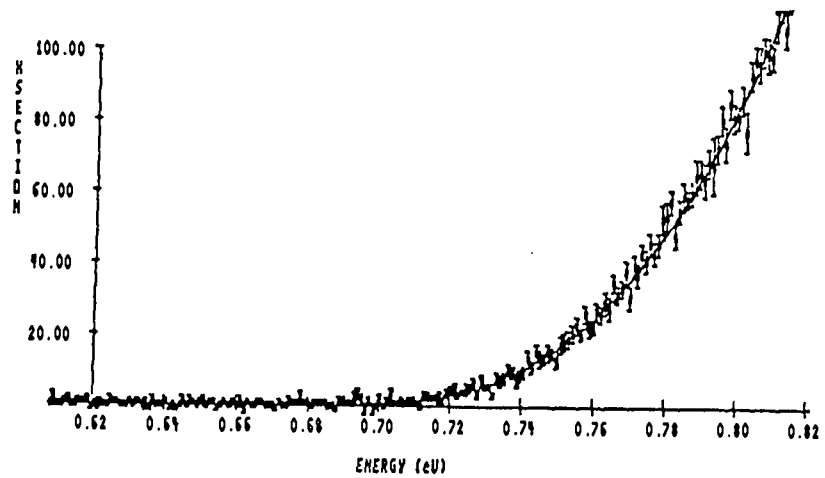
0.35 MV/cm



a:6191

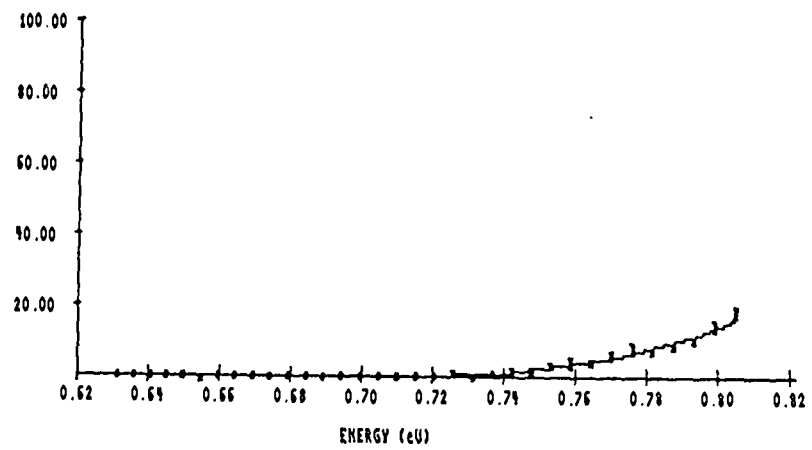


a:6197

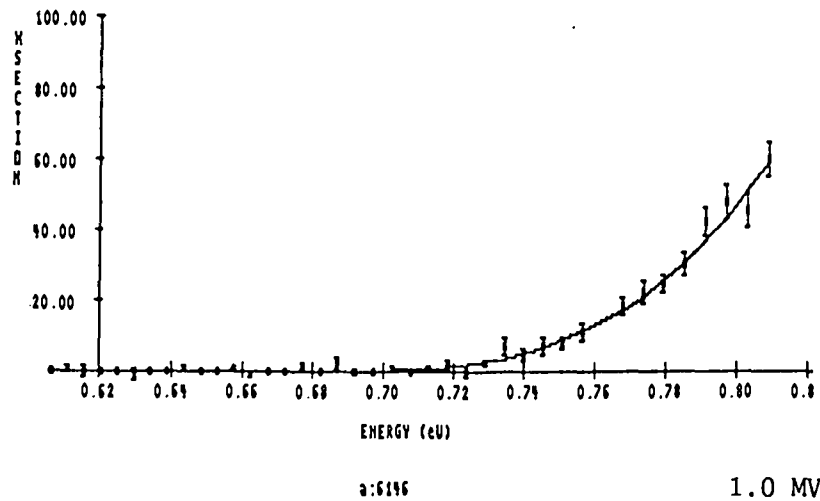
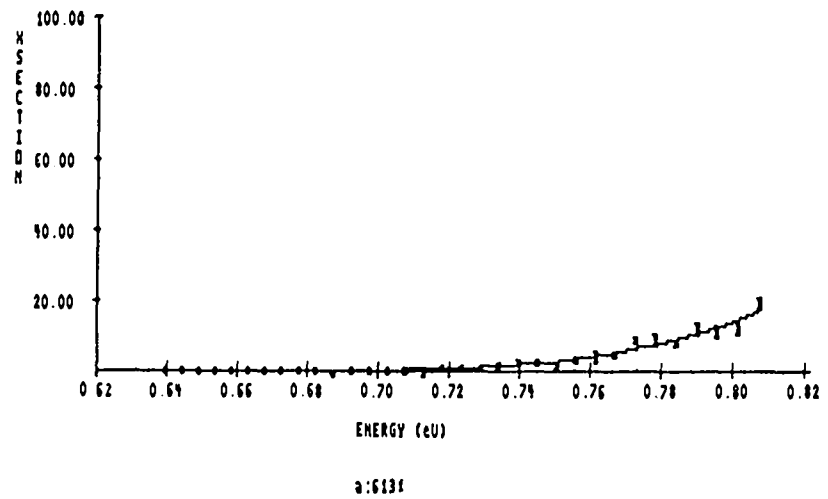
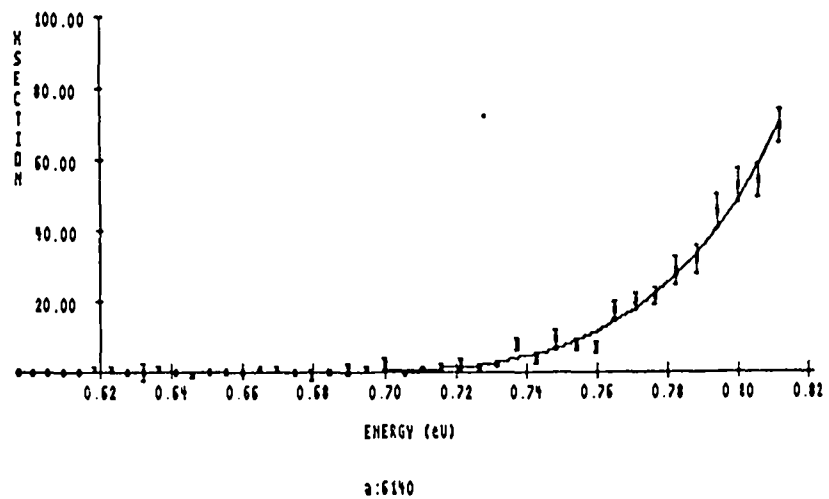


615960

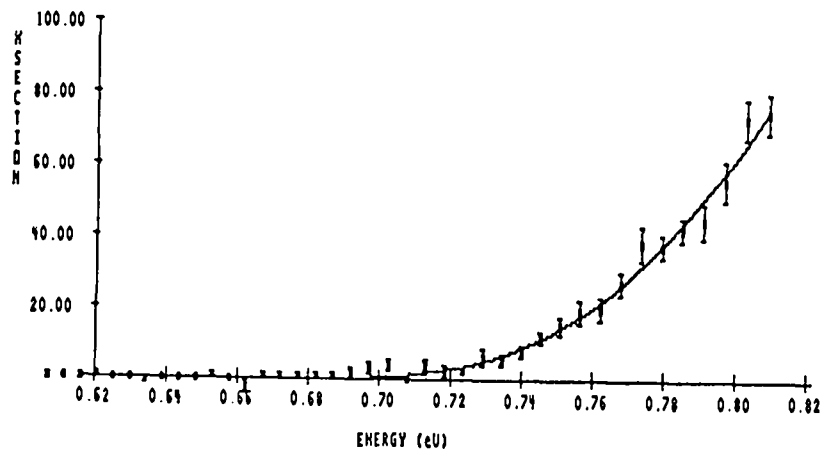
0.68 MV/cm



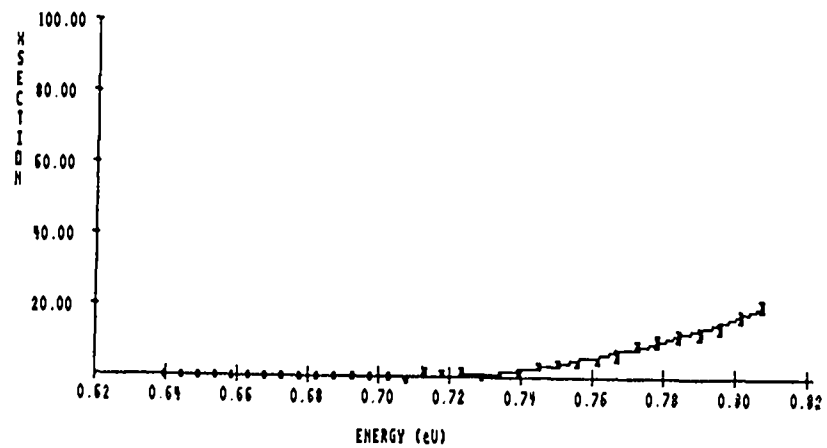
a:6132



1.0 MV/cm

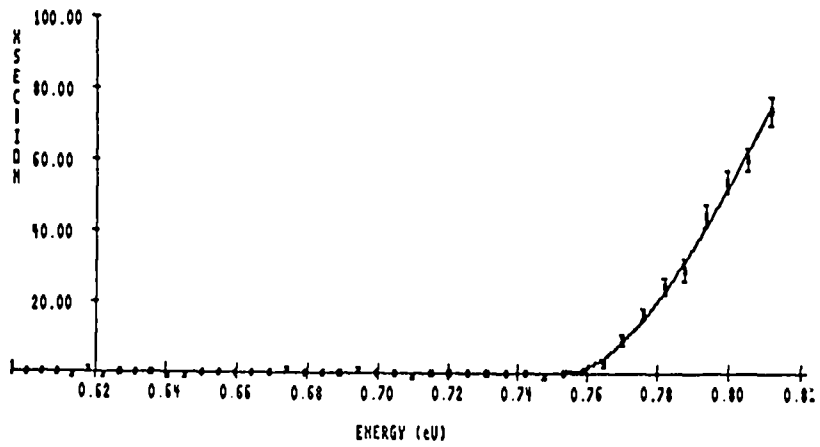


a:6195

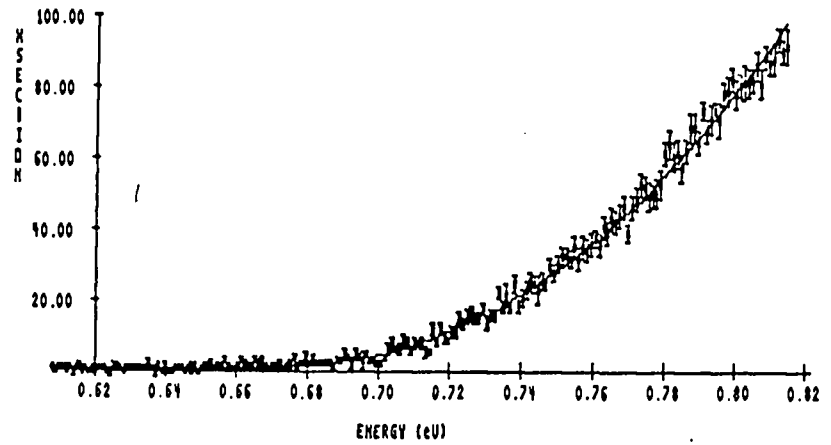


1.18 MV/cm

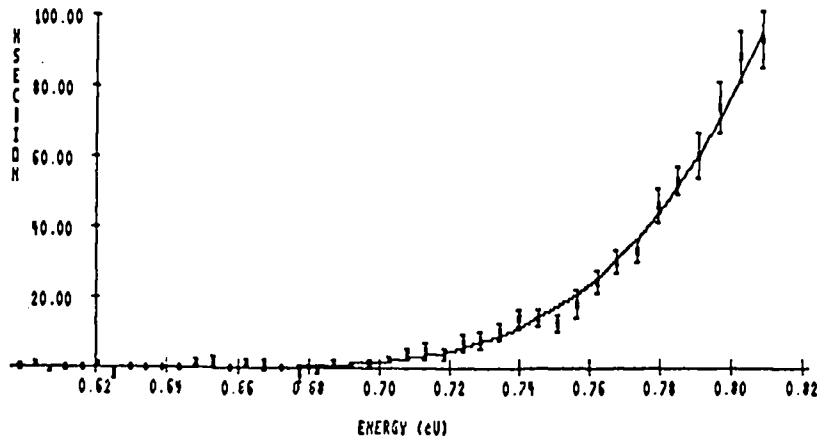
a:6130



a:6138

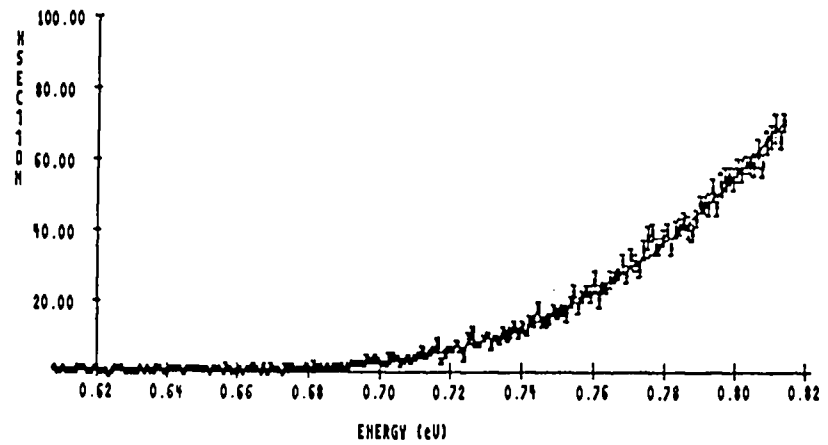


615253

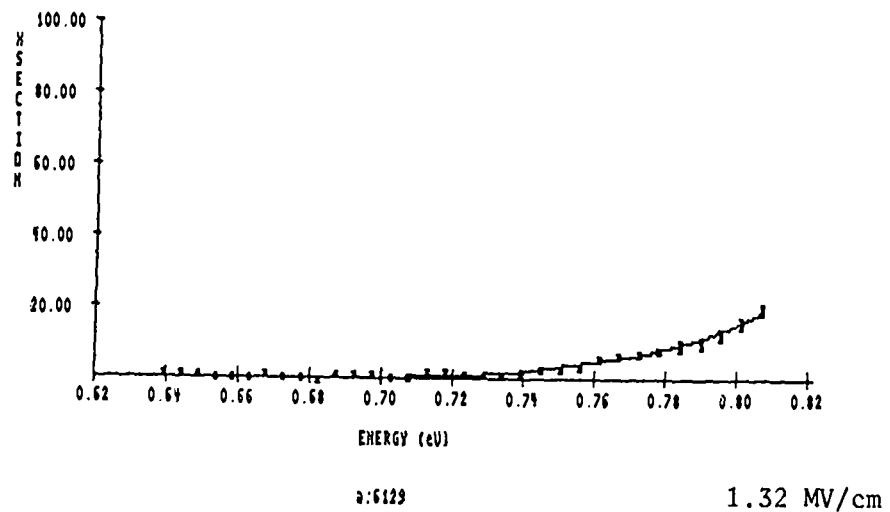
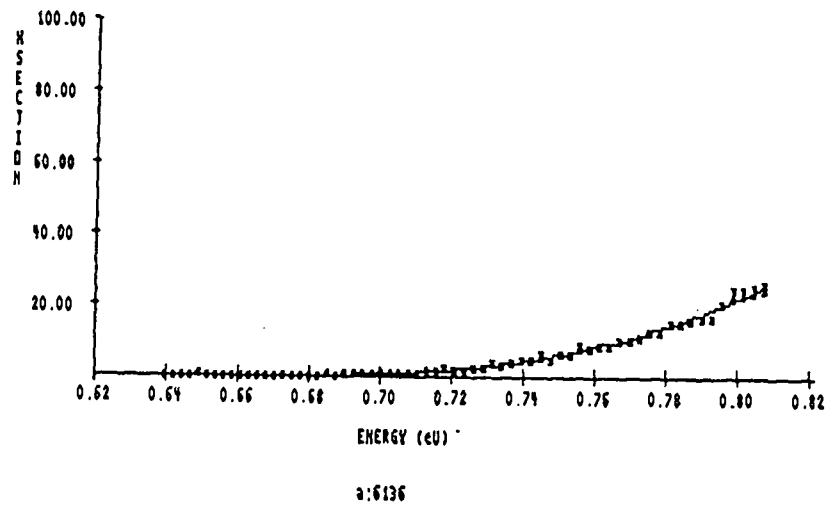
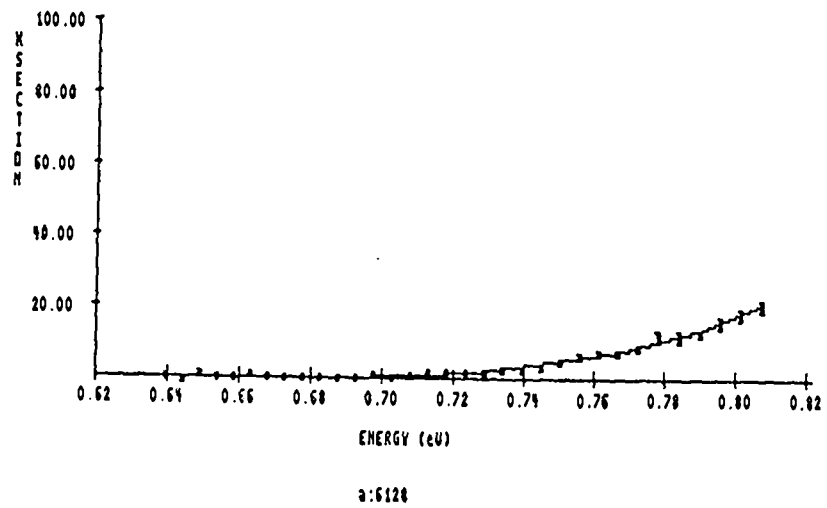


a:6199

1.32 MV/cm



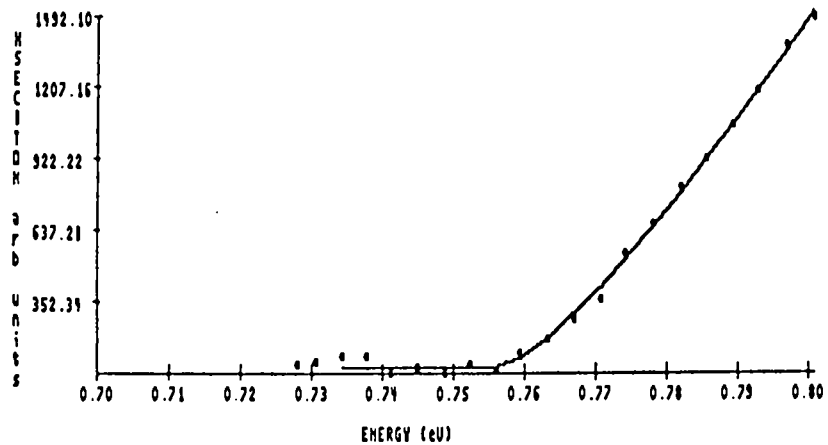
615455



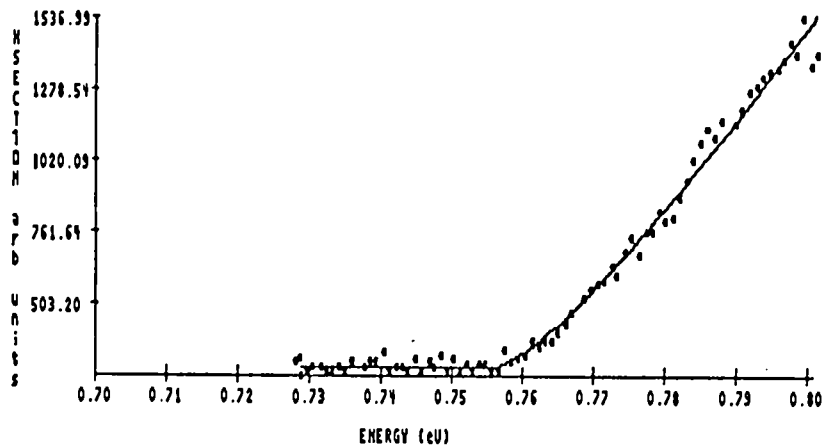
APPENDIX 3

1986 "ZERO FIELD" DATA

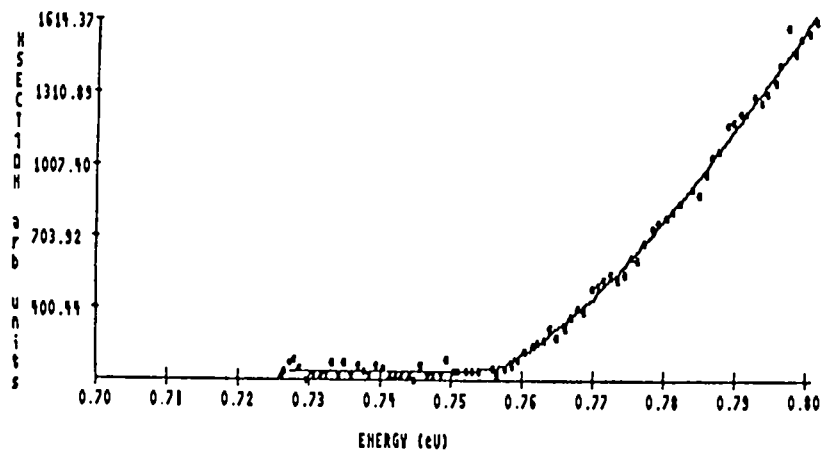
Runs 473 and 474 were taken at 318 MeV with the electrostatic potential well. There was no magnetic hysteresis hence no residual field. These two runs were taken at exactly zero field.



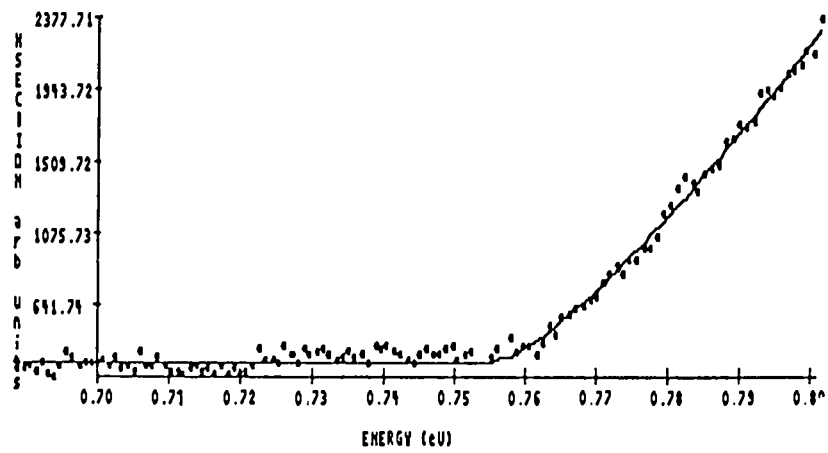
202_5



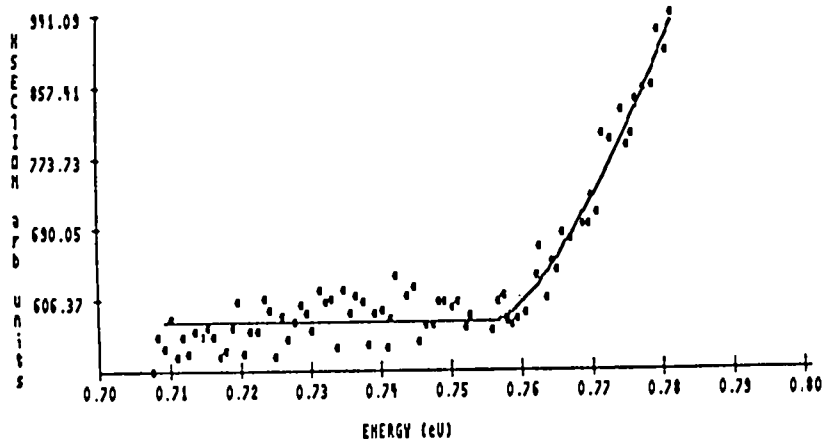
226227_5



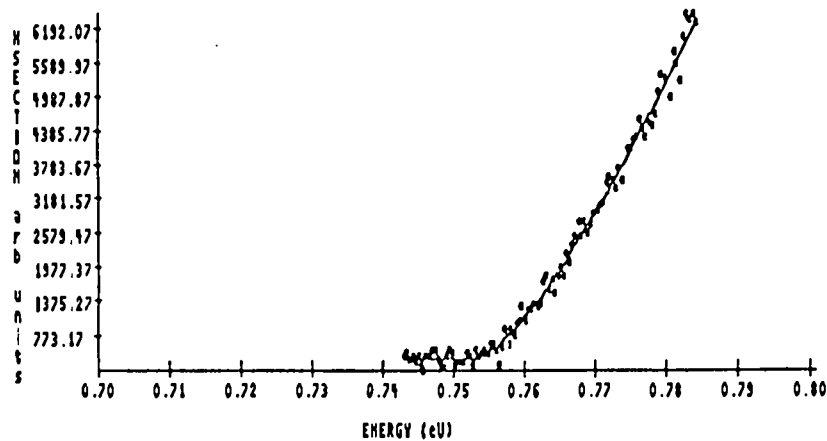
210_5



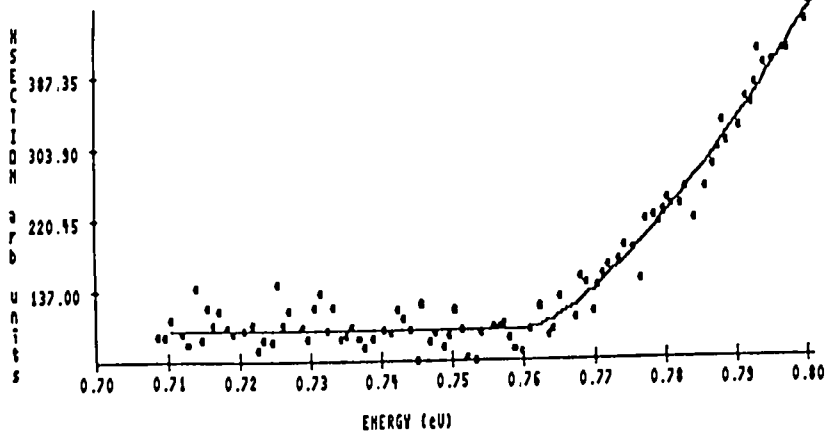
281282_5



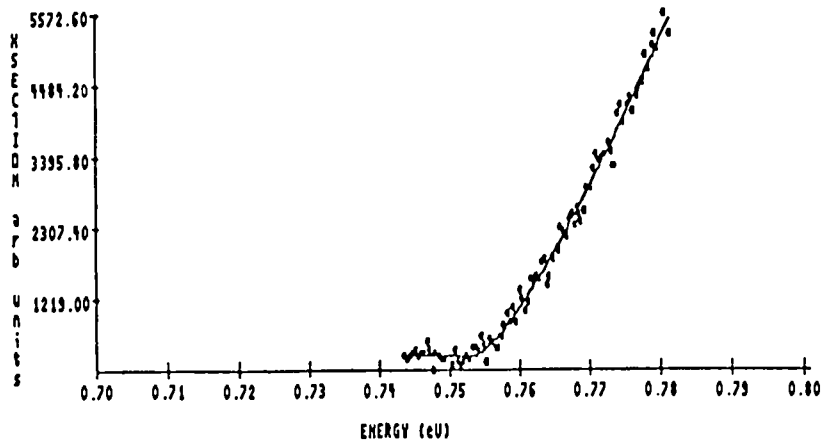
230_3



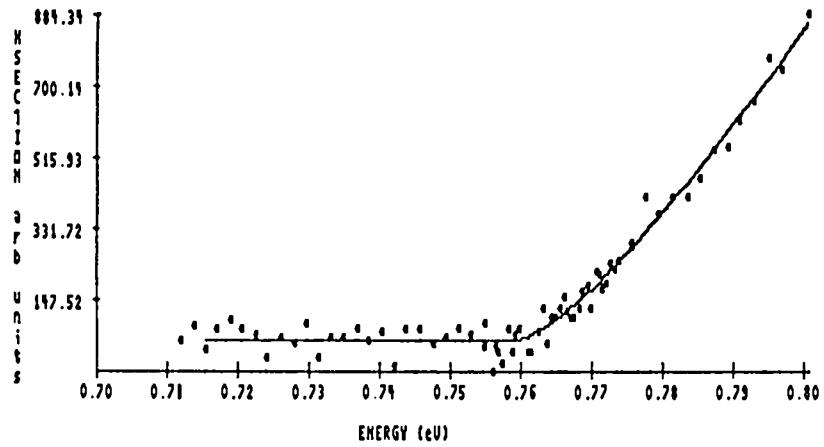
473_3



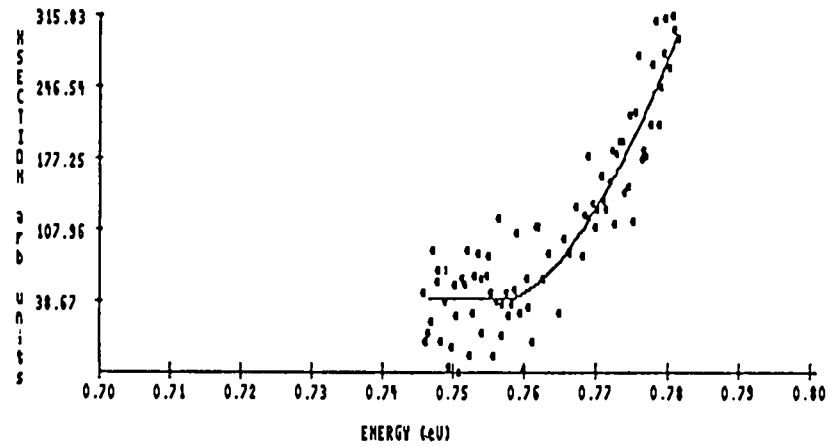
246247_5



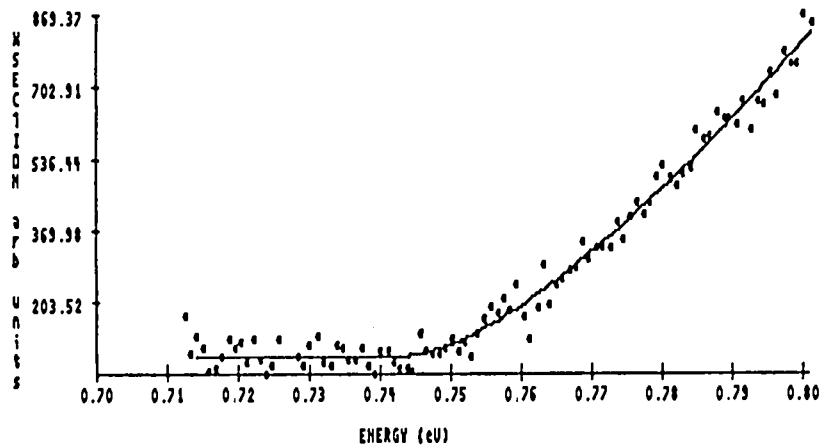
474_3



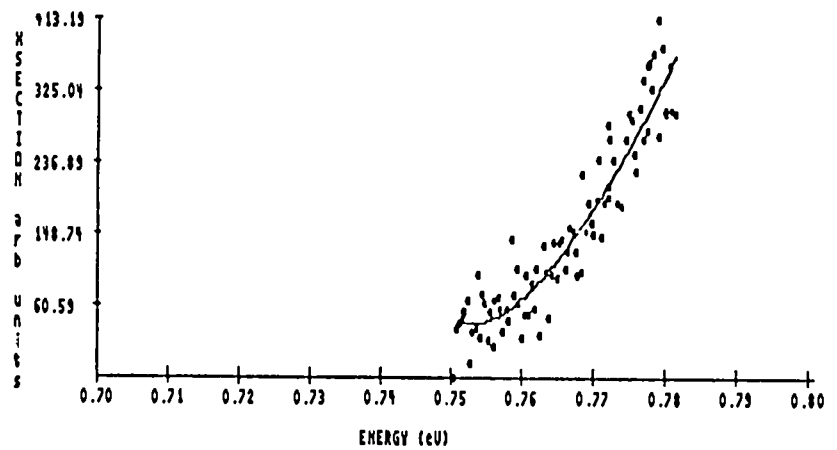
302303_5



319_3



317310_5

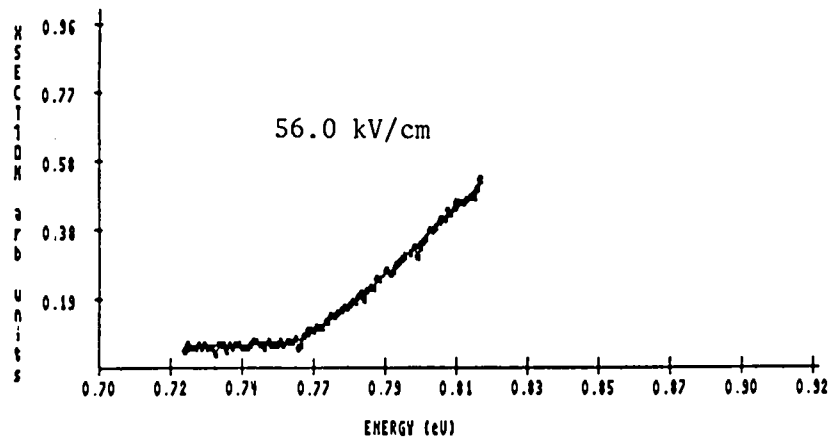


320_3

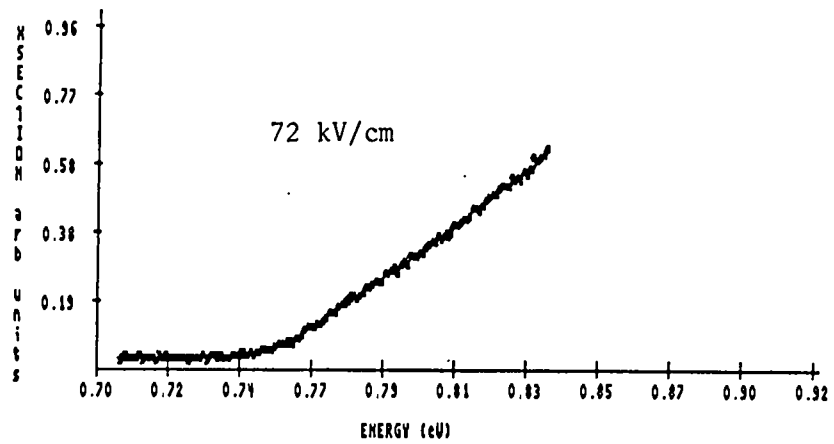
APPENDIX 4

1986 SIGMA POLARIZATION FIELD DATA

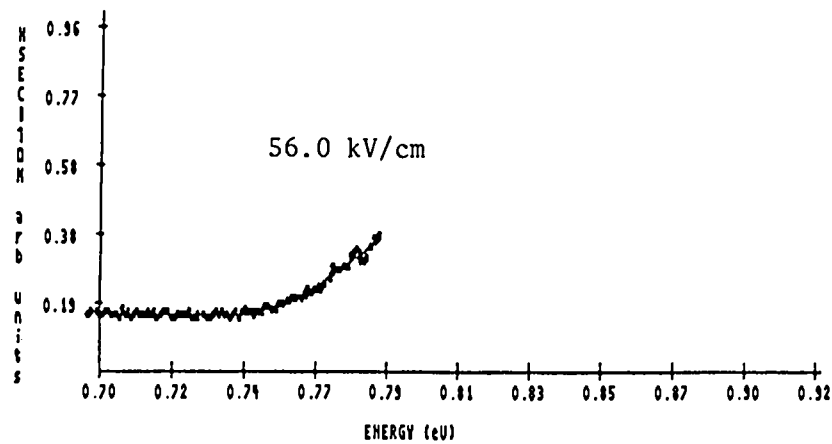
The nominal electric field value is the value of the field at that angle corresponding to 0.7542 eV.



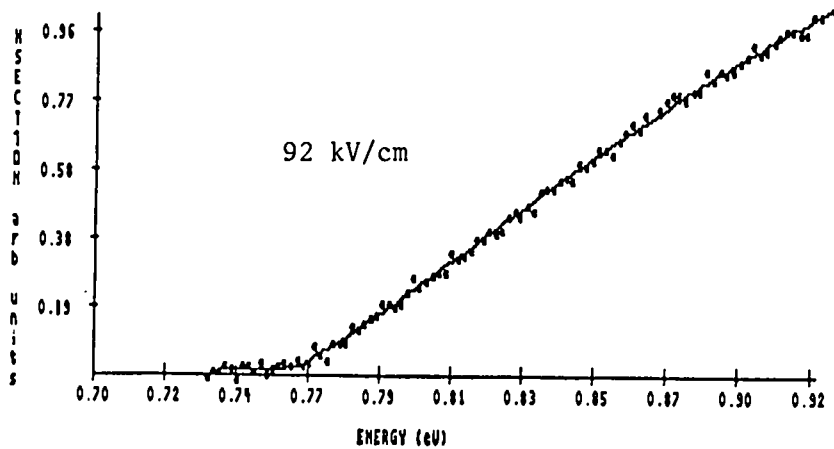
225



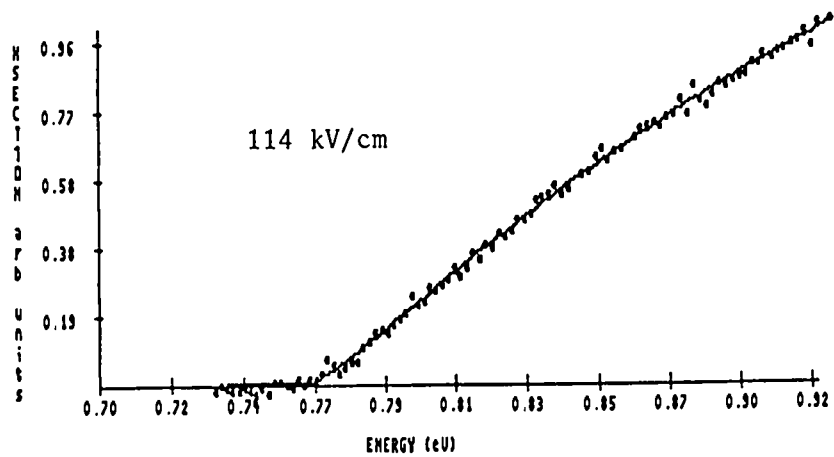
285286



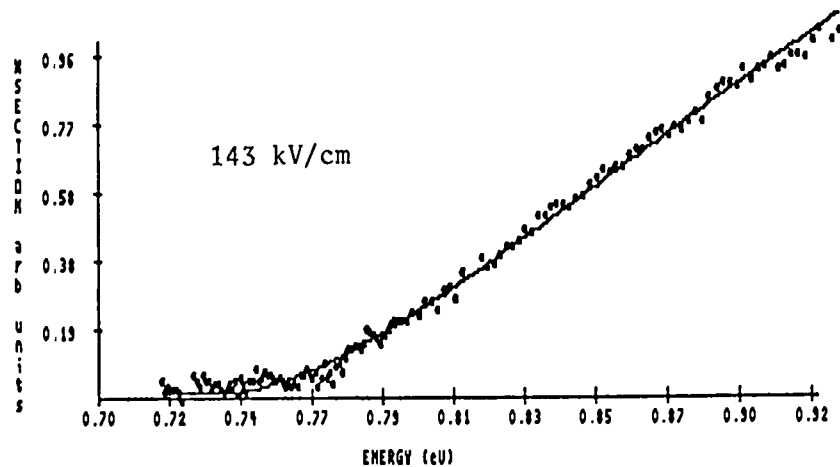
233



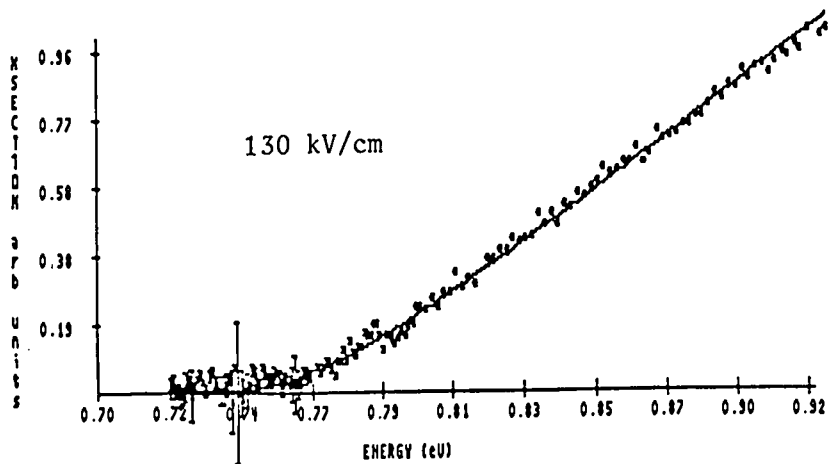
310



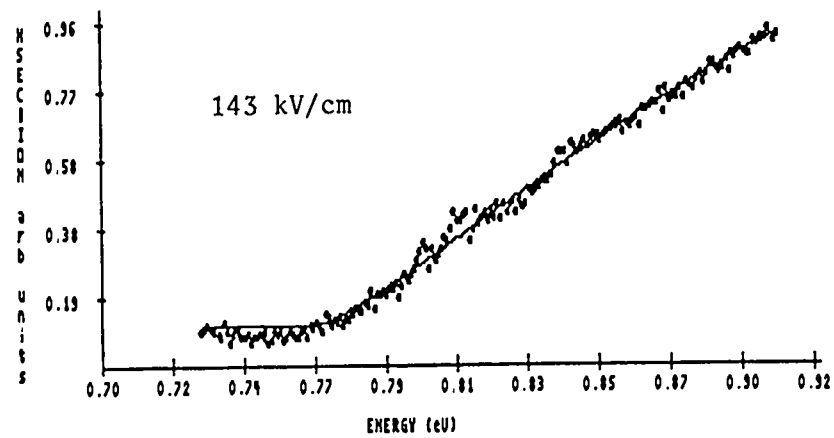
312



315316



313314



32678

APPENDIX 5

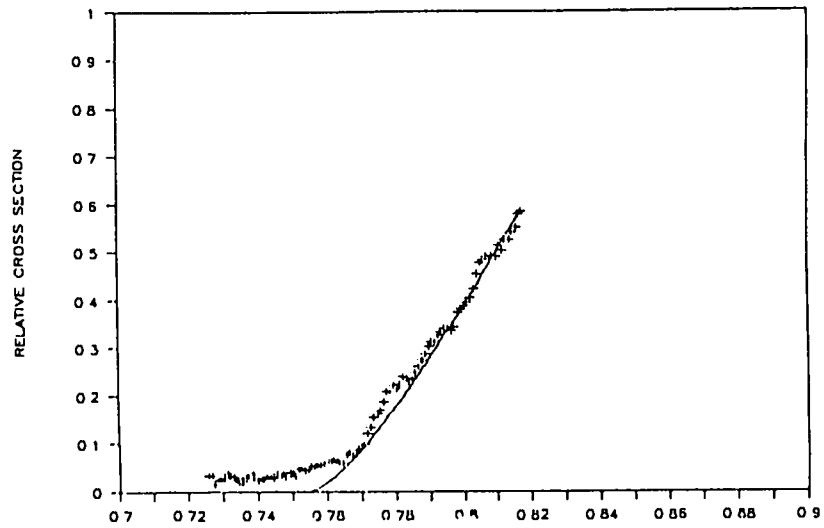
1986 PI POLARIZATION FIELD DATA

The nominal field value is the value of the field at that angle corresponding to 0.7542 eV.

Runs 360, 468, 477, and 478479 were taken at 318 MeV with the electrostatic potential well. The field was constant through each run.

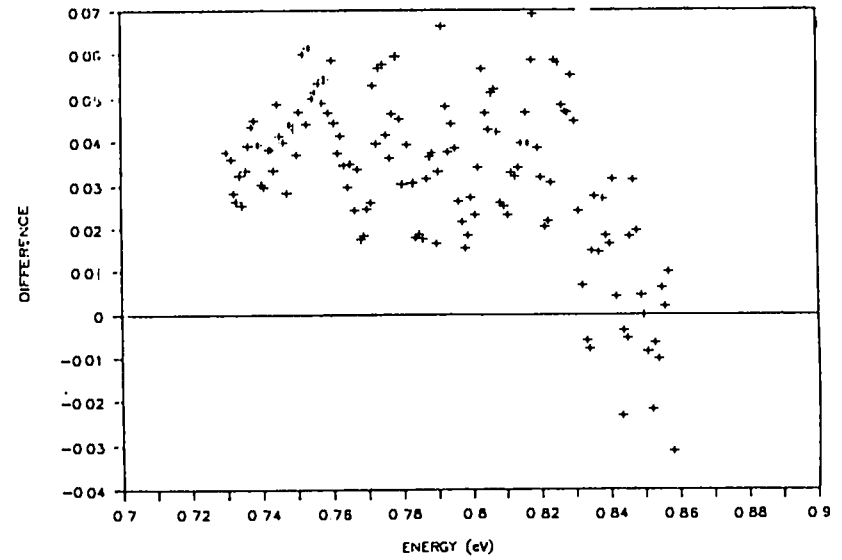
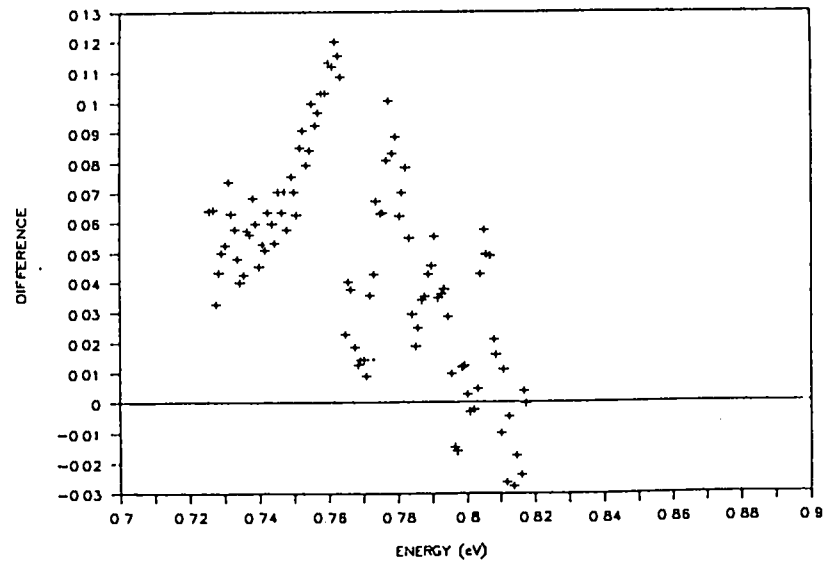
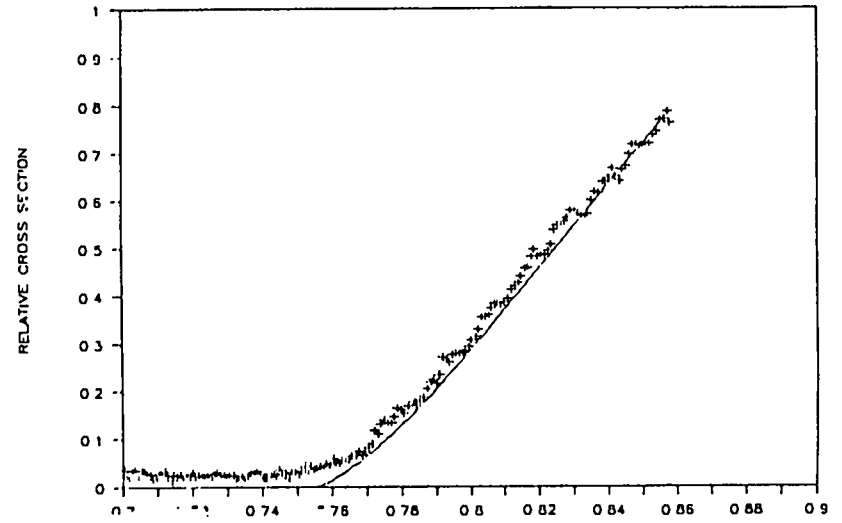
41 kV/cm, PI POLARIZATION

RUN 211



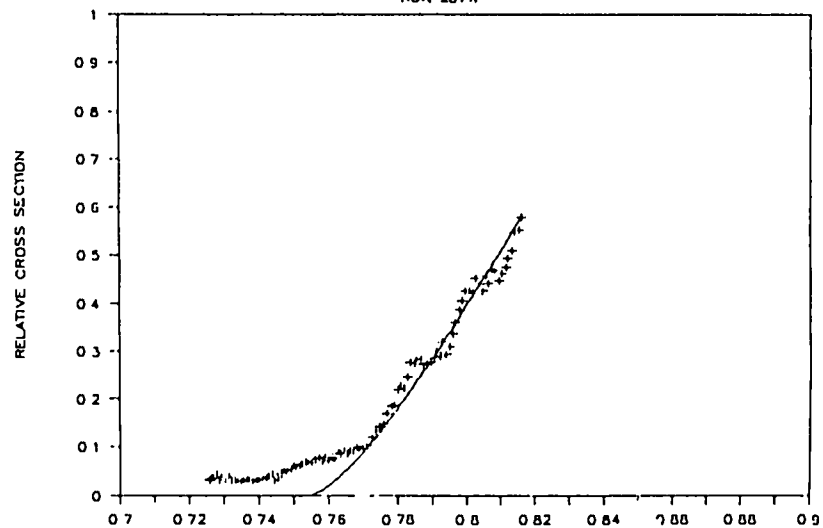
41 kV/cm PI POLARIZATION

RUN 212 213



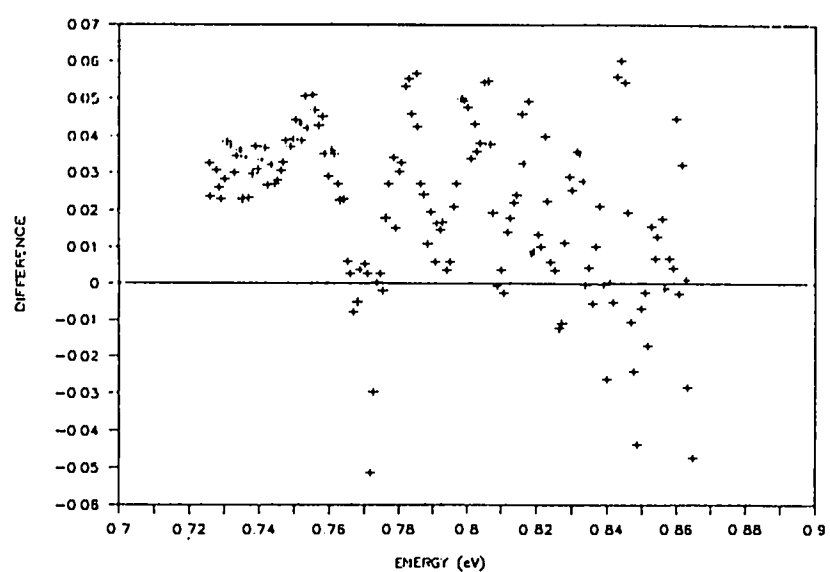
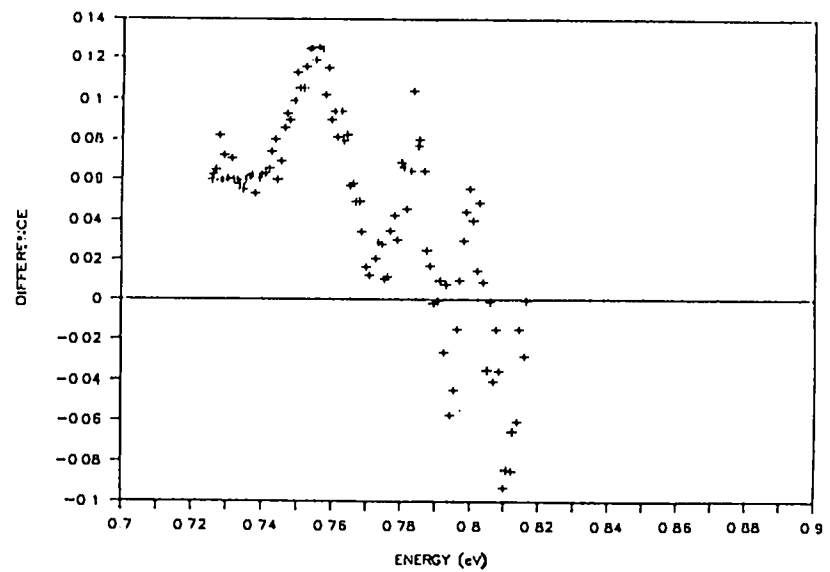
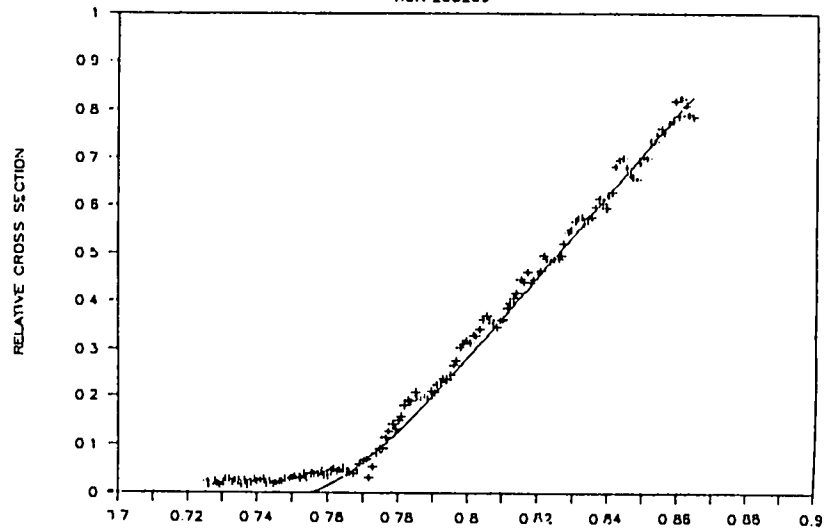
56 kV/cm PI POLARIZATION

RUN 207W



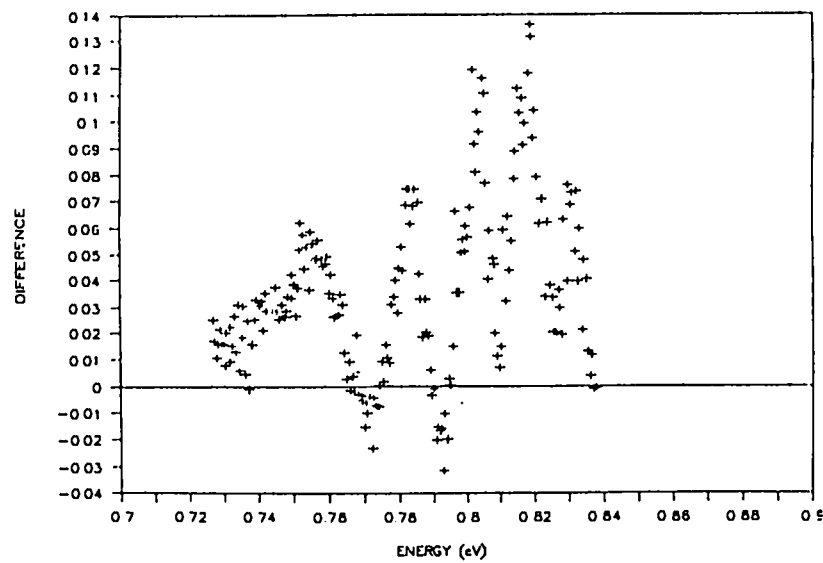
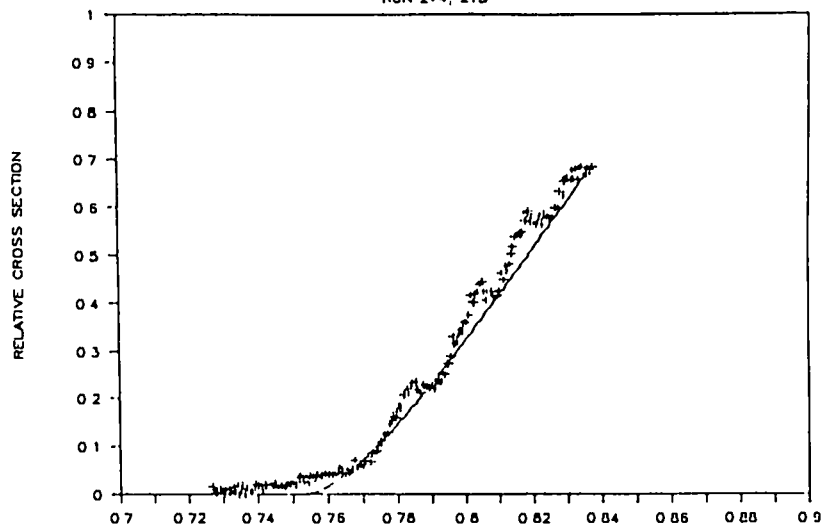
56 kV/cm PI POLARIZATION

RUN 208209



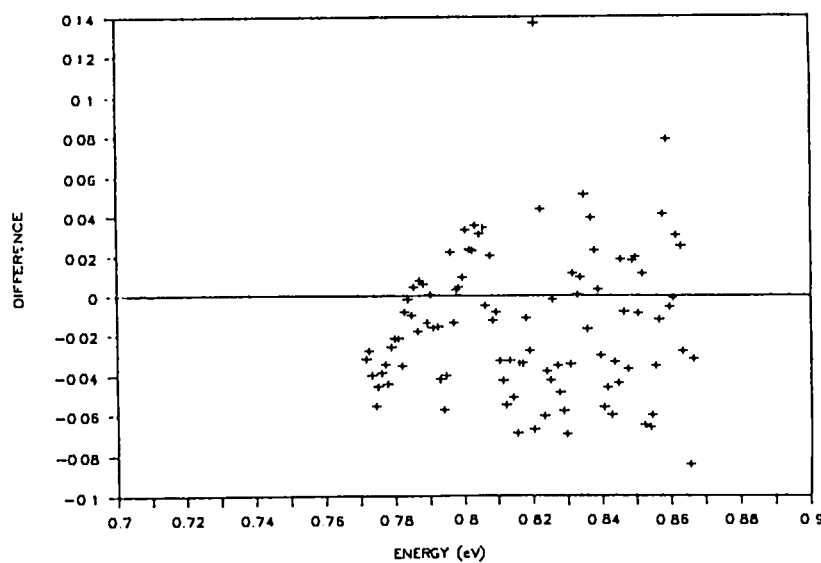
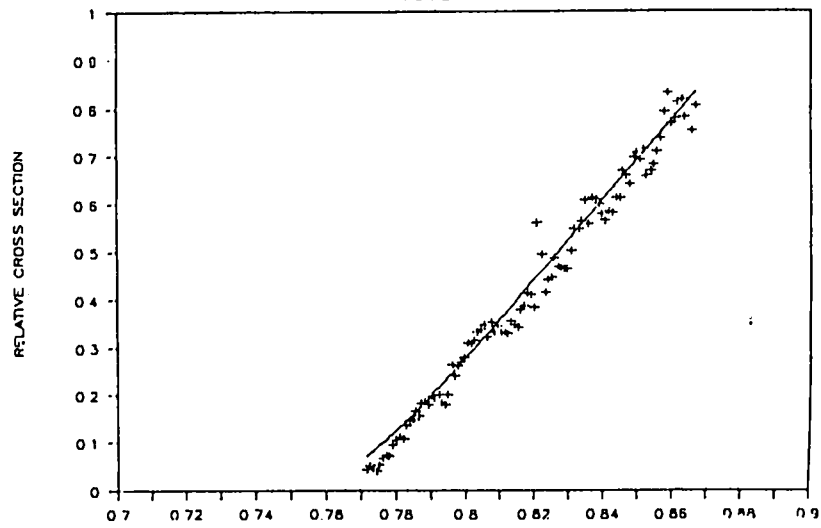
56 kV/cm PI POLARIZATION

RUN 214, 215



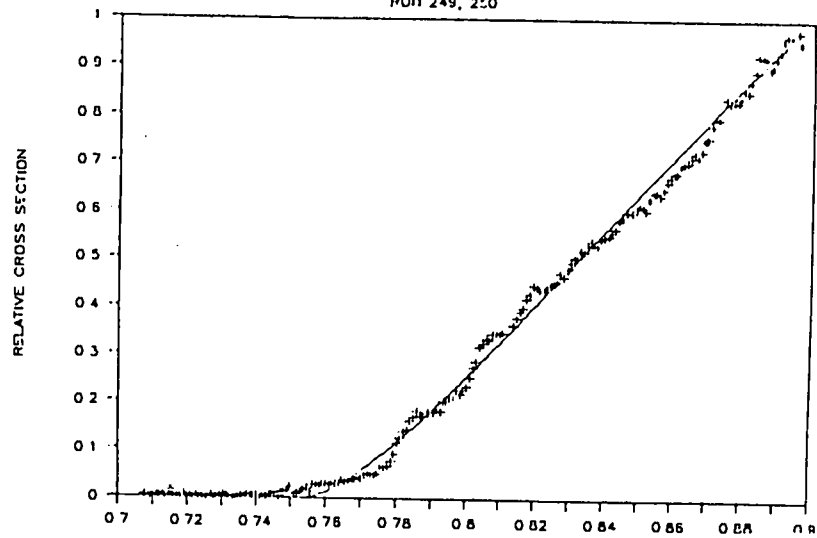
56 kV/cm PI POLARIZATION

RUN 241



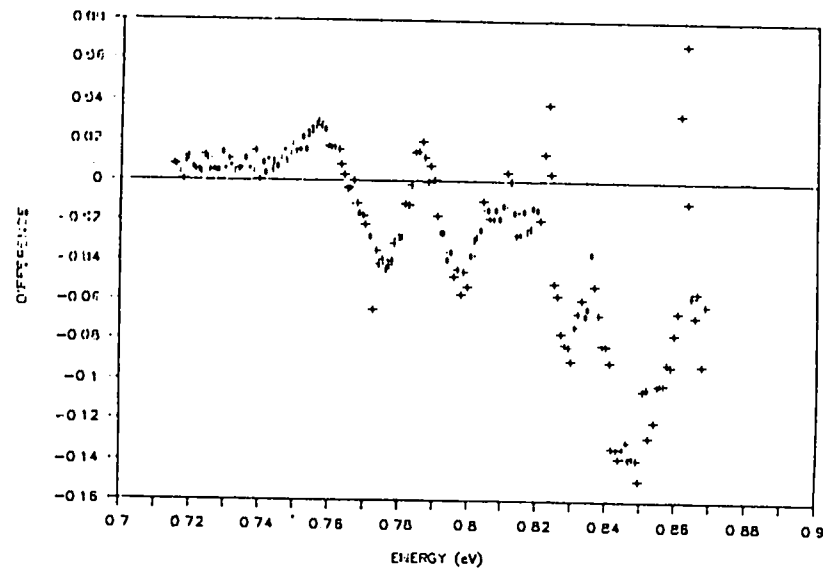
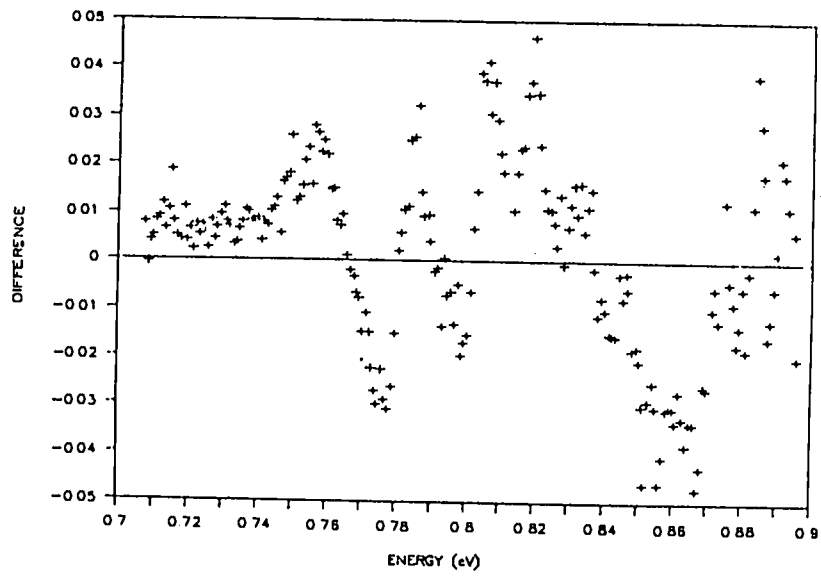
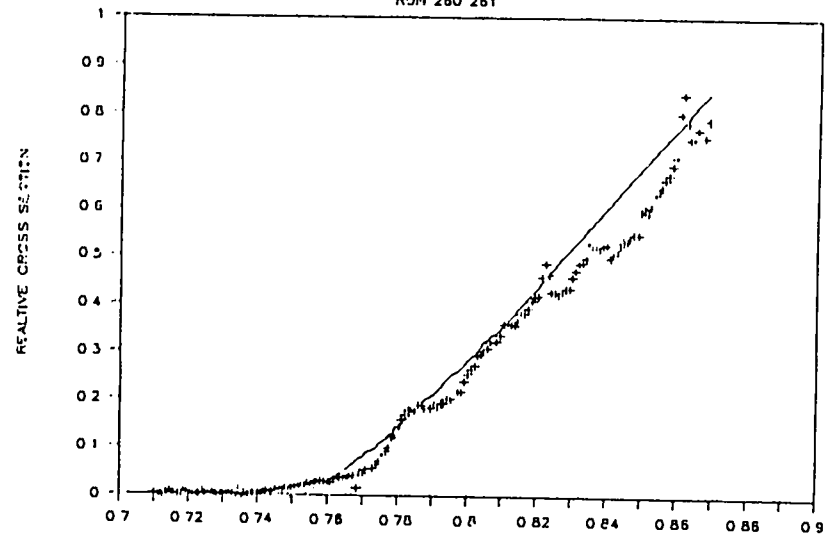
56 kV/cm PI POLARIZATION

RJN 249, 250

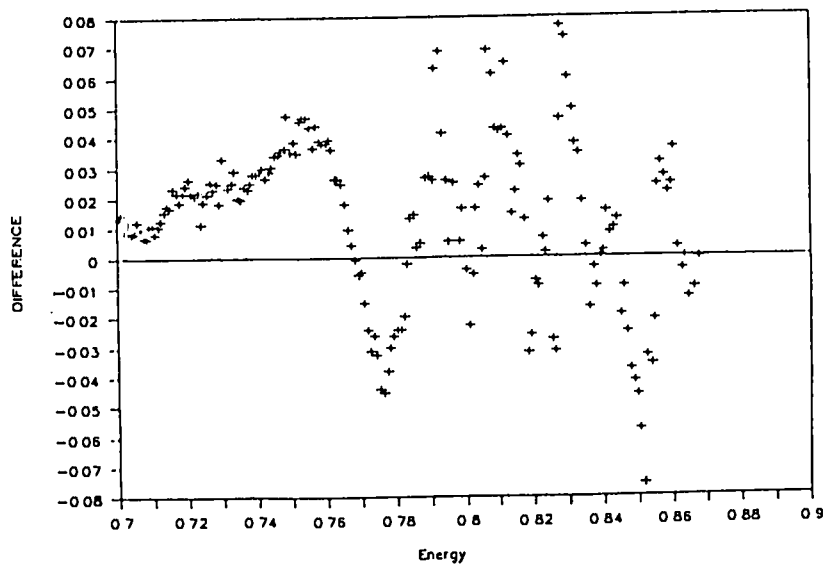
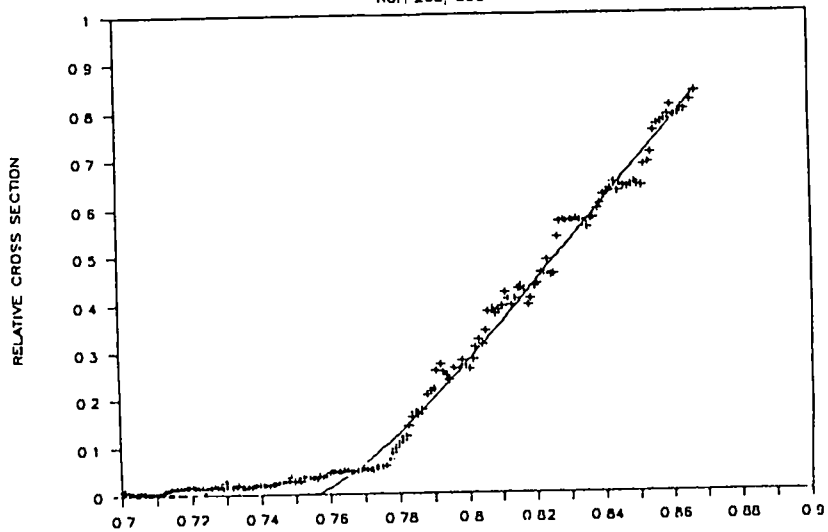


56 kV/cm PI POLARIZATION

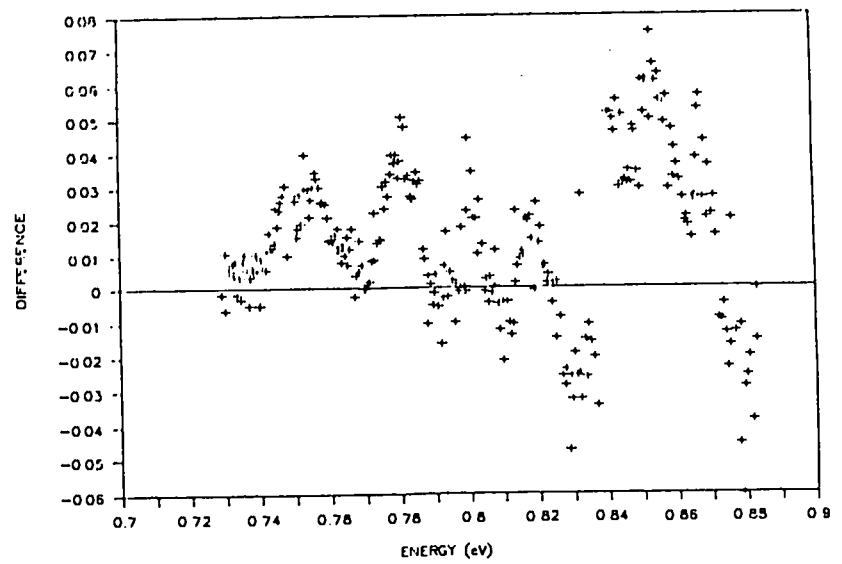
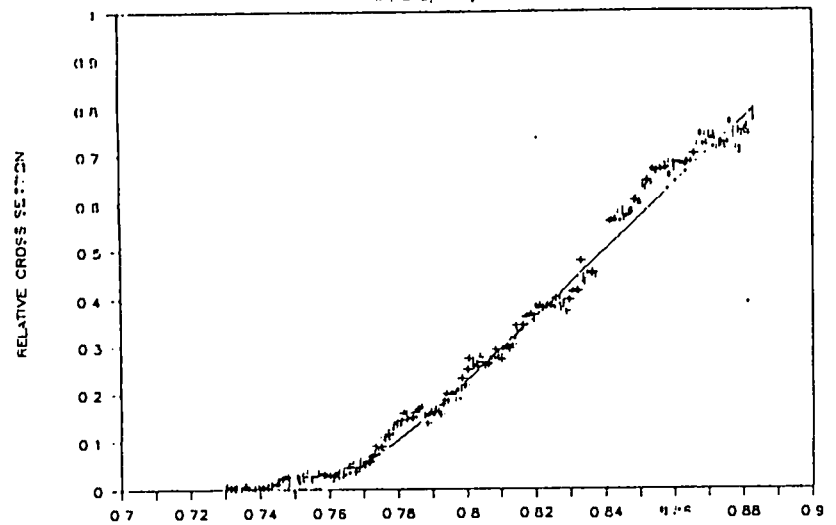
RJN 280 261



64 kV/cm PI POLARIZATION
RUN 252, 253

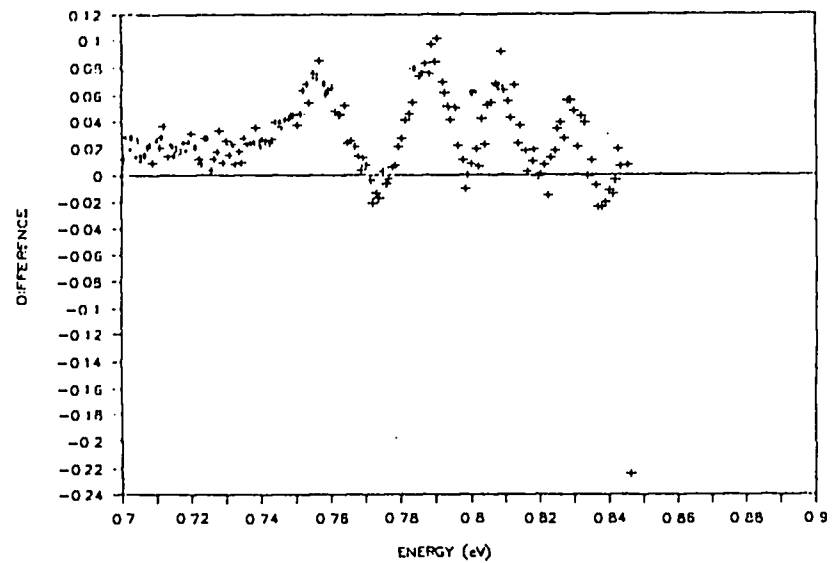
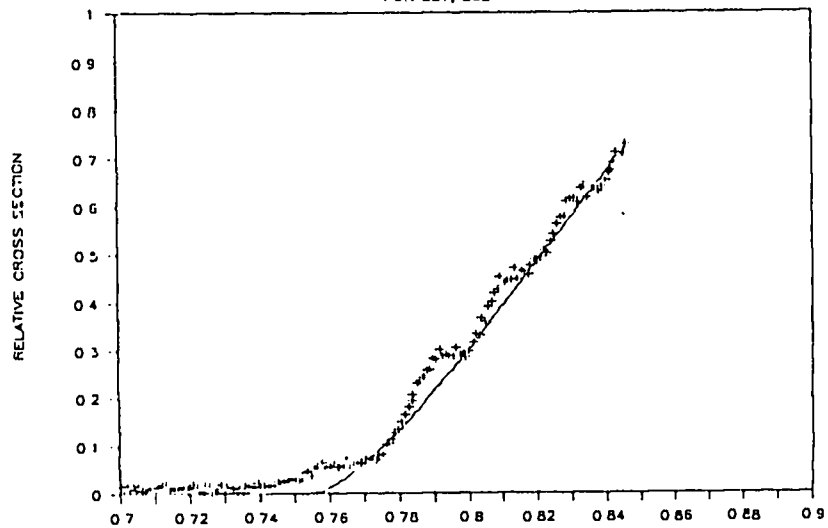


64 kV/cm PI POLARIZATION
PIPI 270, 271, 272



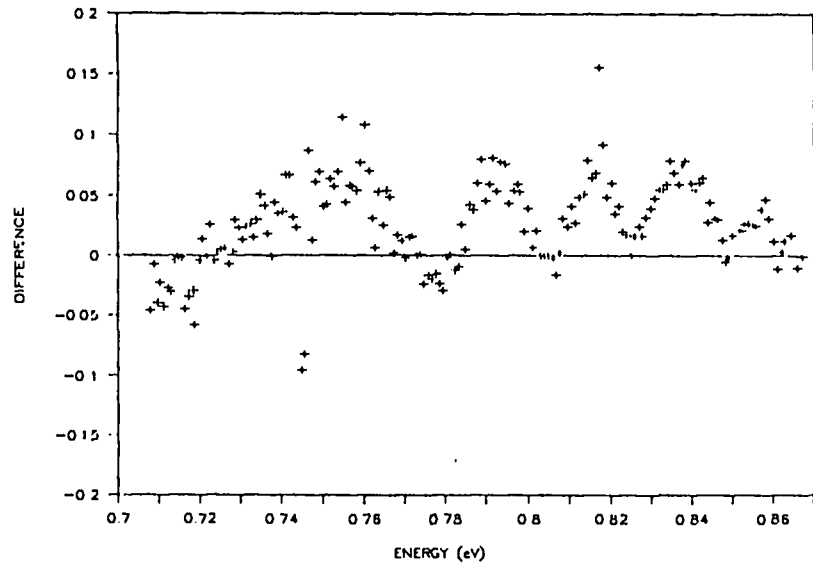
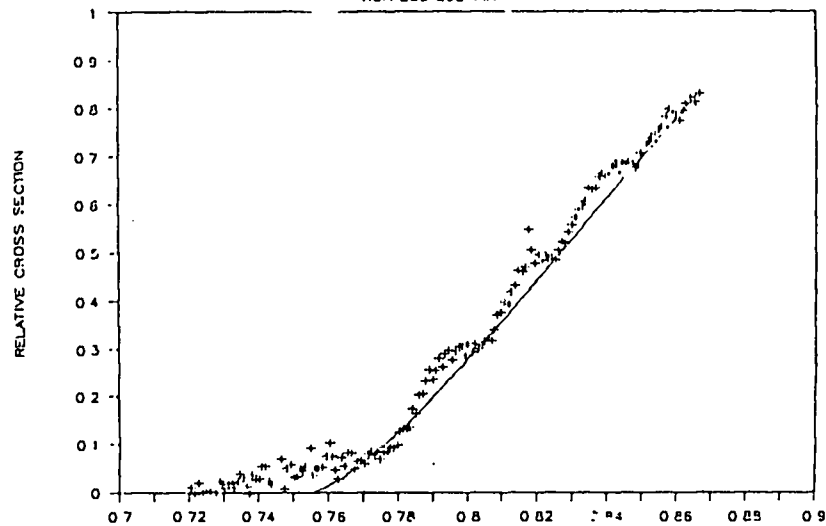
72 kV/cm PI POLARIZATION

RUN 287, 288



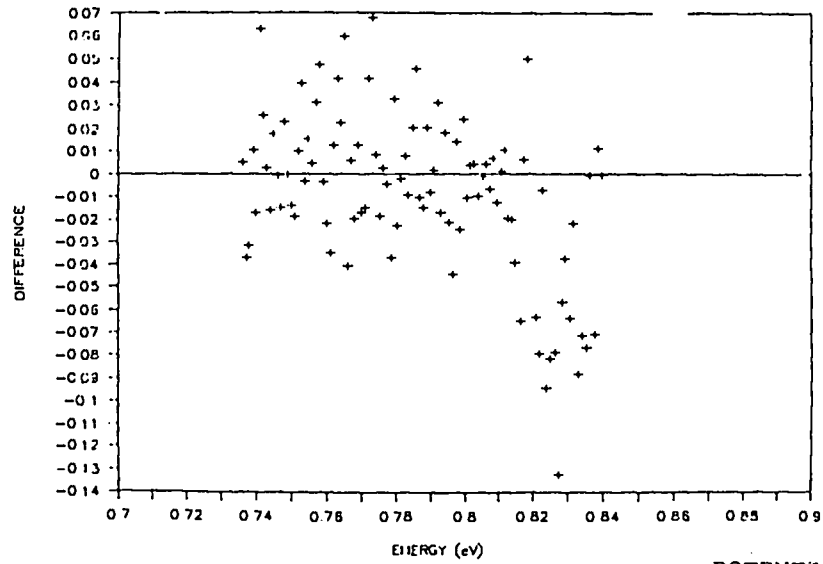
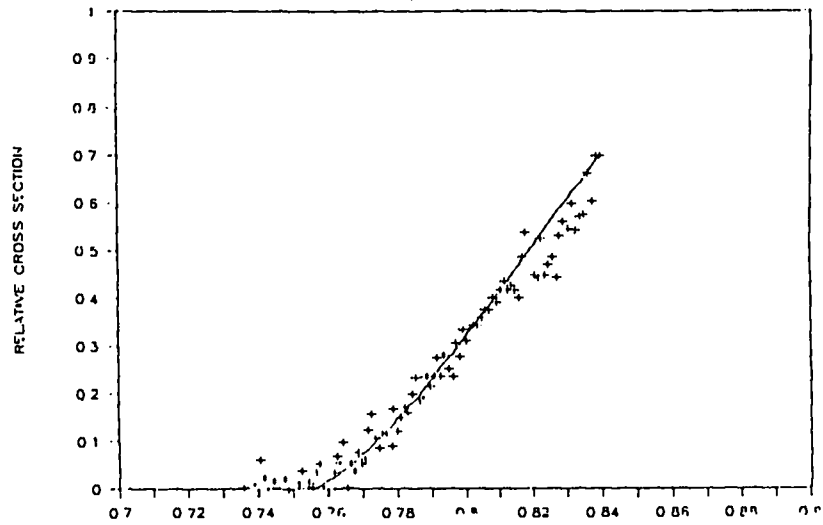
84 kV/cm PI POLARIZATION

RUN 289, 290



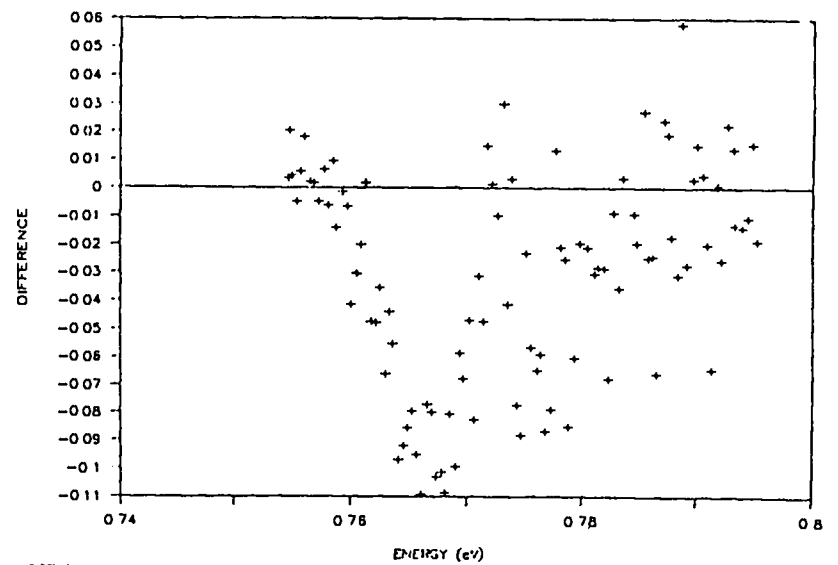
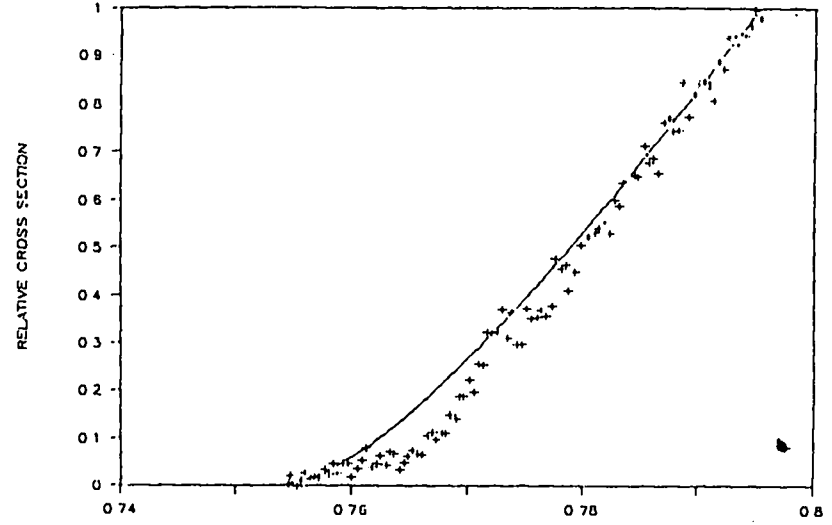
40 kV, PI POLARIZATION

RUN 350W



40 kV, PI POLARIZATION

RUN 45B

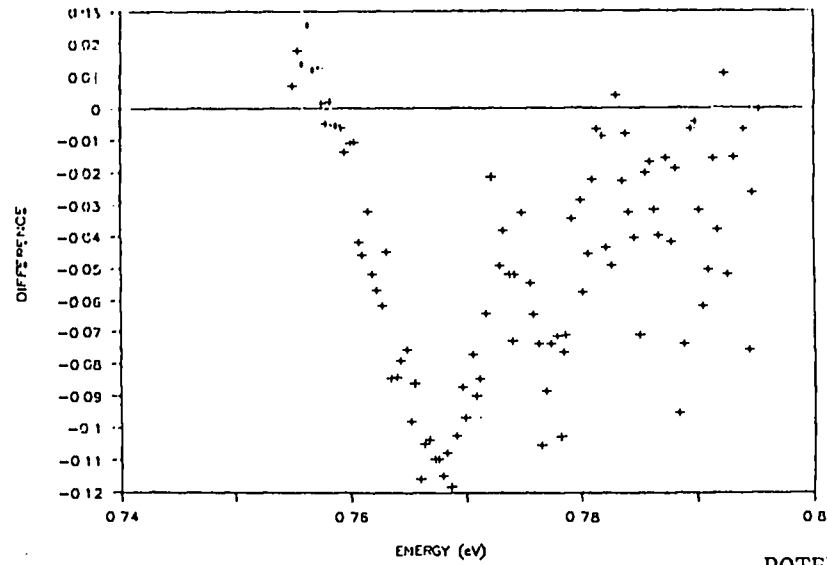
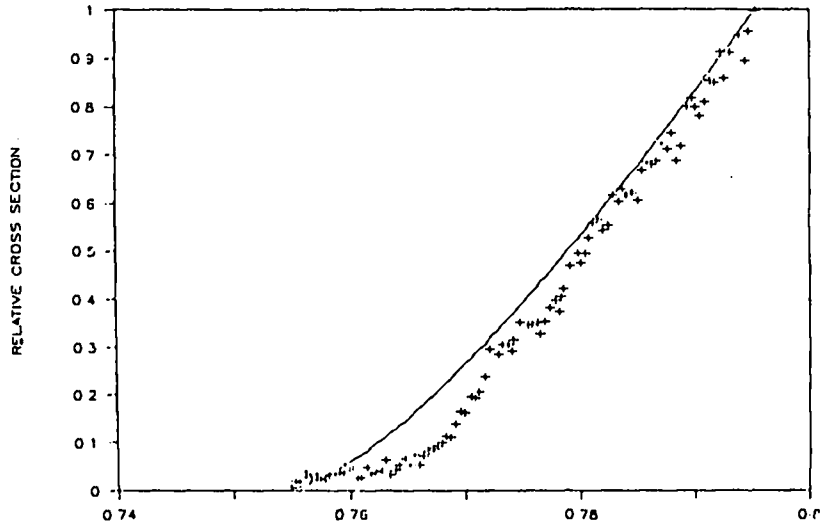


POTENTIAL

WELL

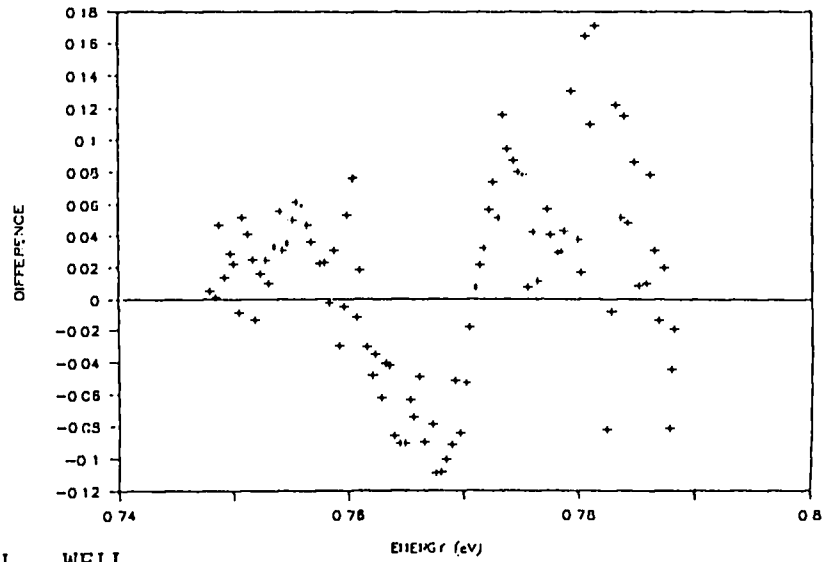
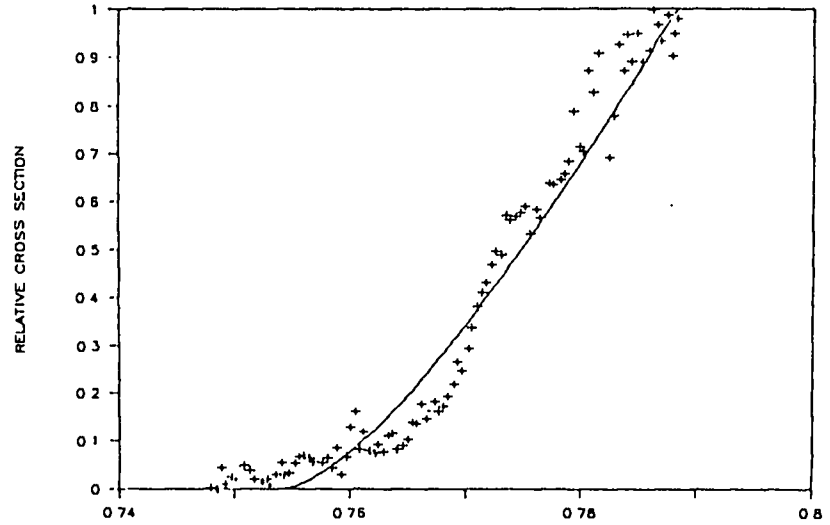
40 kV, PI POLARIZATION

RUI: 469



50 kV, PI POLARIZATION

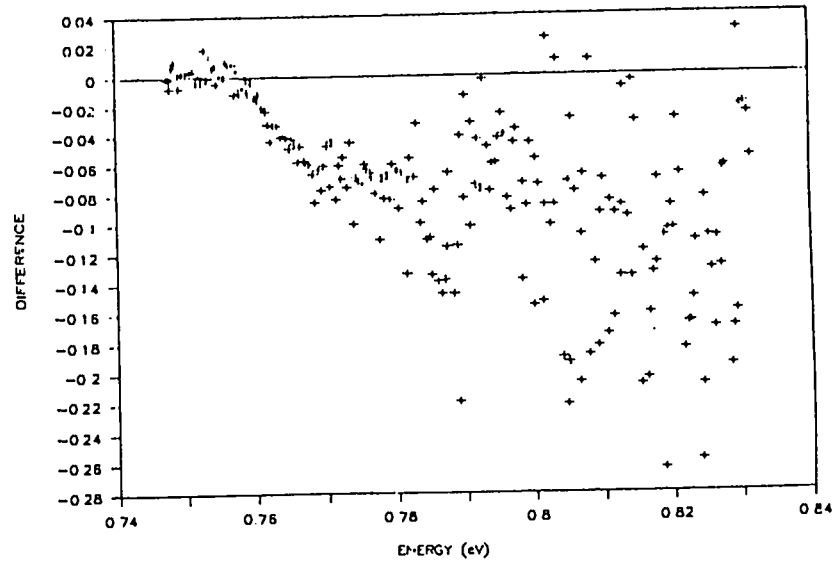
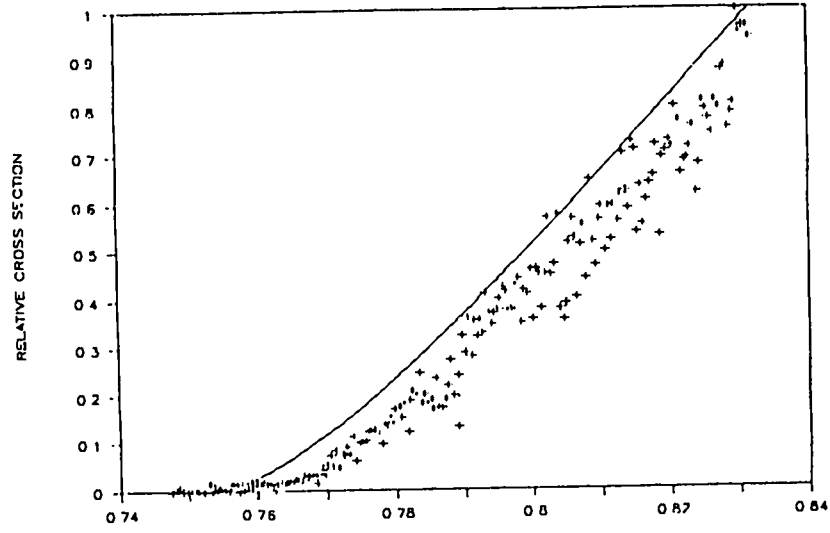
RUI: 477



POTENTIAL WELL

50 kV, PI POLARIZATION

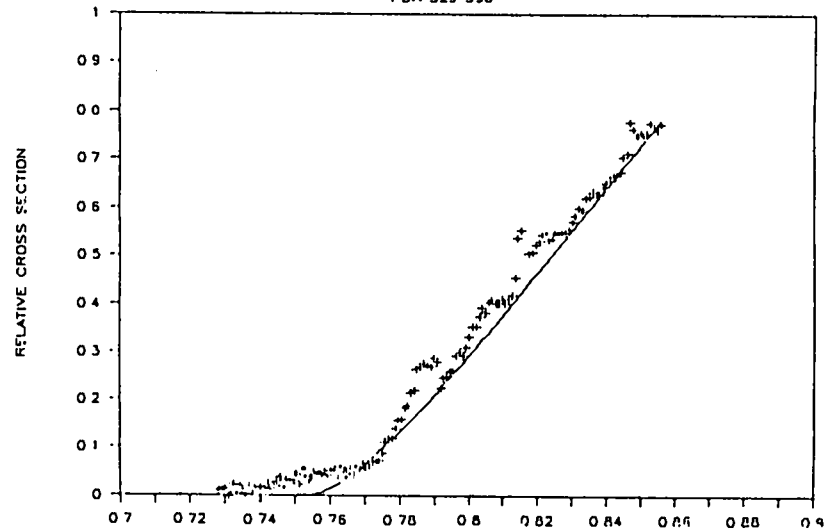
PLATE 478, 479



POTENTIAL WELL

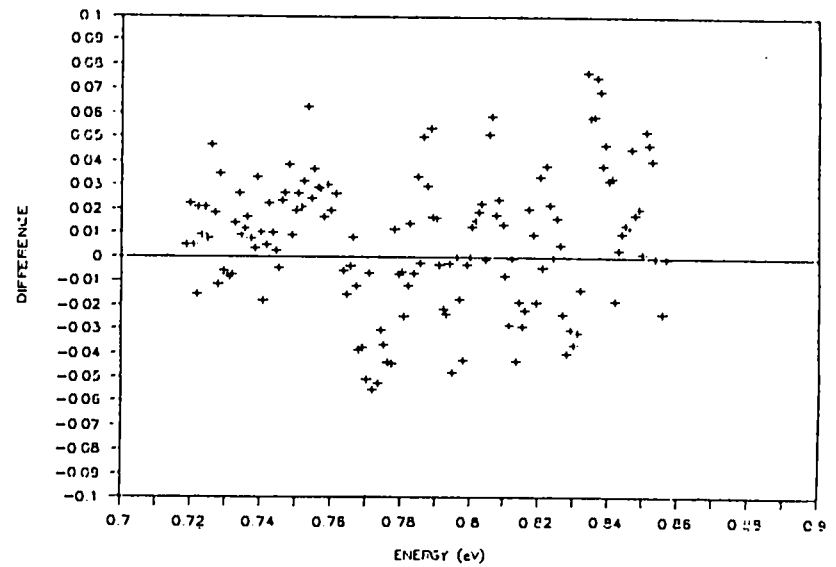
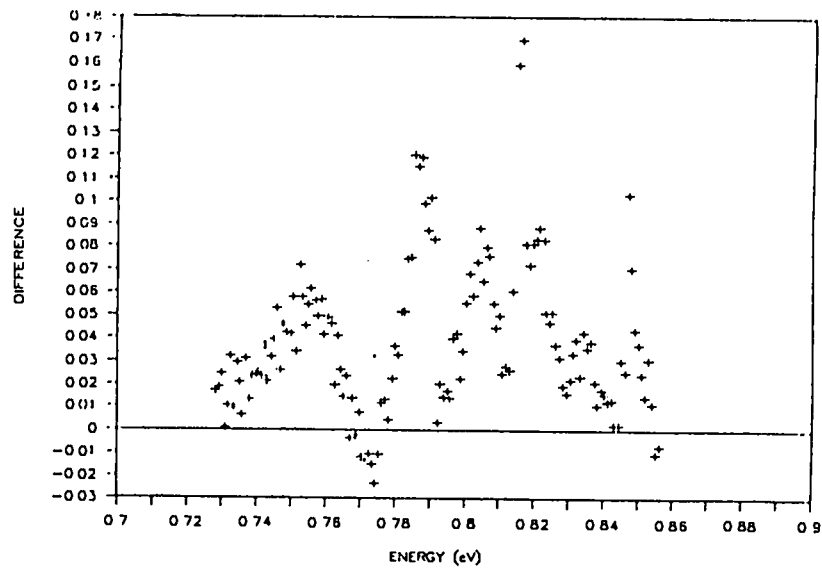
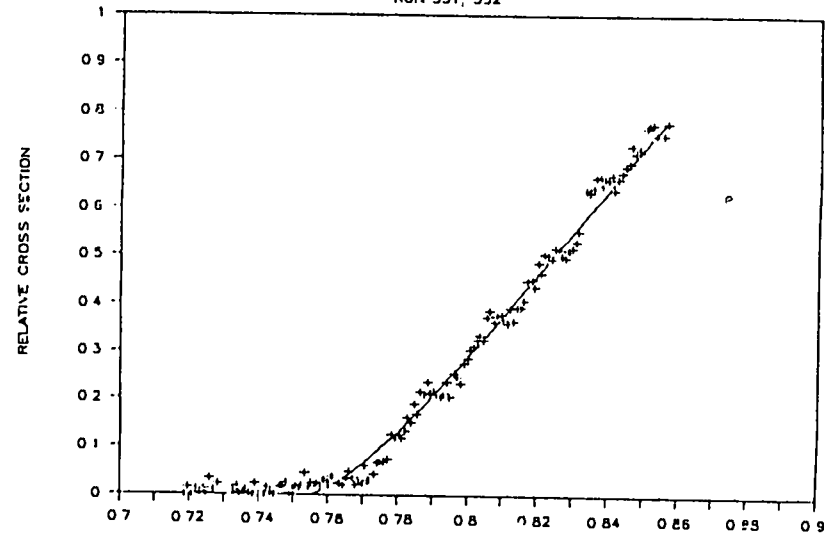
56 kV/cm PI POLRIZATION

RUN 329, 330



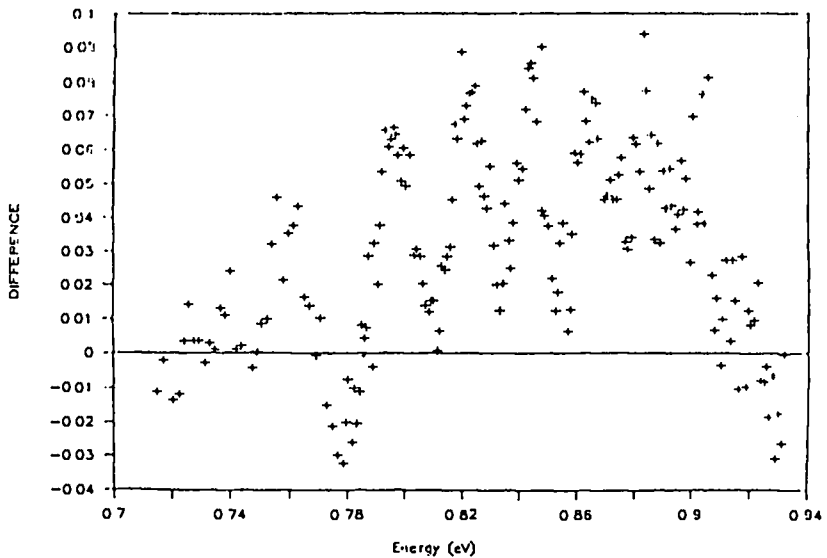
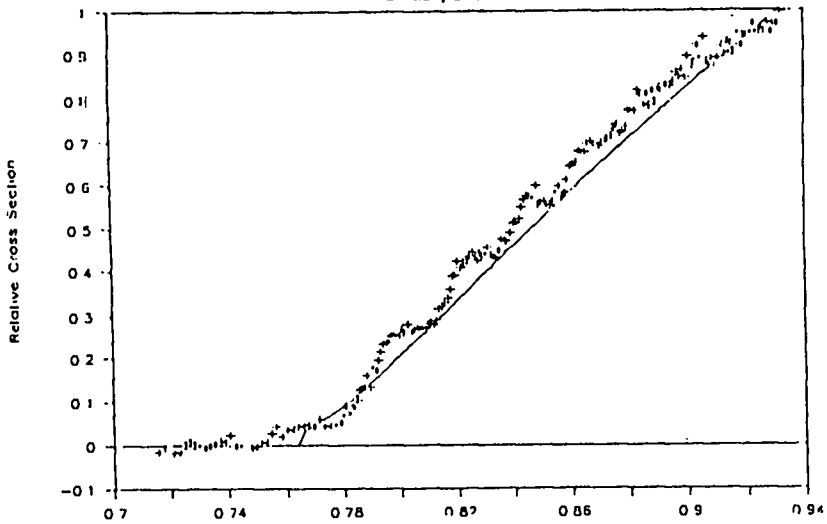
56.4 kV/cm PI POLARIZATION

RUN 331, 332



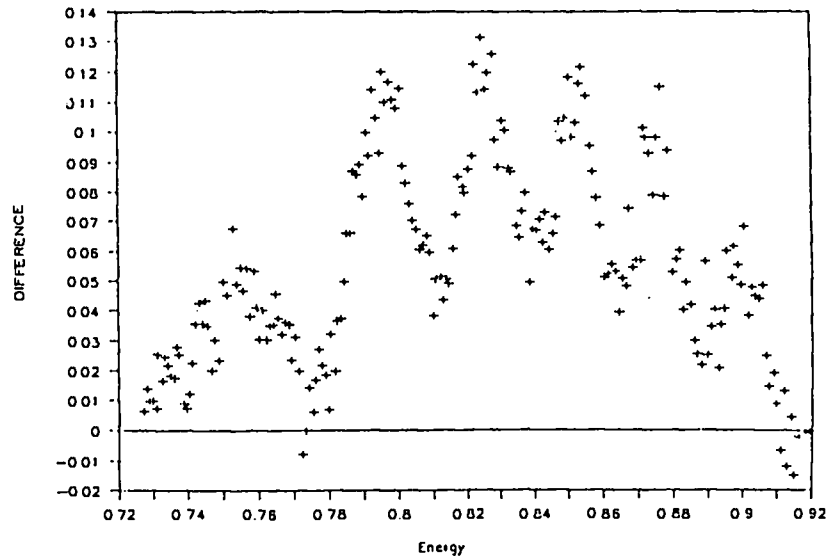
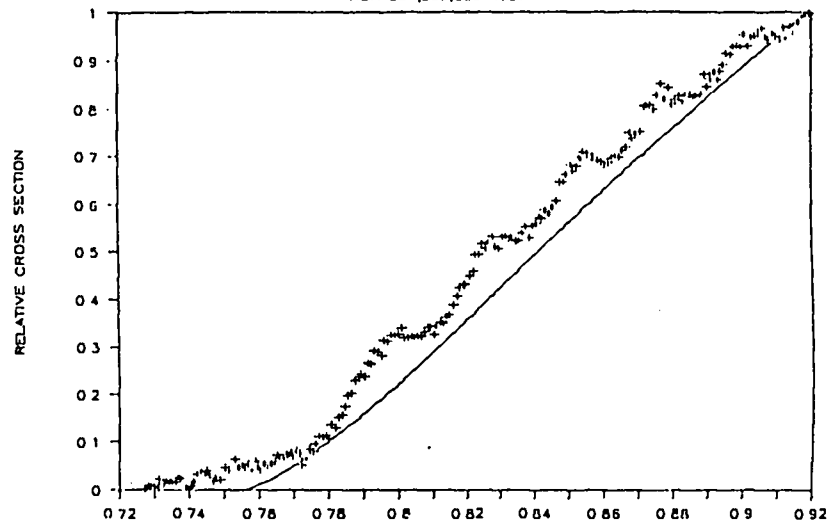
85.4 kV/cm PI POLARIZATION

RUN 307, 308



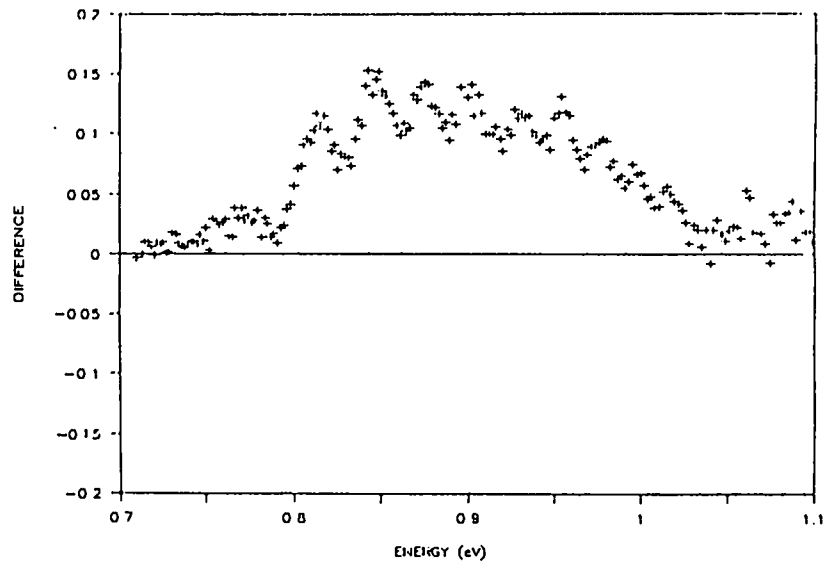
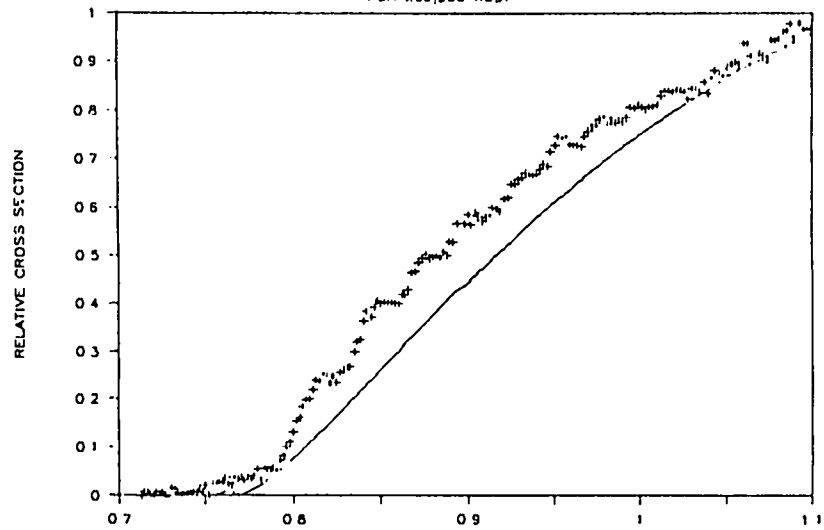
114 kV/cm PI POLARIZATION

RUN 304, 305, 306 WEST



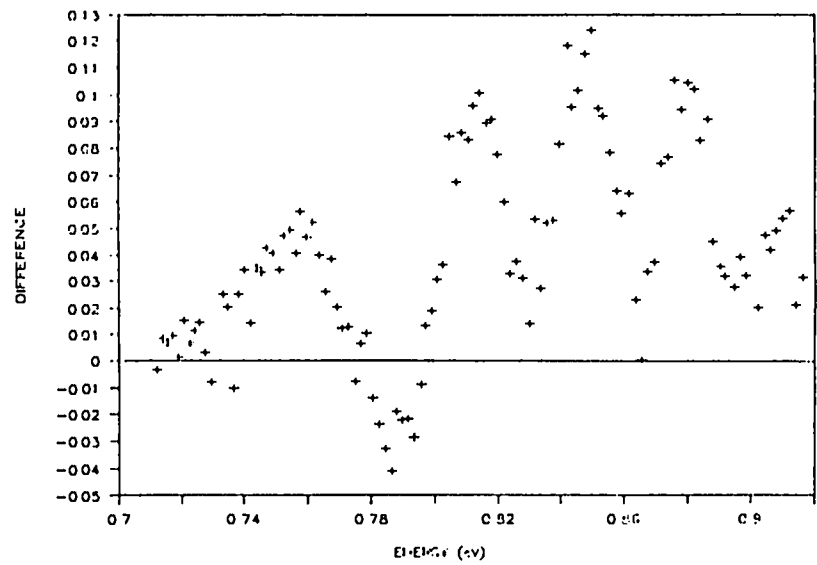
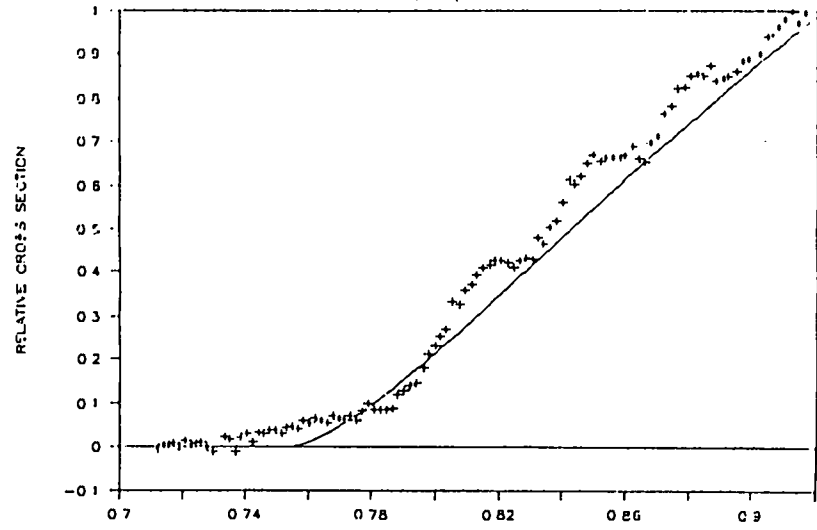
130 kV/cm PI POLARIZATION

RUN 299, 300 WEST



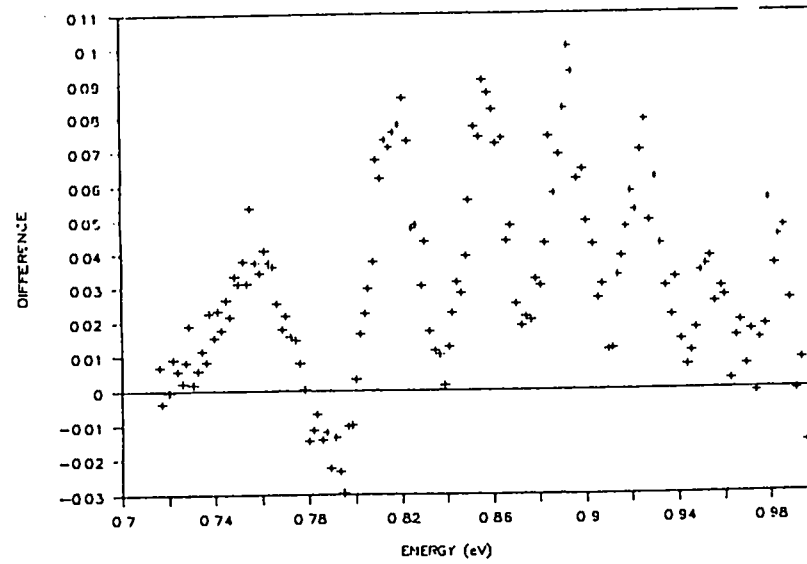
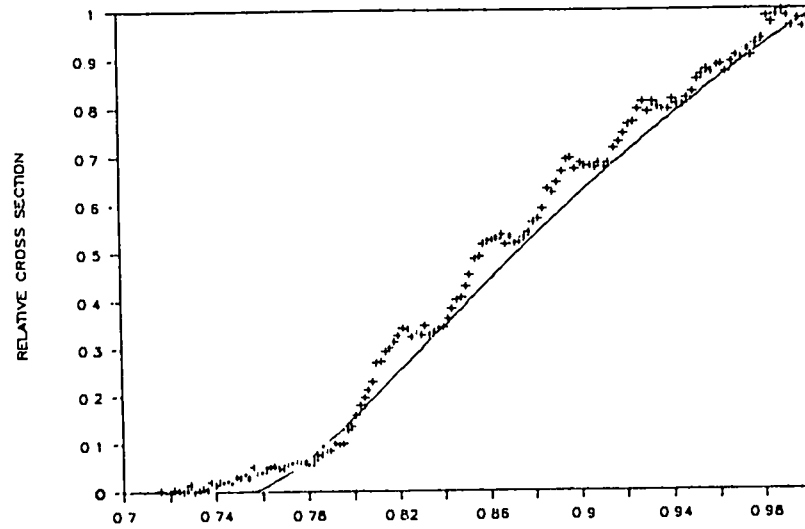
143.4 kV/cm PI POLARIZATION

RUN 297, 298



164 kV/cm PI POLARIZATION

RUN 333 334



REFERENCES

- Abramowitz, M., and I. A. Stegun (eds) Handbook of Mathematical Functions, NBS (1964).
- Armstrong, B. A. Phys. Rev. 131, 1132 (1963).
- Blumberg, W. A. M., R. M. Jopson, and D. J. Larson, Phys. Rev. Lett. 40, 1320 (1978).
- Bryant, H. C., (private Communication) .
- Bryant, H. C., D. Clark, J. B. Donahue, C. A. Frost, K. B. Butterfield, M. Hamm, R. Hamm, W. W. Smith, Atomic Physics with Relativistic Beams, Proceedings, Seventh ICPEAC (1980).
- Bryant, H. C., A. Mohagheghi, J. E. Stewart, J. B. Donahue, C. R. Quick, R. A. Reeder, V. Yuan, C. R. Hummer, W. W. Smith, Stanley Cohen, W. P. Reinhardt, L. Overman, Phys. Rev. Lett. 58, 2412 (1987).
- Bryant, H. C., D. A. Clark, K. B. Butterfield, C. A. Frost, H. Sharifian, H. Tootoonchi, J. B. Donahue, P. A. M. Gram, M. E. Hamm, R. W. Hamm, J. C. Pratt, M. A. Yates, W. W. Smith, Phys. Rev. A 27, 2889 (1983).
- Bryant, H. C., P. A. Lovoi, and G. G. Ohlsen, Phys. Rev. Lett. 27, 1628 (1971).
- Caceci, M. S., W. P. Cacheris, "Fitting Curves to Data" Byte, May 1984.

- Cohen, Stanley, Ph. D. Dissertation, University of New Mexico, 1985.
- Crewe, A. V., M. Isaacson, D. Johnson, Rev. Sci. Instrum. 42, 411 (1971).
- Delone, N. B., I. Yu. Kiyon, V. P. Krainov, V. I. Tugushev, Opt. Spectrosc (USSR) 58, 157 (1985) [Opt. Spectrosk. 58, 262 (1985)].
- Fano, U., Phys. Rev. A 24, 619 (1981).
- Fano, U., R. A. P. Rau, Atomic Collisions and Spectra (Academic, Orlando, 1986), sec. 7.2.4.
- Feneuille, S., S. Liberman, J. Pinard, and A. Taleb. Phys. Rev. Lett., 42, 1404-6 (1979).
- Freeman, R. R., N. P. Economou, G. C. Bjorklund, and K. T. Lu, Phys. Rev. Lett., 41, 1463-7 (1978).
- Frost C.A., Ph. D. Dissertation, University of New Mexico, 1981.
- Greene, C. H., and Rau, A. R. P., Phys. Rev. A 32, 1352 (1985).
- Harmin, D. A., Phys. Rev. Lett., 49, 2, 128-31 (1982).
- Harris, P. G. , (private communication).
- Heller, E. J., J. Chem. Phys., 68, 1066 (1978).
- Littman, M. G., M. M. Kash, and D. Kleppner, Phys. Rev. Lett., 41, 103-7 (1978).
- Lotus 123 v. 2.0, Lotus Development Corp., Cambridge, MA. (1985).
- Luc-Koenig, E., and A. Bachelier, Phys. Rev. Lett., 43, 921-24 (1979).

- Luk, T. S., DiMauro, L., Bergeman, T., and Metcalf, H.,
Phys. Rev. Lett., 47, 83-6 (1981).
- Overman, L., Masters Thesis, University of Pennsylvania,
1985.
- Pekeris, C. L., Phys. Rev. 112, 1649 (1958).
- Rau, A. R. P., J. Phys. B 12, L193 (1979).
- Rau, A. R. P., and K. T. Lu, Phys. Rev. A 21, 1057
(1980).
- Rau, A. R. P., H. Wong, (to be published) .
- Reeder, R. A., (private communication) 1986.
- Reinhardt, W. P., in Atomic Excitation and Recombination
in External Fields, M. H. Nayfeh and C. W. Clark,
eds. (Gordon and Breach, 1985) p 85.
- Ritson, D. M., Techniques of High Energy Physics
(Interscience, 1961).
- Sandner, W. K. A. Safinya, and T. F. Gallagher, Phys.
Rev. A, 23, 2448 (1981).
- Schiff, L. I., Quantum Mechanics, 3rd Ed., McGraw Hill
(1968), p. 265.
- Sellin, Ivan, (private communication).
- Sharifian, H., Ph. D. Dissertation, University of New
Mexico, 1977.
- Smith, S. J. and P. S. Burch, Phys. Rev. 116, 1125
(1959).
- Steffan, G., High Energy Beam Optics (Interscience, 1965).
- Tootoonchi, C. H., Ph. D. Dissertation, University of New
Mexico, 1977.

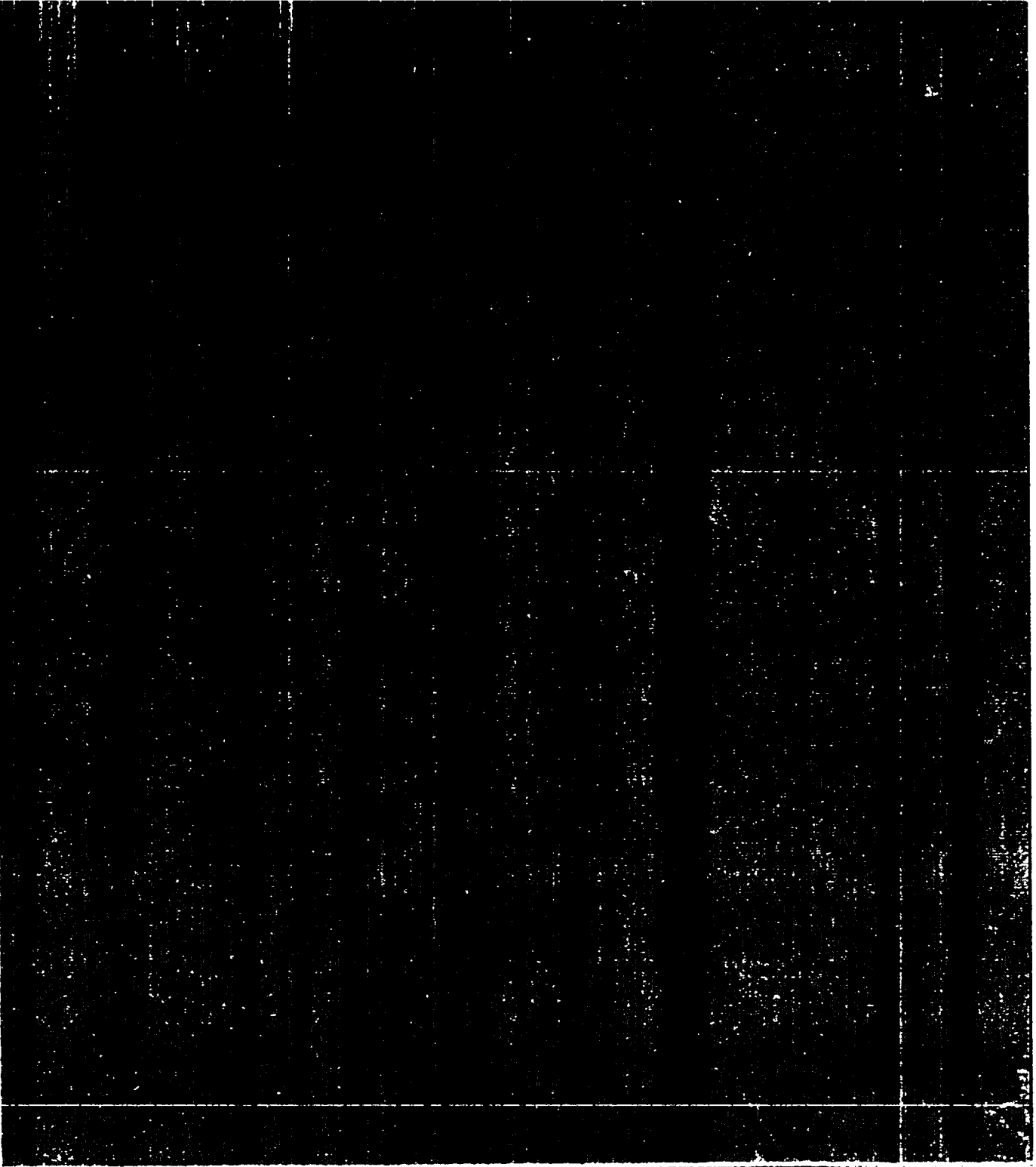
Whitman, Dave, Computer code NONLIN (Baker lab, Cornell
U., 1982).

Wigner, E. P., Phys. Rev. 73, 9, 1002 (1948).

Printed in the United States of America
 Available from
 National Technical Information Service
 US Department of Commerce
 5285 Port Royal Road
 Springfield, VA 22161
 Microfiche (A01)

NTIS		NTIS		NTIS		NTIS	
Page Range	Price Code						
001-025	A02	151-175	A08	301-325	A14	451-475	A20
026-050	A03	176-200	A09	326-350	A15	476-500	A21
051-075	A04	201-225	A10	351-375	A16	501-525	A22
076-100	A05	226-250	A11	376-400	A17	526-550	A23
101-125	A06	251-275	A12	401-425	A18	551-575	A24
126-150	A07	276-300	A13	426-450	A19	576-600	A25
						601-up*	A99

*Contact NTIS for a price quote.



Los Alamos